

Title	Fabrication of Mn-Zn ferrite with the aim of improvement of magnetic and mechanical properties
Author(s)	Hirota, Ken
Citation	大阪大学, 1989, 博士論文
Version Type	VoR
URL	<a href="https://hdl.handle.net/11094/1164">https://hdl.handle.net/11094/1164</a>
rights	
Note	

*Osaka University Knowledge Archive : OUKA*

<https://ir.library.osaka-u.ac.jp/>

Osaka University

Title

Fabrication of Mn-Zn ferrite  
with the aim of  
improvement of magnetic and mechanical  
properties

by  
Ken HIROTA

## Personal career

Ken Hirota is a research scientist at Central Research Laboratory of Matsushita Electric Industrial Co., Ltd.

He received a B.S. degree in material science in 1968, a M.S. degree in material science in 1970, from Osaka University.

He joined Matsushita Electric Industrial Co., Ltd. in 1970. His research activities include powder processing and fabrication, sintering and microstructure development in Mn-Zn ferrites for the magnetic recording head. His current interest is to develop high-toughened Mn-Zn ferrite with the excellent magnetic properties.

発表論文

1. K. Hirota, N. Kinomura, S. Kume and M. Koizumi, "Transition of Sulfospinel to  $\text{Th}_3\text{P}_4$  Type Phase under Pressure", Mat. Res. Bull, 11, 227 ~ 232 (1976)
2. E. Hirota, K. Hirota, M. Satomi and T. Nishikawa, "Hot-pressed Spinel Ferrites Having a Cube Texture." J. Jpn. Soc. of Powder and Powder Metallurgy 25, 307 ~ 310 (1978).
3. K. Hirota, "Spinel Ferrites for Magnetic Recording Head" J. Jpn. Soc. of Mineralogy 16, 3, 265 ~ 273 (1983).
4. K. Hirota, M. Sugimura and E. Hirota, "Hot-press Ferrites for Magnetic Recording Heads", Ind. Eng. Chem. Res. Dev. 23, 323 ~ 330 (1986).
5. K. Hirota, Y. Fujimoto, K. Watanabe and M. Sugimura, "High-B and  $\mu$  Mn-Zn Ferrite with Improved Mechanical Strength", Advances in Ceramics edit. F. F. Wang, State Univ. of New York, New York, 15, 385 ~ 392 (1986).
6. K. Hirota and O. Inoue, "Sodium-doped Mn-Zn Ferrites-microstructure and properties.", Ceram. Bull. 66, 12, 1755 ~ 1758 (1987).
7. O. Inoue, T. Wada and K. Hirota, "Machinability and microstructure of  $(\text{Ni}_{0.8}\text{Mg}_{0.2})\text{O}$  Ceramics.", J. Ceram. Soc. Jpn. 95, 10, 937 ~ 941 (1987).
8. K. Hirota, M. Satomi and K. Kugimiya, "Low Temperature Sintering of Mn-Zn Ferrites.", Proc. of Sintering '87 Tokyo, in press.
9. K. Kugimiya, K. Hirota and M. Satomi, "High B/ $\mu$  MnZn Ferrites for High Hc Media.", J. Mag. Mag. Mat. 72, 275 ~ 278 (1988).

10. K. Hirota, K. Todaka and K. Kugimiya, "Fine Grained Mn-Zn Ferrites with Co-Ca-Zr.", Proc. of Mat. Res. Soc. '88, in press.

11. K. Hirota, M. Satomi and K. Kugimiya, "The Magnetic Head Made of Mn-Zn Ferrites with High  $B_s$ (6300 G).", IEEE Trans. Mag. MAG. in press.

## 資料解説

1. E. Hirota, K. Hirota and K. Kugimiya, "Recent Development of Ferrite Head and Their Materials.", Proc. Conf. Ferrites 3, edit. H. Watanabe, S. Iida and M. Sugimoto, Center for Academic Publication, Jpn. 667 ~ 674 (1980).
2. K. Hirota and E. Hirota, "Synthesis of Grain Oriented Spinel Ferrite Polycrystals.", Bull. of Ceram. Soc. of Jpn. 18, 3, 190 ~ 197 (1983).
3. O. Inoue and K. Hirota, "High Density Mn-Zn Ferrites by Atmosphere-Controlled Sintering Method.", National Tec. Rep. (Jpn.) 31, 3, 139 ~ 144 (1985).
4. K. Hirota and O. Inoue, "DTA and TGA of the starting powder of ferrite.", Basis and application of thermal analysis, Jpn. Soc. of Thermal-Analysis, 98 (1985).

## CONTENTS

Abstract	1
Chapter I Introduction	3
1. Spinel ferrites for magnetic recording heads	3
2. Magnetic recording heads and core materials	3
3. Development of ferrite heads for the usage of both VTR and computer disk memories	5
4. Fabrication process of the polycrystalline ferrites	13
5. References	17
Chapter II Mn-Zn ferrite with a cube-texture	22
1. Introduction	23
2. Experimental procedure	28
2.1 Preparation of $\alpha$ -FeOOH and $\gamma$ -MnOOH	28
2.2 Mixing	28
2.3 Compacting	30
2.4 Sintering	30
2.5 Evaluation	30
3. Results and discussion	32
3.1 $\alpha$ -FeOOH	32
a) seed crystal	32
b) aging	35
c) hydrothermal treatment	35

d) normal and inverse crystal axes	39
3.2 $\gamma$ - MnOOH	42
3.3 Extrusion	42
3.4 Rolling on sheet	42
3.5 Change of the powders during heat treatment	45
3.6 Sintering	48
3.7 Magnetic properties and wear test	48
4. Conclusion	53
5. References	54
 Chapter III. Sodium doped Mn-Zn ferrites	 56
1. Introduction	57
2. Experimental procedure	57
3. Results	60
3.1 Sintering process	60
3.2 Microstructure	60
3.3 Physical properties	66
4. Discussion	66
4.1 Products with 0.001 ~ 0.05 wt% Na	69
4.2 Products with 0.05 ~ 0.1 wt% Na	70
4.3 Products with 0.1 ~ 1.0 wt% Na	71
5. Conclusion	71
6. References	72
 Chapter IV. High-B and $\mu$ Mn-Zn ferrite with improved mechanical strength by triple additions of Na-Zr-Ca	   73



1. Introduction	74
2. Experimental procedure	74
3. Results and discussion	75
4. Conclusion	86
5. References	89

Chapter V. Grain growth of Mn-Zn ferrite with additives  
and its application to the solid state single  
crystal growth

1. Introduction	91
2. Experimental procedure	92
3. Results and discussion	95
3.1 Choice of metal ions for enhancing the grain growth	95
3.2 Grain growth of the ferrites after annealing	98
3.3 Preparation of $B_2O_3$ doped Mn-Zn ferrites with high density	100
3.4 Adhesion of a single crystal plate on polycrystals	101
3.5 Solid state growth of single crystal	106
3.6 Mechanism of single crystal growth	110
3.7 Magnetic properties of grown single crystal	116
4. Conclusion	118
5. References	120

Chapter VI. Summaries

122

Acknowledgement

125

## Abstract

Fabrication of Mn-Zn ferrites were attempted to improve both of their magnetic and mechanical properties, since those were important properties as for the magnetic recording head materials.

In the practical studies, a cube-textured polycrystal ferrite with orientation degree  $Q(110) \geq 95\%$  and  $Q(111) \geq 90\%$  was fabricated. To get high orientation degree, long thin strip shaped powder of  $\alpha$ -FeOOH was newly synthesized and the method of orientating the powders during the compacting process were investigated and topotactic reaction on sintering process was checked. This ferrite was characterized by mechanical anisotropy of cubic spinel for wear resistance against the magnetic tape rubbing.

The effect of a single additive Na or triple additives Na-Ca-Zr on the microstructure of ferrites was investigated from the viewpoint of reducing the grain size and increasing the mechanical strength.

It was cleared that the combination of the amount of additive Na and the sintering condition was important to control the microstructures. The optimum condition was ~ 0.1 wt% Na, heating rate of 300 °C/h to 1250 °C and this resulted in reducing the grain size down to 7  $\mu\text{m}$ .

The triple addition of Na-Ca-Zr raised the resistance to chipping and the permeability at high frequencies. These advantages were obtained by Na addition which decreased the grain size and by Zr and Ca additions which toughened the grain boundaries.

Another effect by the additives, i.e., abnormal grain growth, which occurred during sintering or annealing, was investigated. Among many kinds of additives, mainly  $B_2O_3$  and  $Na_2O$  on the grain growth were studied.  $B_2O_3$  had a strong effect on the grain growth enhancement. In order to make use of the abnormal grain growth of Mn-Zn ferrite polycrystals, the amount of  $B_2O_3$  additives and the critical temperature at which the abnormal grain growth started were measured. By controlling the growth, the polycrystalline ferrite which contacted with a seed crystal, turned into a single crystal from the interface between the poly-single crystals by heat treatment. This solid-state epitaxially grown ferrites showed nearly the same magnetic properties as Bridgman single crystal ferrites. It had such merit as the acquisition of stable magnetic properties due to constant chemical composition in an ingot, which was desirable for the industrial viewpoint. The mechanism of solid-state growth was discussed.

## Chapter I. Introduction

### 1. Spinel ferrites for magnetic recording head

Ferrite is an oxide of cubic spinel type structure and its chemical composition is denoted by a formula  $MFe_2O_4$  where M is a divalent ion of transition elements of 1st group. Since ferrimagnetism of this material was an interesting topics and a useful property, it has long been studied from both sides of technology and basic science.<sup>1)2)</sup>

It is well-known that ferrite has been used as magnetic recording heads because of its excellent magnetic properties at high frequencies and their high wear resistance.<sup>3)-6)</sup> These properties owe to the high electric resistivity, the mechanical hardness, and chemical stability of the substance. Both single and polycrystal are now widely used for the magnetic heads of video tape recorders and for magnetic disks.

### 2. Magnetic recording heads and core material

A magnetic recording head with a polycrystalline ferrites core was precisely studied by Chynoweth.<sup>7)</sup> His survey was concentrated mainly on how to fabricate poreless and high-density ferrite and also how to form a mechanically stable and rigid magnetic gap with strong magnetic field between two opposed pieces of ferrite.

In general, the following characteristics are requested for a magnetic core material: (1) high permeability  $\mu$ , (2) high saturation magnetization  $B_s$ , (3) low coercive force  $H_c$  and low remanent magnetic flux density  $B_r$ , (4) high electric resistivity which leads to high permeability at high frequency, (5) hardness for wear resistance, (6) mechanical strength and durability for ease of precise machining, (7) chemical stability, (8) high Curie temperature  $T_c$ , and (9) reasonable cost.

When the ferrite is used as a magnetic core material, it is desirable for the ferrite to have a high density for forming a mechanically strong magnetic gap. The single crystal ferrite was first adopted as a highly dense magnetic core material and it is still in use for VTR (Video Tape Recorder) heads.<sup>8)-13)</sup> But this kind of head causes a high rubbing noise due to the Barkhausen effect and the material itself is fairly inhomogeneous in composition.<sup>14)-17)</sup>

Among the ferrites, that of Ni-Zn composition has a special character of higher electric resistivity and easiness for machining and now is popular for the flying heads of magnetic disks and drums.<sup>18)</sup>

Hot-pressed ferrites of both Ni-Zn and Mn-Zn ferrite composition were also developed and the dense bodies with a porosity of less than 0.1 % have been obtained.<sup>19)-22)</sup> They show a property of easy fabrication useful for the magnetic recording heads.<sup>23)-29)</sup>

The magnetic recording heads with polycrystalline ferrite cores sometimes have short life due to the pores contained inside. But the polycrystalline ferrites have more homogeneous structure in an ingot than the single crystal ones.

In the assembling process of magnetic head, it is very important to form a magnetic gap of accurate size since this affects the head performance. Various methods to meet this request have been proposed and one of them is a method called glass bonding.

Recently, a fine magnetic gap of 0.4  $\mu\text{m}$  long was produced by sputtering glass on the surface of ferrites and this brought an increase in recording density.

The width of magnetic recording tracks also has been decreased in order to increase the recording density. VHS-type video recording heads and Winchester-type computer disk heads demand, for example, the track width of 20 and 17  $\mu\text{m}$ , respectively.

To obtain higher recording density [bit/unit area], small pore radius, porosity, and grain size, high saturation magnetization density and high permeability at high frequency for the ferrites are demanded.

### 3. Development of ferrite heads for the usage of both VTR and computer disk memories

In the case of the video head, high wear resistance against the magnetic tapes, high power and narrow distribution in signal output are mainly demanded for ferrite.

Although both the Mn-Zn and the Ni-Zn ferrites have cubic structure, their magnetic and mechanical properties show anisotropies which depend on the crystal planes and crystal axes.

As shown in Fig. 1, the wear resistance against the rubbing of tape shows the crystal anisotropy which depends on a combination of the tape-touching surface (crystal plane) and the tape-running direction (crystal axis). When a polycrystalline ferrite is used for the VTR-head material, the tape-touching surface becomes uneven because of the wear anisotropy of each grains on the surfaces.<sup>30)</sup>

And also, there is the anisotropy of the magnetic head output which depends on the crystal axes, as shown in Fig. 2, measured by using single crystal of the Mn-Zn ferrites.<sup>26)</sup> Therefore, the single crystal Mn-Zn ferrite is used for the VTR-head material.

Among the various single crystal preparation, the Bridgman method was chosen to grow single crystals of Mn-Zn ferrite. The advantage of this method is to suppress the evaporation of Zn and also to protect the grown crystal from the contamination of gas atmosphere on processing. A problem, however, arises in case where a binary system forms a complete solid solution. The composition of liquid phase differs from that of solid phase on cooling. The solid phase is enriched with the component of higher melting temperature. Therefore, the subsequent solidifying material contains less amount of this component.



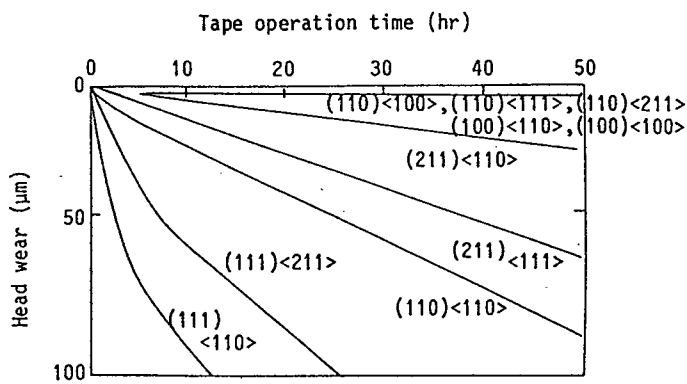


Fig.1 Wear of single crystal video heads of Mn-Zn ferrite having various crystal planes and axes as tape-touching surface: ( ), tape-touching surface; < >, tape-running direction; tape:  $\text{CrO}_2$ , head: core width, 110  $\mu\text{m}$ ; penetration depth, 180  $\mu\text{m}$ ; relative tape speed, 11 m/s.

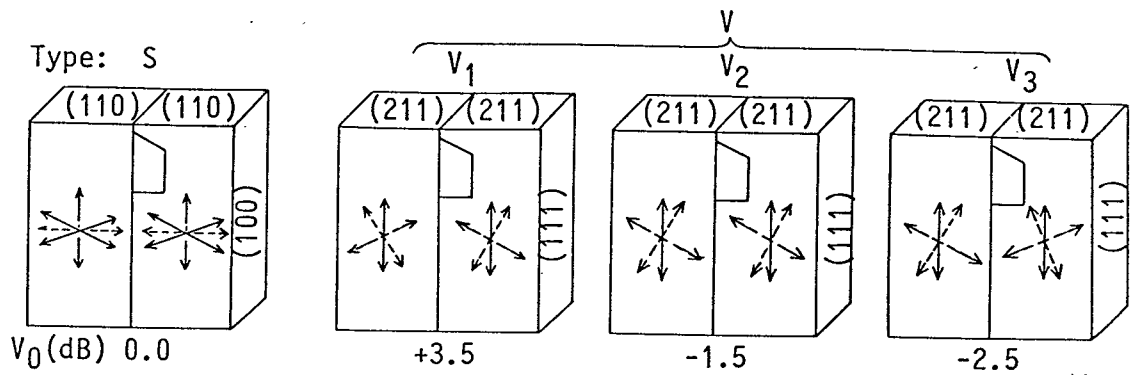


Fig.2 Comparison between relative outputs ( $V_0$  at 5 MHz) of various crystal planes and axes as the tape-touching surface and running direction. Measuring condition: type, VHS-VTR heads; relative tape speed, 5 m/s; tape,  $\gamma\text{-Fe}_2\text{O}_3$  ["Avyline" trade mark, TDK Co.,Ltd] tape;

$\langle 211 \rangle, \longleftrightarrow$ ;  $\langle 110 \rangle, \leftarrow \rightarrow$ ;  $\langle 100 \rangle, \leftarrow \dashrightarrow$ .

As a result, the final product has a large compositional gradient in the growth direction, instead of strong requirement of homogeneity.

Another disadvantage exists in the Bridgman method. In the Bridgman method, a platinum crucible is usually used as a container at temperatures above 1600 °C. Consumption of precious platinum crucible makes the production cost high.

On the other hand, one way to avoid the above-stated demerits is the use of polycrystalline ferrites. The homogeneity of the sintered body and the low production cost can be expected for this kind of materials.

From the viewpoint of adopting the merit of the polycrystal production, the grain oriented Mn-Zn ferrite was studied,<sup>31)-43)</sup> because, by arranging the grains of the polycrystals, the mechanical and magnetic anisotropy which depend on the crystal plane or axis could be used.

It would be more progressive to use a grain-oriented ferrite in which the dominant characters of polycrystals are available in addition to those of mechanical and magnetic anisotropies.

The fabrication of the grain-oriented ferrite is based on the usage of shape anisotropy of starting powders and topotactic growth of powders during sintering. Details of this method will be described in Chapter II.

In the case of the disk memory head, the polycrystalline ferrites meet the demand of mass productivity at low cost.

The polycrystalline ferrites have been improved to reduce the grain size and to increase the mechanical strength. These properties are important to get long durability for machining in the head assembling process,<sup>44)-48)</sup> and to obtain the narrow distribution of signal output of head which makes the track narrow.

As far as the reduction of the grain size is concerned, there is a relatively strong relation between the grain size and the scattering of the head performance of the polycrystalline ferrite head. As the grain size becomes smaller, narrower scattering of the head performance is available, approaching to that of a single-crystal ferrite head (Fig. 3).<sup>26)30)</sup> The signal output of the head changed with the tape operation time for about 60 min, which is the early stage of the work and then stays constant afterwards.

The initial variation of signal output which relates with the magnetic tape operation time is dependent on the average grain size of the ferrite materials (Fig. 4). In this paper, the effect of Na on the microstructure of the Mn-Zn ferrites, such as the reduction of the grain size, will be described in Chapter III.<sup>49)</sup>

To improve the mechanical strength, especially the durability to chipping or grain pull-out during cutting or polishing the ferrites, a triple addition of  $ZrO_2$ , CaO and Na was studied by the present author.<sup>50)</sup> The result will be described in Chapter IV.

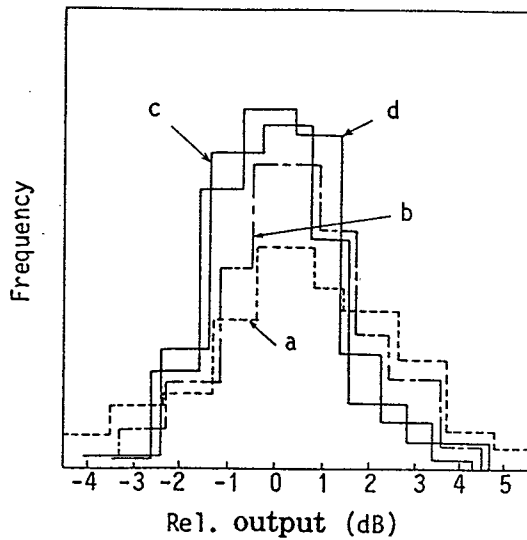


Fig.3 Distribution of the output of video heads made of polycrystalline ferrites of average grain size of 60 and 5  $\mu\text{m}$ . Comparisons are made with that of single crystal head and (111)-oriented ferrite head: (a) polycrystalline ferrite head (average grain size = 60  $\mu\text{m}$ ); (b) polycrystalline ferrite head (average grain size = 5  $\mu\text{m}$ ); (c) (111)-oriented ferrite head; (d) single crystal ferrite head.

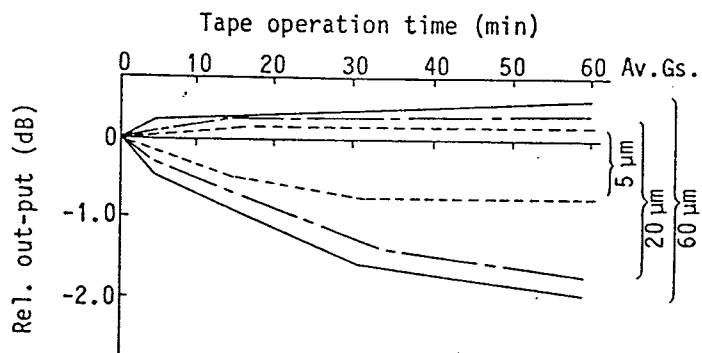


Fig.4 Initial variation of head output as a function of the average grain size of ferrite materials: 60, 20 and 5  $\mu\text{m}$ .

In relation to these surveys, the abnormal grain growth of Mn-Zn ferrite polycrystals enhanced by additives such as Na and B was observed. By optimizing the amount of additives and sintering condition, the abnormal growth could be controlled. To apply this method, crystal growth in solid state was attempted. These results will be described in Chapter V.

#### 4. The fabrication process of the polycrystalline ferrites

Three kinds of manufacturing processes are known to produce dense sintered ferrites; (i) a vacuum sintering,<sup>51)</sup> (ii) a hot press sintering, (iii) a hot isostatic press (HIP) sintering.<sup>52)53)</sup>

In the vacuum sintering, low cost of production, easy control of sintering atmosphere and no recurrence of pores in the sintered body after aging are counted as the merits. But some demerits exist such that the densification strongly depends on the properties of starting powders and also there is a difficulty to produce the fine grained ferrites with high density.

The hot press sintering has merits that it can produce the sintered body with high density which is relatively free from the properties of starting powders. The HIP sintering used for the production of ferrites is a capsule-free method; i.e., HIP sintering uses the presintered bodies which have  $\geq 92 \sim 95$  % of theoretical density.

These pressure sintering method have demerit that the control of sintering atmosphere is not easy, sometimes pores recur in the sintered body after aging and the cost is high. But there is enough merit that they can produce the fine grained ferrites with density higher than 99 %.

In this paper, the hot press sintering was mainly adopted because of the properties of starting powder and in order to fabricate fine grained ferrites. Figure 5 shows the manufacturing process of the hot press ferrites. Figure 6 is the photomicrograph of coprecipitated ferrite powder prepared by wet process whose particle size is small and sintering activity is high.<sup>54)-56)</sup> They are often used in the hot press sintering.<sup>57)-58)</sup>



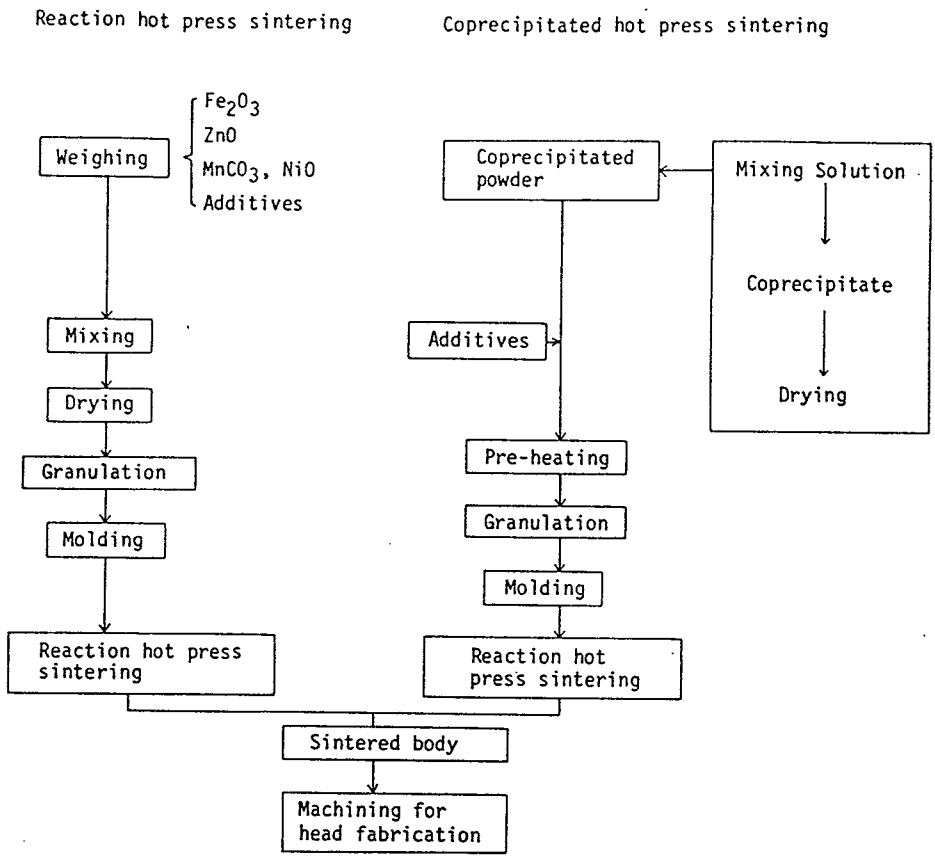


Fig.5 Manufacturing process of the hot press ferrite materials.



Fig.6 Coprecipitated Mn-Zn ferrite powder.

## 5. References

1. J. Smit and H. P. J. Wijn, "Ferrite", Philips Technical Library(1959).
2. Y. Kato and T. Takei, Denki Gakkaishi (Jpn.) 53, 408 ~ 412 (1933).
3. F. Bergman, U.S.Patent 2,809,237 (BASF).
- R. Iderr, Electronics Apr. 124 (1951) (3M).
- H. F. Olson, W. D. Houghton, A. R. Morgan, M. Artzt, J. A. Zenel and J. G. Woodward, RCA Rev., 17, 330 ~ 338 (1956).
4. Jpn. Utility Model 36-27312.
- H. Nishinomiya and H. Abe, NHK Tech. Journal (Jpn.) 18, 1 ~ 20 (1966).
5. A. L. Stuijts, J. Verweel and H. P. Peloschek, IEEE Trans. Comm. and Elect. 83, 726 ~ 736 (1964).
6. Jpn. Utility Model 40-14931, U.S. Patent 3,843,541.
7. W. R. Chynoweth, Tele-Tech and Elect. Ind., 14, 82 (1955), IRE Nat. Conv. Rec., 3, 7 (1955).
8. M. Sugimoto, Proc. Int. Conf. Ferrites 2 edit. Y. Hoshida, S. Iida and M. Sugimoto, Univ. of Tokyo Press, 318 ~ 322 (1970).
9. S. Kobayashi, I. Yamagishi and R. Ishii, *ibid.*, 326 ~ 328 (1970).
10. S. Harada and Y. Nojo, *ibid.*, 310 ~ 313 (1970).
11. R. D. Fisher, J. M. Magee, I. J. Lowe and V. Morton, *ibid.*, 340 ~ 342 (1970).

12. Y. Matsumoto, K. Miyamoto, T. Miyamoto, S. Komoda and Y. Takahashi, Proc. of Spring Conf. of Jpn. Soc. of Powder and Powder Metallurgy, 138, 144, 146 (1972).
13. T. Iwasa and H. Abe, Proc. Int. Conf. Ferrites 2, edit. Y. Hoshino, S. Iida, and M. Sugimoto, Univ. of Tokyo Press, 349 ~ 351 (1970).
14. Th. J. Berben and D.J. Perduijn, Proc. Int. Conf. Ferrites 3, edit. H. Watanabe, S. Iida and M. Sugimoto, Center for Academic Publication, Jpn. 722 ~ 725 (1980).
15. Tominaga, Proc. of Autumn Conf. of Jpn. Soc. of Powder and Powder Metallurgy, 143 (1968).
16. O. Konei, U.S. Patent 2,866,011 (Clevite).
17. M. Torii, U. Kihara and I. Maeda, Proc. Int. Conf. Ferrites 3, edit. H. Watanabe, S. Iida and M. Sugimoto, Center for Academic Publication, Jpn. 717 ~ 721 (1980).
18. H. Watanabe, Tohoku Metal Technical Review (Jpn.) 2, 1, 48 (1963).
19. W. W. Malinofsky and R. W. Babbitt, J. Appl. Phys. 32, 3, 237S (1961).
20. T. Nishikawa, A. Ikeda and H. Chiba, Denshi Zairyo (Jpn.) 4, 8, 19 ~ 24 (1965).
21. H. Sugaya, IEEE Trans. Mag. MAG-4, 295 ~ 301 (1968).
22. E. Hirota, T. Mihara, A. Ikeda and H. Chiba, ibid., MAG-7, 337 ~ 341 (1971).
23. E. Hirota, Oyo Buturi (Jpn.) 42, 630 ~ 634 (1973).
24. A. Ikeda, National Tech. Rep. (Jpn.) 13, 255 ~ 261 (1967).

25. A. Ikeda, M. Satomi, H. Chiba and E. Hirota, Proc. Int. Conf. Ferrites 2, edit. Y. Hoshino, S. Iida and M. Sugimoto, Univ. of Tokyo Press, 337 ~ 339 (1970).
26. E. Hirota, K. Hirota and K. Kugimiya, Proc. Int. Conf. Ferrites 3, edit. H. Watanabe, S. Iida and M. Sugimoto, Center for Academic Publication, Jpn. 667 ~ 674 (1980).
27. E. Hirota and K. Kugimiya, National Tech. Rept. (Jpn.) 22, 6, 753 ~ 773 (1976).
28. E. Hirota and S. Hayakawa, Electro-Ceramics (Jpn.) Summer 34 (1977).
29. E. Hirota, Oyo Buturi (Jpn.) 39, 4, 342 (1970).
30. F. Kobayashi, J. Inst. Telev. Eng. Jpn, 32, 882 (1970).
31. K. Kugimiya, E. Hirota and Y. Bando, IEEE Trans. Mag. MAG-10, 907 ~ 909 (1974).
32. E. Hirota, K. Kugimiya and T. Nishio, J. Jpn. Soc. of Powder and Powder Metallurgy, 26, 4, 123 ~ 130 (1979).
33. K. Kugimiya and E. Hirota, U.S. Patent 3,931,642.
34. K. Kugimiya and K. Hirota, Proc. of Spring Conf. of Jpn. Soc. of Powder and Powder Metallurgy, 2-20 (1980).
35. E. Hirota, K. Hirota and M. Satomi, J. Jpn. Soc. of Powder and Powder Metallurgy, 25, 307 ~ 310 (1987).
36. K. Hirota and E. Hirota, Bull. of Ceram. Soc. of Jpn., 18, 3, 190 ~ 197 (1983).
37. T. Takada, K. Iwase and Y. Bando, Jpn. Patent S48-42008, 49-81415.
38. T. Nishikawa and Kodama, Proc. Conf. of Ceram. Soc. of Jpn., S-52 147 (1977).

39. Y. Wang and P. Liu, Proc. Int. Conf. Ferrites 3, edit. H. Watanabe, S. Iida, and M. Sugimoto, Center for Academic Publication, Jpn., 55 ~ 58 (1980).
40. S. Nobuoka, Rept. of the Government Ind. Res. Institute, Osaka, 331, 23 ~ 32 (1969).
41. K. Tahara, N. Yamamoto, Y. Bando, M. Kiyama and T. Takada, Proc. of Spring Conf. of Jpn. Soc. of Powder and Powder Metallurgy, 2-12 (1968).
42. K. Tahara, N. Yamamoto, Y. Bando, M. Kiyama and T. Takada, Proc. of Autumn Conf. of Jpn. Soc. of Powder and Powder Metallurgy, 2-10 (1971).
43. K. Hirota and K. Kugimiya, *ibid.*, Spring 2-6 (1977).
44. M. Kanbayashi, K. Nakata and M. Makino, Bull. Jpn. Soc. of Prec. Eng. 16, 1, 37 ~ 42 (Mar. 1982).
45. Y. Namba and H. Tsuwa, Annals of CIRP 27/1, 511 ~ 516 (1978).
46. Y. Namba and H. Tsuwa, *ibid.*, 28/1, 425 ~ 429 (1979).
47. E. G. Visser, Philips Technical Library (1983).
48. T. Yonezawa, K. Yokoyama and N. Ito, Prec. Eng. Yamanashi 116 (1978), National Tech. Rept. (Jpn.) 25, 6 ~ 17 (1979).
49. K. Hirota and O. Inoue, Ceram. Bull. 66, 12, 1755 ~ 1758 (1987).
50. K. Hirota, Y. Fujimoto, K. Watanabe and M. Sugimura, Advances in Ceramics edit. F. F. Wang, State Univ. of New York, New York, 15, 385 ~ 392 (1985)

51. Y. Shichijo and E. Takama, Proc. Int. Conf. Ferrites 2 edit. Y. Hoshida, S. Iida and M. Sugimoto, Univ. of Tokyo Press, 210 ~ 213 (1970).
52. K. H. Hardtl, Ceram. Bull. 54, 201 ~ 207 (1975).
53. E. Takama and M. Ito, IEEE Trans. Mag. MAG-15, 6, 1858 ~ 1860 (1979).
54. T. Takada and M. Kiyama, Proc. Int. Conf. Ferrites 2 edit. Y. Hoshida, S. Iida, and M. Sugimoto, Univ. of Tokyo Press, 69 ~ 71 (1970).
55. T. Takada, Proc. Int. Conf. Ferrites 3, edit. H. Watanabe, S. Iida and M. Sugimoto, Center for Academic Publication, Jpn., 3 ~ 6 (1980).
56. H. Robbins, *ibid.*, 7 ~ 10 (1980).
57. T. Akashi, I. Sugano, T. Okauda, and T. Tsuji, NEC Res. and Dev. (Jpn.), 19, 89 ~ 93 (1970).
58. K. Kugimiya and E. Hirota, IEEE Trans. Mag. MAG-13, 5, 1472 ~ 1474 (1977).

## Chapter II. Mn-Zn ferrites with a cube-texture

### Abstract

A study was carried out to fabricate a Mn-Zn hot pressed ferrite with a cube-texture in order to make use of an anisotropy (especially mechanical anisotropy like "wear resistance against the running magnetic tapes") and to utilize the productivity of the sintered polycrystals.

To fabricate a cube-texture ferrite, a) preparation of raw materials, b) compacting process, and c) sintering process were studied. Large thin strip shape  $\alpha$ -FeOOH was newly synthesized, which consists of two processes i.e., synthesis of a seed crystal and hydrothermal treatment of the seed crystal. As far as compacting process is concerned, the combination of extrusion of a green sheet and rolling of the extruded sheet was adopted. By double hot pressing (1200 °C 2 hr and 1350 °C 2hr, 30 MPa) on calcined compact, a Mn-Zn ferrite with high orientation magnitude such as  $Q(110) \geq 95\%$  and  $Q(111) \geq 90\%$  was developed. The Mn-Zn ferrite with a cube-texture had intermediate magnetic properties between that of a conventional polycrystal and a single crystal. It also showed nearly the same wear resistance as a single crystal under the same measuring conditions.



## I. Introduction

Extensive surveys have been continued to give anisotropic properties of magnetism to sintered ferrites.

Magnetoplumbite type hexagonal ferrite,  $MFe_{12}O_{19}$  ( $M=Ba, Sr, Pb$ ), is characterized by its anisotropy whose easy axis is parallel to  $\langle 0001 \rangle$  direction (c-axis). If the dominant proportion of grain is oriented to this direction on sintering, the product shows strong anisotropy. This is known as "grain-oriented hard magnet"<sup>1)2)</sup>. This anisotropic ferrite magnet is produced by the following process; (1) fine ferrite particles are placed in magnetic field to align their c-axis parallel, (2) pressed into compacts and, (3) sintered.

"Soft magnetic ferrite" has been invented by using another hexagonal ferrite,  $Ba_3Co_2Fe_{24}O_{41}$  ( $Co_2$ -Z type)<sup>3)</sup>. This substance possesses easy plane of magnetization parallel to c-plane and shows high permeability at high frequency. The fabrication of the substance consists of two stages of processing; (1) compaction of starting material (mixed powder of  $2BaFe_{12}O_{19}$ ,  $3BaO$  and  $1CoO$ ) in magnetic field and (2) topotactic reaction on sintering.

Subsequent development has made it possible to produce "soft magnetic ferrite" using cubic spinel ferrites such as  $MnFe_2O_4$ ,  $CoFe_2O_4$ , or  $MgFe_2O_4$ <sup>4)</sup>.

It is found that the mixture of  $\alpha$ -FeOOH and one of the following components,  $\gamma$ -MnOOH,  $Co(OH)_2$  or  $Mg(OH)_2$ , the shapes of which are platy or strip-like, is useful starting material to make the produced ferrite anisotropic.

When the mixed powders are uniaxially compressed, their crystal orientations align along almost perpendicular to (111) plane or  $\langle 111 \rangle$  axis. A topotactic reaction takes place by the following heat treatment and the product possesses the preferred orientation.

"Soft magnetic ferrites" have been noticed to be suitable for the magnetic recording head. High performance, however, is required for this usage and Mn-Zn ferrite has been developed since it shows superior properties in high magnetic flux density, high permeability and high mechanical strength for precise machining and wear resistance.

In hot pressed Mn-Zn ferrite, the preferred orientation of  $\langle 111 \rangle$  axis  $\geq 90\%$  and also the porosity  $\leq 0.01\%$  has been succeeded<sup>5)</sup> and mainly used as a video recording magnetic head. They are manufactured by the process shown in Fig. 1; (1)  $\alpha\text{-Fe}_2\text{O}_3$  of thin hexagonal plate,<sup>6)</sup>  $\gamma\text{-MnOOH}$  of thin strip and reagent grade ZnO are mixed to the expected ratio of composition in wet process, (2) the mixed slary is compressed uniaxially in a die, (3) the obtained green compact is hot pressed with the same direction, among these three oxides it takes place to produce the spinel ferrite grains arranged to (111) plane.<sup>7)</sup>

In addition to the uniaxial anisotropy mentioned above, ferrites with cube-texture having a two-dimensional anisotropy, have been investigated.<sup>8)</sup>

Ni-ferrite, which is prepared from the mixed powder of thin strip shape  $\alpha$ -FeOOH and reagent grade NiO, possesses about 60 % orientation of (110) and 40 % of (111) planes, respectively.

The author and his colleagues have extended the idea to the fabrication of hot pressed Mn-Zn ferrite with the cube-texture, since this substance is expected to behave highly anisotropic comparable to a single crystal and also to remain the high productivity of polycrystals.<sup>9)10)</sup>

In this fabrication, the preferred orientation is performed by the compression of starting powders with shape anisotropy and by the subsequent topotactic reaction on sintering. Therefore, three steps of preparation of starting material, its compaction<sup>11)</sup> and sintering are important to complete the synthesis.

As the starting powders, both  $\alpha$ -FeOOH and  $\gamma$ -MnOOH of thin strip shape are adopted as shown in Fig. 1. Figure 2 shows the topotaxy of these hydroxides at the time of spinel ferrite formation in the correlation of platy  $\alpha$ -Fe<sub>2</sub>O<sub>3</sub> which was an intermediate product on the reaction. The plane of strips of these powders turn to (111) and the longitudinal axes change into  $\langle 110 \rangle$  of spinel structure. The finally obtained polycrystals array their axes parallel to  $\langle 111 \rangle$  and  $\langle 110 \rangle$  directions.

This chapter will describe fabrication processes, magnetic and mechanical properties of Mn-Zn ferrite with a cube-texture.

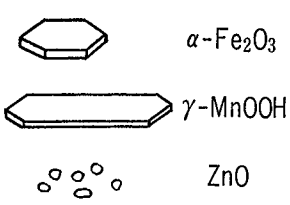
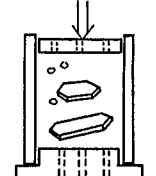
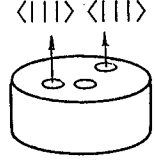
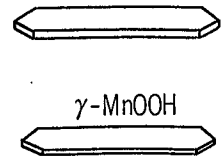
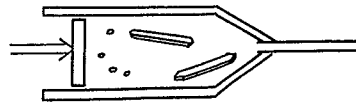
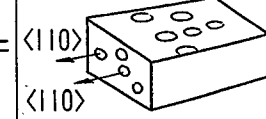
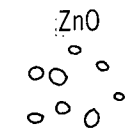
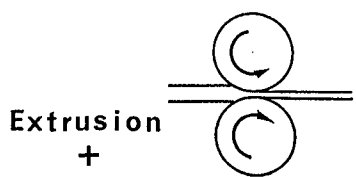
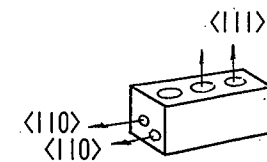
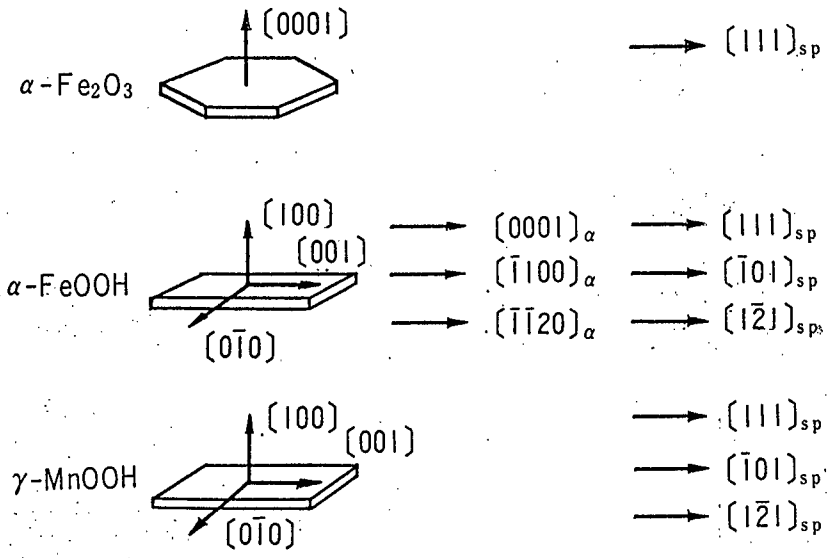
	Orient. axes	Starting powder	Forming methodes	Sintered bodies
One axis orientation	$\langle 111 \rangle$	 $\alpha\text{-Fe}_2\text{O}_3$ $\gamma\text{-MnOOH}$ $\text{ZnO}$	 <b>Wet uniaxial pressing</b>	 $\langle 111 \rangle \langle 111 \rangle$
	$\langle 110 \rangle$	 $\alpha\text{-FeOOH}$ $\gamma\text{-MnOOH}$	 <b>Extrusion</b>	 $\langle 110 \rangle$ $\langle 110 \rangle$
Two axes orientation	$\langle 110 \rangle$ $\langle 111 \rangle$	 $\text{ZnO}$	 <b>Extrusion + Rolling</b>	 $\langle 111 \rangle$ $\langle 110 \rangle$ $\langle 110 \rangle$

Fig. 1. The sketch of fabrication process for the uniaxial grain oriented Mn-Zn ferrites and a Mn-Zn ferrite with a cube-texture.



**Crystal axes of  
starting powders**

**Crystal axes of  
powders changed  
into spinel phase**

Fig. 2 Topotactic reaction of  $\alpha\text{-Fe}_2\text{O}_3$ ,  $\alpha\text{-FeOOH}$ , and  $\gamma\text{-MnOOH}$  in spinel ferrite formation.

## 2. Experimental procedure

### 2.1 Preparation of $\alpha$ -FeOOH and $\gamma$ -MnOOH

$\alpha$ -FeOOH powder was synthesized as follows; NaOH was added to  $\text{FeSO}_4$  solution and mixed in a 4 liter beaker and then  $\text{Fe}(\text{OH})_2$  was precipitated at  $40^\circ\sim 45^\circ\text{C}$ , and  $\text{pH} \geq 14$ . After that, by air flow oxidation ( $\sim 1$  l/min) for 80 ~ 260 hr,  $\text{Fe}(\text{OH})_2$  was oxidized into  $\alpha$ -FeOOH. The conditions of preparation are listed in Table 1. As the products obtained above procedure were not large enough as a starting powder, the  $\alpha$ -FeOOH is used as "seed crystal" powder. Aging of  $\alpha$ -FeOOH was carried out in the  $\text{FeSO}_4$  solution with iron ingots at  $60\sim 80^\circ\text{C}$  for 24 ~ 150 hr. The obtained  $\alpha$ -FeOOH was hydrothermally treated in 1 ~ 10 mol/l NaOH solution at  $150^\circ\sim 200^\circ\text{C}$  for 6 ~ 8 hr in a 200cc Morey-type reactor ("Autoclave" vessel) with a filling up ratio about 60 %. The pressure at hydrothermal treatment was estimated about 5 ~ 10 MPa.

$\gamma$ -MnOOH was synthesized by adding  $\text{NH}_4\text{OH}$  into  $\text{MnSO}_4$  solution to precipitate  $\text{Mn}(\text{OH})_2$ , aging it in titrating hydrogen peroxide  $\text{H}_2\text{O}_2$  and blowing oxygen into the solution.<sup>14)</sup>

### 2.2 Mixing

$\alpha$ -FeOOH,  $\gamma$ -MnOOH and reagent grade ZnO were mixed to the desired compositional ratio of 53 mol%  $\text{Fe}_2\text{O}_3$ , 28 mol% MnO and 19 mol% ZnO with a binder system.

Sample No.	FeSO <sub>4</sub> ·7H <sub>2</sub> O (mol/l)	NaOH (mol/l)	Time (hr)	Product		
				length,	width (μm)	
1S	0.072	0.43	90	0.3~0.5	0.05	branches
2S	0.072	1.5	90	0.5	0.07	
3S	0.072	3.5	90	0.5	0.05~0.1	
4S	0.072	7.0	260	0.5~2.5	0.05~0.1	
5S	0.10	7.0	240	0.5~1.5	0.03	
6S	0.15	7.0	165	0.5~1.5	0.03	
7S	0.25	1.5	90	0.5	0.07	branches
8S	0.25	7.0	125	0.8~1.8	0.05	
9S	0.30	1.5	160	0.5~0.8	0.03~0.15	branches
10S	0.30	7.0	80	0.7~1.3	0.05	
11S	0.35	2.1	160	0.6~0.8	0.03~0.1	branches
12S	0.35	7.0	260	0.5~2.5	0.05	abnormal compound

Table 1 Synthesis conditions of α-FeOOH and the properties of products in this study.

The mixing ratio of powder to binder was about 60/40 wt%.

The binder system consisted of methylcellulose ( $C_6H_{10}O_5$ ), glycerine ( $C_3H_8O_3$ ) and  $H_2O$ .

### 2.3 Compacting

A mixture was extruded into a sheet with 2 ~ 3 mm thick at the extrusion velocity of 1 ~ 18 cm/sec by applying pressure on the mixture in the die, which was designed for the extrusion process. Then the extruded sheet was rolled under the rotating velocity 1.5 ~ 5 cm/sec with pressure about 150 ~ 200 MPa by twin stainless steel rolls of 20 cm in diameter. The rolled sheet was laminated into the compacts.

### 2.4 Sintering

After the binder was taken out (800°C 2 hr in air), the compacts were calcined in  $N_2$  at 1100°~ 1300°C to get  $\alpha-Fe_2O_3$  precipitates in the body reduced.

The calcined body was put into the SiC die with  $Al_2O_3$  powder as a pressing media and hot pressed. The hot press sintering, whose pressing direction was perpendicular to the sheet planes, was undertaken at 1100°~1350°C and 30 MPa for 2 hr in air.

### 2.5 Evaluation



The sintered bodies were cut into pieces approximately 15 by 15 by 0.5 mm, which were used to measure the grain orientation. The orientation  $Q(HKL)$  [denotes  $Q(110)$ ,  $Q(111)$ ] was calculated from the following equations.

$$Q(HKL) = [\sum I'(HKL) / \sum I(hkl) - \sum I^{\circ}(HKL) / \sum I^{\circ}(hkl)] / [1 - \sum I^{\circ}(HKL) / \sum I^{\circ}(hkl)]$$

$\sum I'(HKL)$  = summation of only  $I(HKL)$ ,  $I(2H2K2L)$  and  $I(3H3K3L)$

$\sum I(hkl)$  = summation of all  $I(hkl)$

Here,  $I(hkl)$ s denote intensities of X-ray diffraction of  $(hkl)$  planes which were measured from the rotating samples, and  $\sum I(hkl)$  means the summation of  $I(hkl)$  for all  $(hkl)$  planes concerned about a cube-texture ferrites and  $\sum I^{\circ}(hkl)$  about Mn-Zn ferrite powder.

A microscope, a scanning electron microscope (SEM), and a transmission electron microscope (TEM) were used for the observations.

The average grain size,  $G_s$ , was measured from the photographs taken of a lapped and etched surface of ferrites. The electron diffraction analysis also was done to identify the crystal structure of starting powders.

Thermal gravimetry analysis (TGA) was used to identify powders under heat treatment.

Then,  $8\Phi-4\Phi-3t$  and  $8\Phi-4\Phi-0.5t$  mm ferrite troids were used to measure the properties of B/H curves by a B/H curve-tracer and permeability  $\mu$  by a vector-impedancemeter, respectively.

Wear resistance against the running tape was measured by using  $\text{CrO}_2$  tape at the relative speed of 5.8 m/sec between the test piece and running tape at room temperature and relative humidity Rh 50 ~ 60 %.

### 3. Results and discussion

#### 3.1 $\alpha$ -FeOOH

$\alpha$ -FeOOH powder is about 0.2 ~ 0.5  $\mu\text{m}$  long, which is commercially sold as the starting powder for hard magnetic  $\gamma$ - $\text{Fe}_2\text{O}_3$  of recording media.

From the study of grain oriented Mn-Zn ferrite, it is cleared that the starting powder of  $\alpha$ -FeOOH for a cube-texture ferrite should have a length of several  $\mu\text{m}$  and the ratio of length/width be about 5/1 ~ 10/1 in order to array its direction during compacting process.

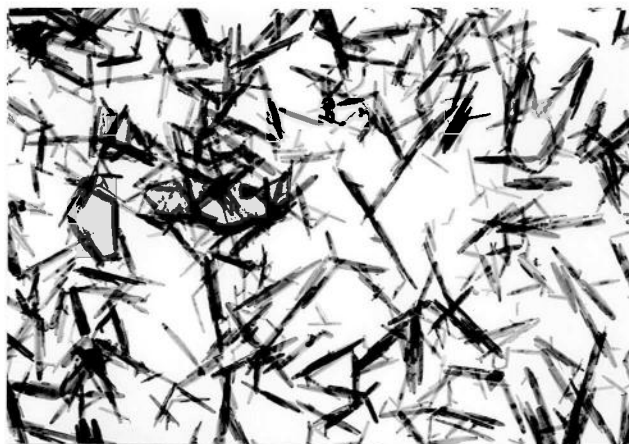
##### a) a seed crystal

The conditions of the synthesis and their products of this study are listed in Table 1. TEM photographs of each product synthesized under various conditions are presented in Figs. 3 and 4.

From Table 1 and Fig. 3, it is seen that when the low ratio of  $\text{NaOH}/\text{FeSO}_4$  and high concentration of  $\text{FeSO}_4$  are used,  $\alpha$ -FeOOH particles have branches and consist of a mixture of large and fine grains.

NaOH (mol/l)

0.43



1.5



3.5



7.0



1  $\mu\text{m}$

Fig. 3 Powder shape of  $\alpha$ -FeOOH seed crystal versus NaOH solution concentration varied from 0.43, 1.5, 3.5 to 7.0 mol/l under the constant concentration of  $\text{FeSO}_4 \cdot 7\text{H}_2\text{O}$  of 0.072 mol/l (Runs No. 1S ~ 4S of Table 1).

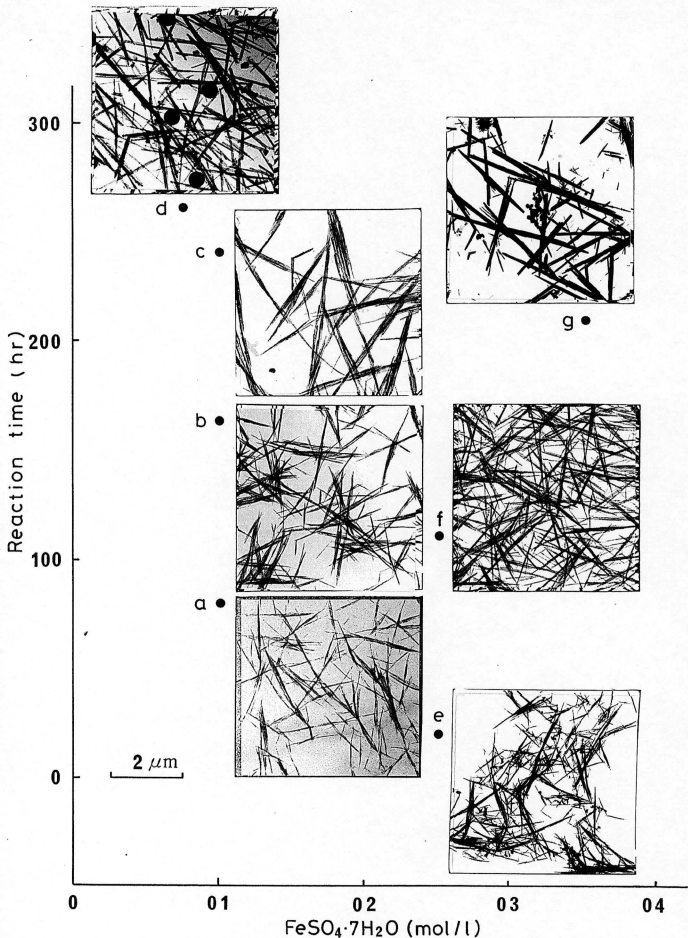


Fig. 4 Powder shape and product of  $\alpha$ -FeOOH seed crystal versus the concentration of  $\text{FeSO}_4 \cdot 7\text{H}_2\text{O}$  and reaction time under the constant NaOH solution as 7 mol/l at  $40^\circ \sim 45^\circ \text{C}$ . In Fig. 4-d,  $\alpha$ -FeOOH particles with standard spheres of  $0.5 \mu\text{m}$  in diameter were shown as a comparison.

These products are not suitable for the starting materials because they are not homogeneous powder.

Long chemical reaction (> 80 hr), and the use of combination of dil  $\text{FeSO}_4 \cdot 7\text{H}_2\text{O}$  solution (0.25 ~ 0.3 mol/l) and conc NaOH solution (7 mol/l), bring a good result and a needle like  $\alpha\text{-FeOOH}$  with the dimension of 0.5 ~ 2.5  $\mu\text{m}$  long and about 0.05  $\mu\text{m}$  wide (Fig. 4-f) is synthesized.

#### b) aging

The needle like  $\alpha\text{-FeOOH}$  particles grow up to 0.3 ~ 0.4  $\mu\text{m}$  in width but not the length by aging as shown in Fig. 5. The relations between aging duration and the change of shape are shown in the TEM photographs of Fig. 6.

#### c) hydrothermal treatment

Hydrothermal treatment was tried for ripening of  $\alpha\text{-FeOOH}$  seed crystals. The conditions and the kinds of products of hydrothermal treatment are listed in Table 2.

When  $\alpha\text{-FeOOH}$  is soaked in NaOH solution under hydrothermal condition, needle-like seed crystals grow up in their width and homogenize their shapes by dissolution of fine particles into NaOH solution and reprecipitation to large crystals.

From the results shown in Table 2, it is cleared that soaking in NaOH with high concentration > 5 mol/l produces  $\alpha\text{-Fe}_2\text{O}_3$ .

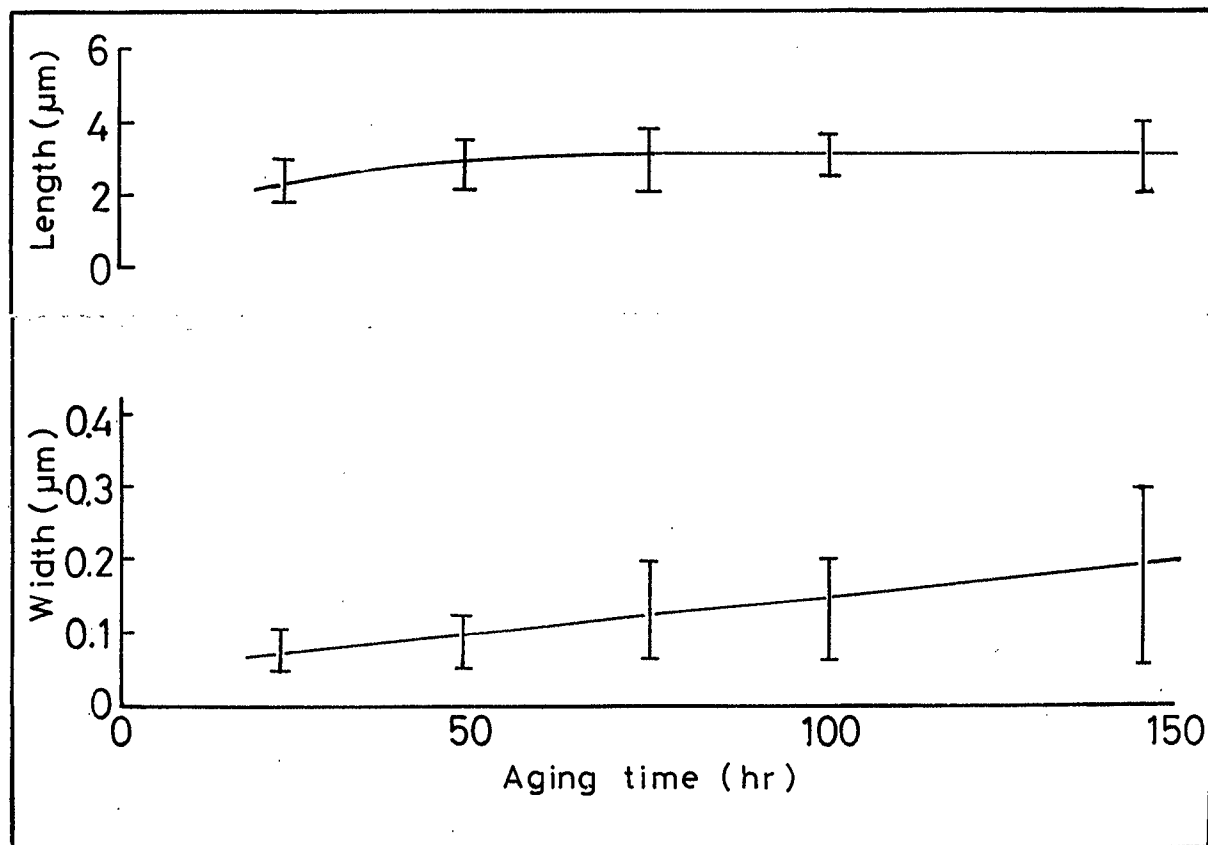
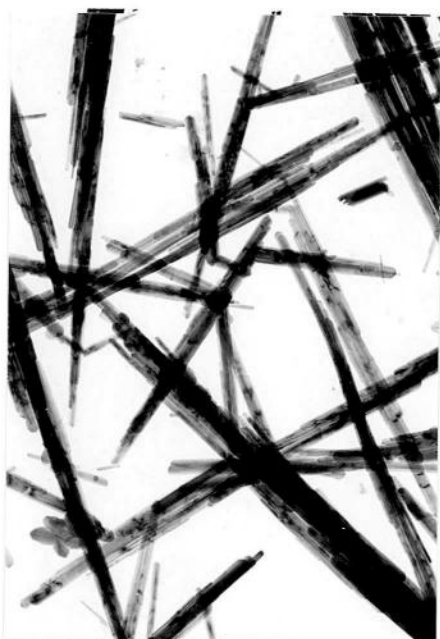


Fig. 5 Powder shape change with aging time for  $\alpha$ -FeOOH. Seed crystal is the sample of No. 8S of Table 1 and that of Fig. 4-f.



24 hr



48 hr



78 hr



145 hr

1  $\mu$ m

Fig. 6 TEM photographs of  $\alpha$ -FeOOH after 24, 48, 78 and 145 hr aging. Starting seed crystal is  $\alpha$ -FeOOH of Sample No.8S of Table 1 and of Fig. 4-f.

Sample NO.	NaOH (mol/l)	Temp. (°C)	Time (hr)	Starting $\alpha$ -FeOOH*	Product length( $\mu$ m), width( $\mu$ m), crystal structure
Au1	1	160	6	8S	1.0~2.5      0.05 $\alpha$ -FeOOH
Au2	1	200	8	8S	1.5~2.5      0.1~0.2 $\alpha$ -FeOOH
Au3	1	200	8	8S-90hr aged	$\alpha$ -Fe <sub>2</sub> O <sub>3</sub>
Au4	1	200	8	Y-LOP** (commercial product)	0.3~0.6      0.05~0.1 $\alpha$ -FeOOH branches, twin
Au5	5	200	8	8S	$\alpha$ -Fe <sub>2</sub> O <sub>3</sub>
Au6	10	200	8	8S	$\alpha$ -Fe <sub>2</sub> O <sub>3</sub>

\* :Symbols correspond to samples in Table 1.

\*\*: $\alpha$ -FeOOH powder produced by Titan Kogyo Co.,Ltd.

Table 2 Hydrothermal conditions for  $\alpha$ -FeOOH.

The dimensions of products are also shown.



When an aged  $\alpha$ -FeOOH is used instead of a seed crystal as starting powder, it also turns into  $\alpha$ -Fe<sub>2</sub>O<sub>3</sub>, but small and thin  $\alpha$ -FeOOH particles with length of 0.2 ~ 0.5  $\mu$ m (commercial products) remain unchanged by hydrothermal treatment. An optimum condition of hydrothermal treatment is decided that the concentration of NaOH is 1 mol/l and reaction temperature-time is about 200 °C - 8 hr, respectively. By these conditions,  $\alpha$ -FeOOH with 1.5 ~ 2.5  $\mu$ m long and 0.1 ~ 0.2  $\mu$ m wide is synthesized.

TEM photographs of  $\alpha$ -FeOOH grown by hydrothermal treatment is shown in Fig. 7.

#### d) normal and inverse crystal axes

The electron diffraction patterns of grown-up  $\alpha$ -FeOOH show that there are two kinds of  $\alpha$ -FeOOH characterized by the alignments of crystal axes; one has  $\langle 100 \rangle$ -axis parallel to the vertical strip plane and  $\langle 0\bar{1}0 \rangle$ -axis vertical to the elongated side plane (normal  $\alpha$ -FeOOH), and the other one has axes inversely (inverse  $\alpha$ -FeOOH) as seen in Fig. 8.

When the solution temperature increases over 50 °C in a short time during the preparation of  $\alpha$ -FeOOH seed crystal, some portion of  $\alpha$ -FeOOH turns into the inverse.

On the topotactic reaction related to  $\alpha$ -FeOOH and  $\gamma$ -MnOOH, the normal  $\alpha$ -FeOOH is preferable in order to produce a cube-texture ferrite as is understood from the experimental results shown in Figs. 1 and 2.



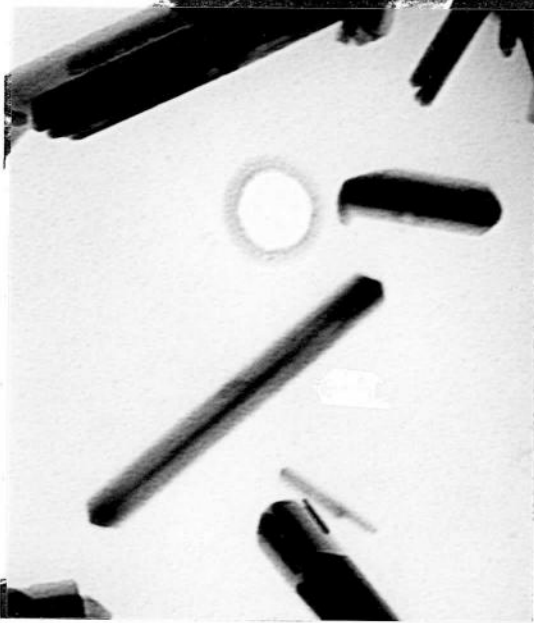
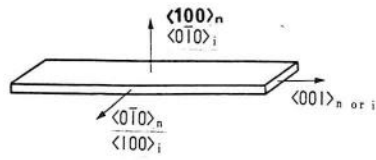
(A)

1  $\mu\text{m}$



(B)

Fig. 7 TEM photographs of  $\alpha\text{-FeOOH}$  before and after hydrothermal treatment. (A) is  $\alpha\text{-FeOOH}$  of Sample No. 8S of Table 1 and (B) is  $\alpha\text{-FeOOH}$  of Sample No. Au2 of Table 2.



6  $\mu\text{m}$

Normal



1  $\mu\text{m}$

Inverse

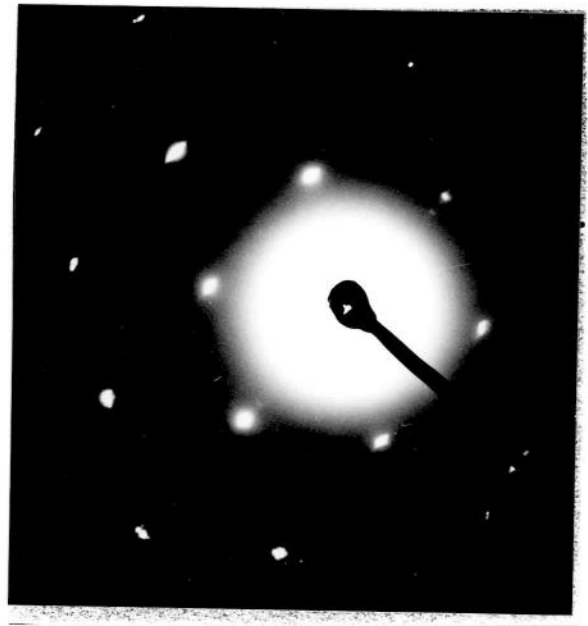


Fig. 8 Crystal growth habits of normal and inverse  $\alpha$ -FeOOH and their electron diffraction patterns.

### 3.2 $\gamma$ -MnOOH

The shape and topotaxy of synthesized acicular  $\gamma$ -MnOOH of several  $\mu\text{m}$  long is shown in Fig. 9.

### 3.3 Extrusion

SEM photographs of Fig. 10 show the arrangement of longitudinal axes of acicular powders parallel to the extruded direction (Fig. 10-a, b) and perpendicular to the extruded direction (Fig. 10-c)

From the results, it is cleared that the optimum speed of extrusion is about 10 cm/sec, because the orientation is accelerated by increasing the velocity, but the sheet becomes distorted at the speed beyond 10 cm/sec. At this suitable speed,  $Q(110)$  reaches to about 35 % and  $Q(111)$  to about 25 %, showing that an extrusion process is effective to the longitudinal axes of acicular powders parallel to the extruding direction.

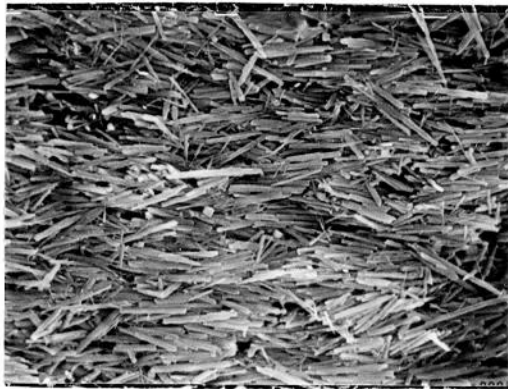
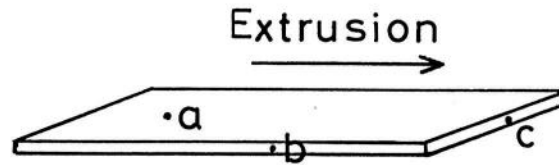
### 3.4 Rolling on sheet

As the orientation magnitude induced by extrusion was not high enough to fabricate the cube-texture ferrites, a rolling process was introduced for the extruded sheet. In the case of the  $\langle 111 \rangle$  axes of grain orientated ferrites, 60 ~ 70 % orientation of raw material powder is obtained parallel to the (111) planes in the molded compacts under 30 MPa.

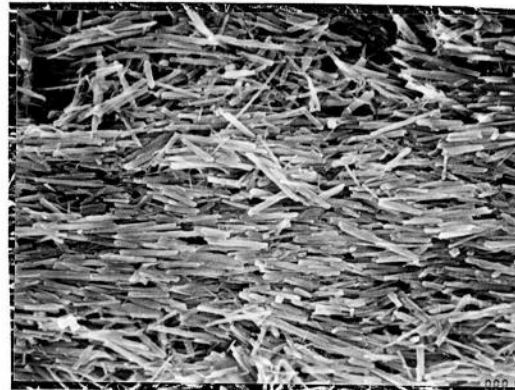


1  $\mu\text{m}$

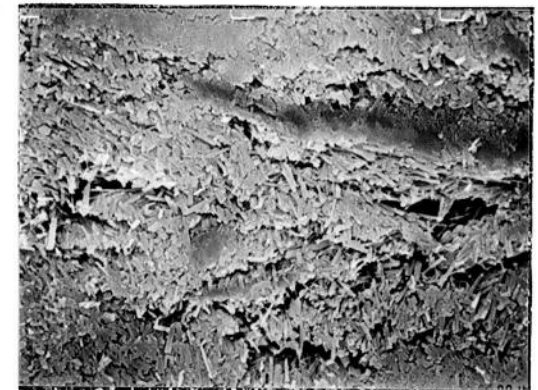
Fig. 9 Shape of  $\gamma$ -MnOOH powder used in this experiment.



(a)



(b)



(c)

5  $\mu$ m

Fig. 10 SEM photographs of powder arrangement in an extruded sheet.

The rotating velocity has a little influence on the orientation. An increase in both Q(110) and Q(111) of the rolled sheet is about 5 % at optimum condition of 5 cm/sec of the rotating velocity. The relationship between the increase of both Q(110) and Q(111) and rolling ratio  $(d_1 - d_0)/d_0 \times 100$  [ $d_0, d_1$ : thickness of sheet before and after rolling, respectively] is plotted in Fig. 11. From Fig. 11, it is seen that not only the orientation of Q(111) due to the transverse particle orientation induced by pressing, but also the longitudinal orientation of Q(110) were increased by rolling. This increase in Q(110) is the result of the longitudinal orientation of the acicular powders due to the elongation of sheet by the rolling.

### 3.5 Change of the powder during heat treatment

To investigate the derangement of arranged powders, TGA and an SEM observation of the powders and their arrangement before and after heat treatment were carried out. TGA curves for  $\alpha$ -FeOOH,  $\gamma$ -MnOOH and a mixture of these hydroxides with methylcellulose are shown in Fig. 12. The mixture was dehydrated at 250°~ 300°C and turned into Mn-ferrite at about 1000°C. There was no change of powder arrangement in the sheet before and after heat treatment of 1300°C in air, which was confirmed by an SEM observation. From this, derangement of powder arrangement was thought not to occur during increasing temperature with dehydration or burning of binder system.

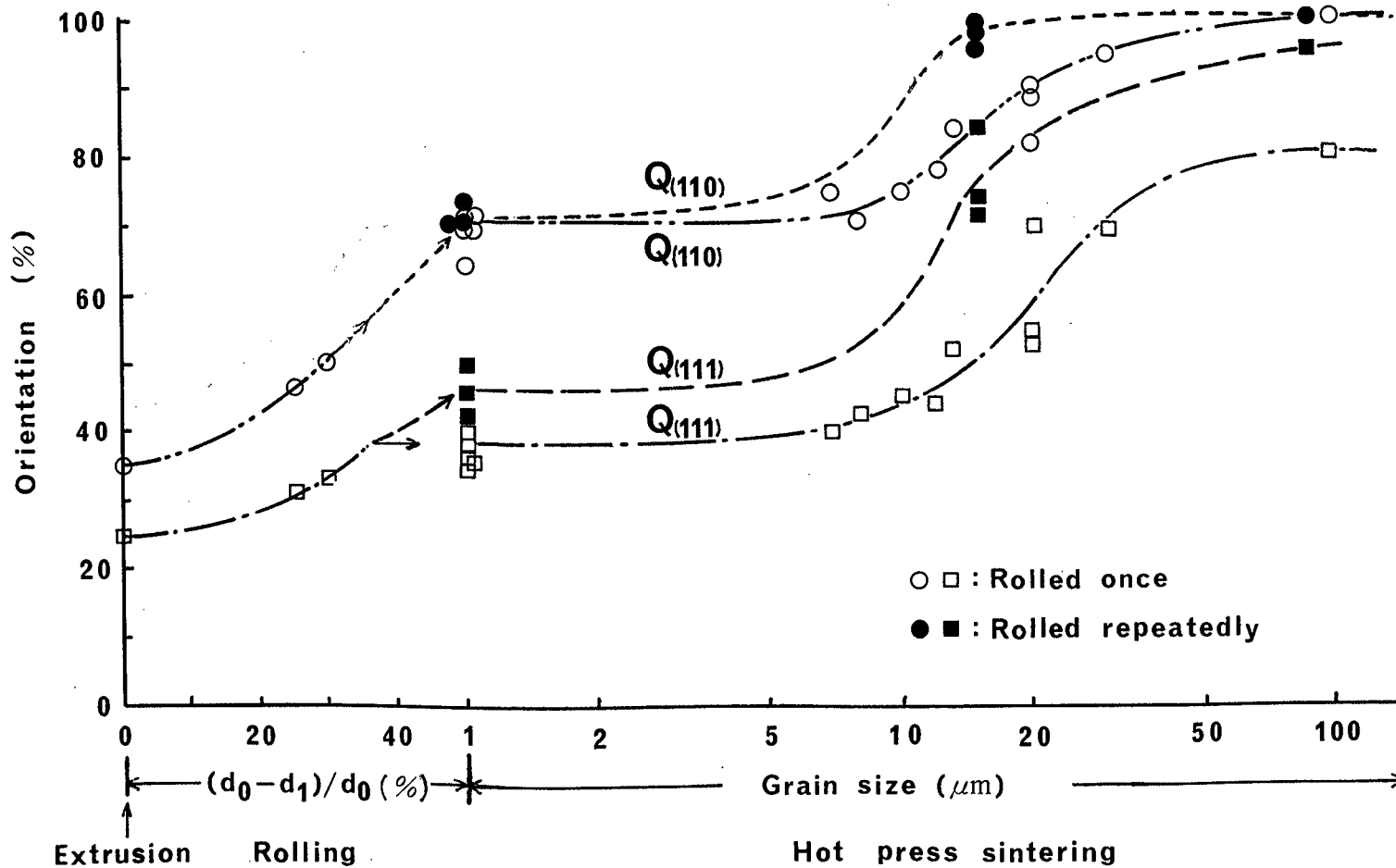


Fig. 11 The relationship between orientation and the process factors, the grain size of the hot pressed Mn-Zn ferrite with a cube-texture.



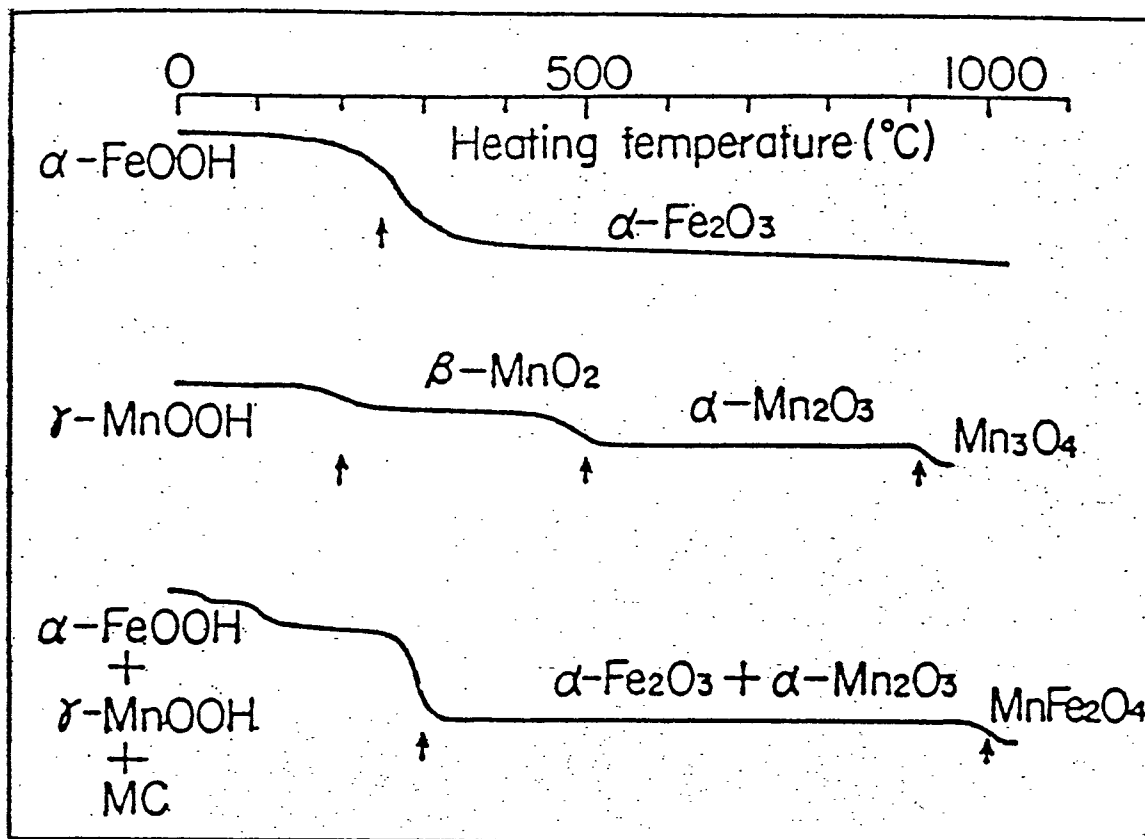


Fig. 12 TGA curves for  $\alpha$ -FeOOH,  $\gamma$ -MnOOH and a mixture of these hydroxides with methylcellulose. Heat-up rate is 300°C/h in air.

### 3.6 Sintering

The orientation and the grain size of sintered body have close correlation, i.e., when the grain size becomes large, the orientation gets high values, as the same as studied before about  $\langle 111 \rangle$  axes of grain oriented ferrites.<sup>5)</sup> This result and the contribution of each fabrication process to the orientation are summarized and shown in Fig. 11.

The dependence of the hot press sintering pattern on the orientation and densification of the sintered body was studied. Improvement for obtaining both high orientation and dense sintered body was done by a double hot pressing i.e., first pressing at 1200°C and second 1350°C for 2 hr at 30 MPa. The first pressing densifies the sintered body at the temperature that grain growth does not occur after ferrite formation ( $G_s < 10 \mu\text{m}$ ). The second pressing at higher temperature induces grain growth to 100  $\mu\text{m}$ . The second hot compression increases the orientation by inducing dominant grain growth to the pressing direction.

The representative X-ray diffraction patterns of both a cube-texture ferrite and an  $\langle 111 \rangle$  axes of grain oriented ferrite are shown in Fig. 13. The former has both  $Q(110) \geq 95\%$  and  $Q(111) \geq 90\%$ , and the latter does  $Q(111) \geq 95\%$ , respectively. The  $G_s$  of these are about 100  $\mu\text{m}$ .

### 3.7 Magnetic properties and wear resistance

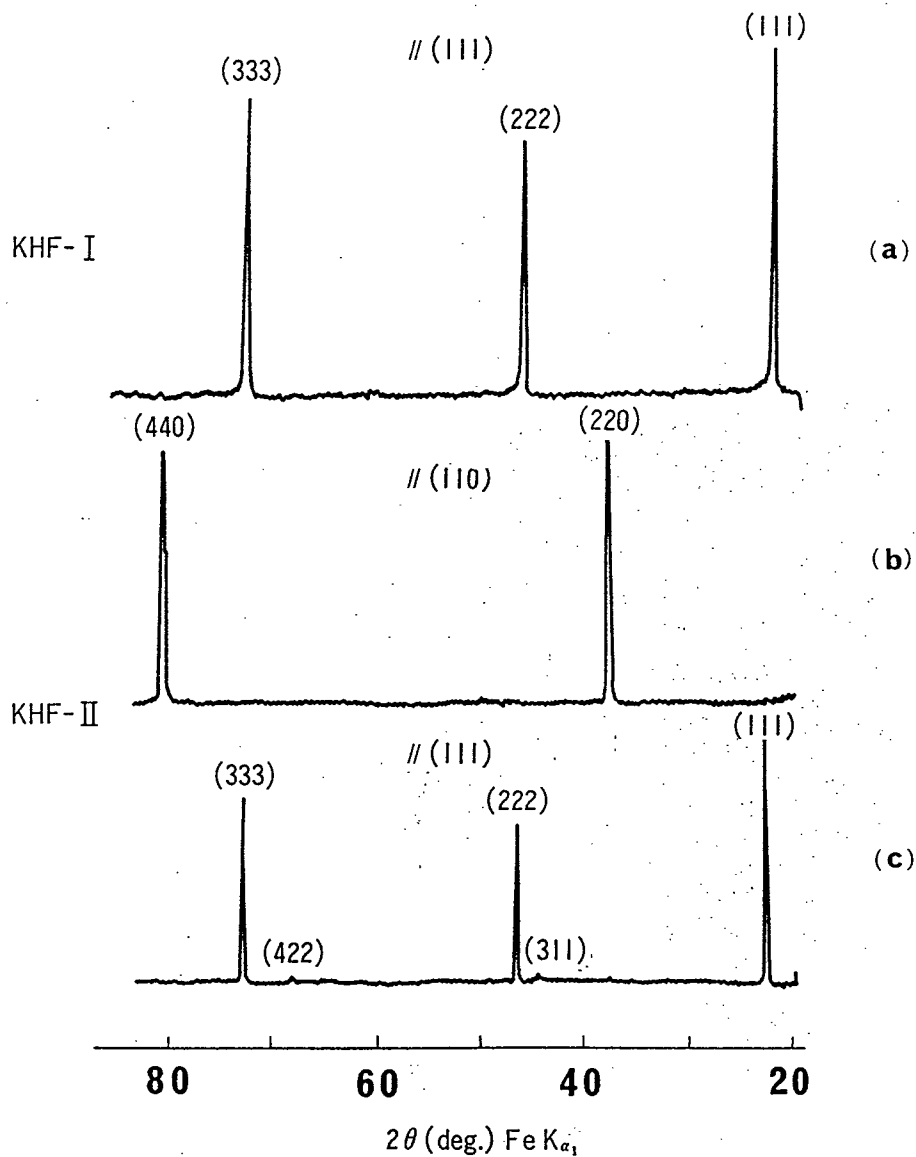


Fig. 13 Representative X-ray diffraction patterns of  $\langle 111 \rangle$  axes of grain oriented Mn-Zn ferrite (KHF-I), and Mn-Zn ferrite with a cube-texture (KHF-II): (a) and (c) show diffractions from the samples parallel to (111) plane of KHF-I and KHF-II, respectively, (b) shows diffraction from the sample parallel to (110) plane of KHF-II.

The magnetic properties of Mn-Zn ferrite polycrystals with a cube-texture, a normal (randomly oriented grain) texture, and a single crystal ferrite are listed in Table 3. Their composition is nearly the same (53 mol%  $\text{Fe}_2\text{O}_3$ , 28 mol% MnO, and 19 mol% ZnO). As the magnetocrystalline anisotropy constant  $K_1$  is negative value<sup>20)</sup> for this composition, an easy magnetic axis is  $\langle 111 \rangle$ , which is perpendicular to an  $\langle 110 \rangle$  axis. The measurement of a cube-texture and a single crystal ferrites were done along  $\langle 110 \rangle$  axis of the ferrite perpendicular to the plane of toroid. Therefore, the toroidal samples have an easy magnetic axis parallel to the plane.

The result on a cube-texture ferrite shows that its property is intermediate between that of a polycrystal and a single crystal.

Although the structure of a Mn-Zn ferrite is cubic, the substance has the magnetic and mechanical anisotropy, suggesting the anisotropic wear of the head composed of single crystal. Figure 14 shows the curves representing the head wear made of single crystal and grain oriented ferrites. The magnitude of wear depends on the tape-touching surface and the tape-running direction defined with the combination of the principal planes (hkl) and axes  $\langle uvw \rangle$ . It is noted that the head made of a cube-texture ferrite shows nearly the same wear as that of the single crystal with  $(110)\langle 111 \rangle$ , and that there is little difference in wear resistance between a single crystal and a polycrystal if the grains of polycrystal are oriented.

Magnetic properties	polycrystal ferrite	ferrite with a cube-texture	single crystal ferrite
magnetic flux density B (T)	0.45	0.45	0.45
coercive force Hc (A/m)	6.36	7.96	3.98
Curie Temp. Tc (°C)	150	150	150
permeability			
0.1 MHz	2750	2400	3000
0.5 MHz	2200	2000	2000
1.0 MHz	1650	1550	1500
5.0 MHz	540	500	300
7.0 MHz	350	320	180
10.0 MHz	220	200	100

Table 3 Magnetic properties of a Mn-Zn ferrite polycrystal with a cube-texture, a conventional polycrystal and a single crystal with the same composition.

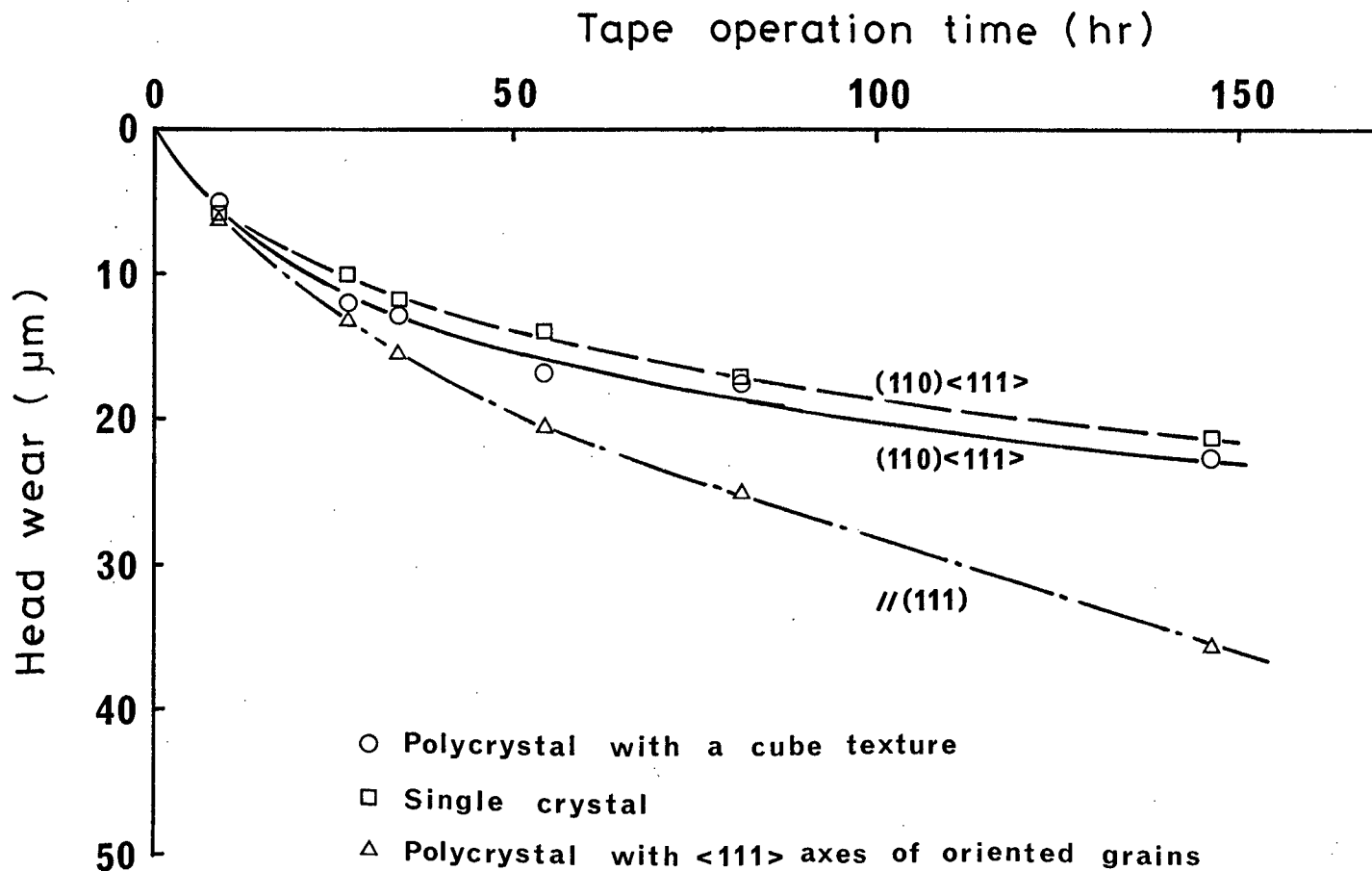


Fig.14 Anisotropic wear of magnetic heads made of a Mn-Zn ferrites;  $(hkl)\langle uvw \rangle$  denotes combination of  $\text{CrO}_2$  tape-touching surface and tape-running direction, the relative speed between the heads and the tape was 5.8 m/sec.

The magnitude of wear depends on the tape-touching direction and the tape-running direction, regardless a polycrystal or a single crystal ferrite.

#### 4. Conclusion

A study was carried out to fabricate the Mn-Zn hot press ferrite with a cube-texture in order to make use of an anisotropy (especially mechanical anisotropy like "wear resistance against the running tapes") and utilize the productivity of the sintered polycrystalline ferrites.

To fabricate the cube-texture ferrite, a) preparation of raw materials, b) compacting process, and c) sintering process were studied. Large  $\alpha$ -FeOOH powder was newly synthesized, which consisted of two process i.e., synthesis of a seed crystal under the condition that  $\text{FeSO}_4$  0.25 ~ 0.3 mol/l with NaOH 7 mol/l solution at 40°~ 45°C for more than 100 hr, and hydrothermal treatment of a seed crystal of  $\alpha$ -FeOOH under the condition that heat treatment temperature is 200°C for 8 hr in NaOH 1 mol/l solution. By these process,  $\alpha$ -FeOOH with several  $\mu\text{m}$  in length and 0.1 ~ 0.2  $\mu\text{m}$  in width was synthesized. As far as compacting process is concerned, the combination of extrusion of a green sheet and rolling on the extruded sheet was adopted. The rolling ratio and the grain size of the sintered body had strong influence on the orientation magnitude.

By a double hot pressing (1200°C-2 hr and 1350°C-2 hr 30 MPa) of the calcined compacts, a Mn-Zn ferrite with high orientation such as  $Q(110) \geq 95\%$  and  $Q(111) \geq 90\%$  was developed.

The Mn-Zn ferrite with a cube-texture had the intermediate magnetic properties between that of a polycrystal and a single crystal and showed the same wear resistance as a single crystal under the same conditions.

## 5. References

1. G. W. Rathenan, J. Smit and A. L. Stuijts, *Zeit fur Phys.*, 133, 250 (1952).
2. T. Takada, Y. Ikeda, H. Yoshinaga and Y. Bando, *Proc. Int. Conf. Ferrites*, edit. Y. Hoshino, S. Iida and M. Sugimoto, Univ. of Tokyo Press, 275 ~ 278 (1970).
3. J. Smit and H. P. J. Wijn, "Ferrites", Philips Technical Library (1959).
4. Y. Ikeda, Y. Bando and T. Takada, *Proc. of Spring Conf. of Jpn. Soc. of Powder and Powder Metallurgy*, 2-22 (1972).
5. K. Kugimiya, E. Hirota and Y. Bando, *IEEE Trans. Mag. MAG-10*, 3, 907 ~ 909 (1974).
6. S. Nobuoka, Report of the Government Ind. Res. Institute, Osaka, 331, 108 ~ 116 (1969).
7. Y. Ikeda, Y. Bando and T. Takada, *Proc. of Spring Conf. of Jpn. Soc. of Powder and Powder Metallurgy*, 2-22 (1971).
8. T. Nishikawa and Kodama, *Proc. of Conf. Ceram. Soc. of Jpn.* 147 (1977).



9. E. Hirota, K. Hirota, M. Satomi and T. Nishikawa, J. Jpn. Soc. of Powder and Powder Metallurgy, 25, 307 ~ 310 (1978).
10. K. Hirota and E. Hirota, Bull. of Ceram. Soc. of Jpn. 18, 3, 190 ~ 197 (1983).
11. K. Kugimiya and K. Hirota, Proc. of Spring Conf. of Jpn. Soc. of Powder and Powder Metallurgy, 2-20 (1980).
12. S. Nobuoka, Report of the Government Ind. Res. Institute, Osaka, 331, 23 ~ 32 (1969).
13. T. Takada and M. Kiyama, Proc. Int. Conf. Ferrites, edit. Y. Hoshino, S. Iida and M. Sugimoto, Univ. of Tokyo Press, 69 ~ 71 (1970).
14. K. Tahara, N. Yamamoto, Y. Bando, M. Kiyama and T. Takada, Proc. of Autumn Conf. of Jpn. Soc. of Powder and Powder Metallurgy, 2-12 (1968), and ibid. 2-10 (1971).
15. E. Hirota, Oyo Buturi, 42, 6, 630 ~ 634 (1973).
16. K. Hirota, M. Satomi, K. Kugimiya, E. Hirota and T. Nishikawa, Proc. of Spring Conf. of Jpn. Soc. of Powder and Powder Metallurgy, 2-26 (1979).
17. T. Asai, S. Nobuoka and K. Ando, J. Jpn. Chem. Soc. 5, 654 ~ 658 (1978).
18. K. Hirota and K. Kugimiya, Proc. of Spring Conf. of Jpn. Soc. of Powder and Powder Metallurgy, 2-6 (1977).
19. K. Kugimiya and E. Hirota, Proc. of Spring Conf. of Jpn. Soc. of Powder and Powder Metallurgy, 2-23 (1976).
20. K. Ohta, J. Phys. Soc. of Jpn. 18, 5, 685 ~ 690 (1963).

### Chapter III. Sodium doped Mn-Zn ferrites

#### Abstract

The effects of adding Na in the range of 0.001 ~ 1.0 wt% on the properties of Mn-Zn ferrites were investigated. The microstructure changed with both the concentration of Na and the sintering conditions especially the ramping rates (50 ~ 300 °C/h) and the firing temperatures (1150° ~ 1250°C).

The effects of Na doping on the microstructure were characterized by three categories; (I) 0.001 ~ 0.05, (II) 0.05 ~ 0.10, (III) 0.10 ~ 1.0 wt%. High density ( $\geq 99.9\%$  of  $d_0$ ; theoretical density) ferrites composed of fine grain of 8  $\mu\text{m}$  in average were sintered in (I), low density (98 ~ 99 % of  $d_0$ ) ferrites of large or exaggerated grains of 1000  $\mu\text{m}$  in (III). Heat-up condition strongly affected the microstructure in (II).

## 1. Introduction

The magnetic and mechanical properties of the sintered Mn-Zn ferrites depend on the microstructure as well as the composition and the sintering condition.

There have been many studies on the effects of additives on the magnetic properties of Mn-Zn ferrites, including a study on CaO-SiO<sub>2</sub> doped Mn-Zn ferrites<sup>1)</sup>, the loss of which at high frequency was diminished by high electric resistive layers at grain boundaries. Also there have been many works on the effects of additives on the microstructure of Mn-Zn ferrites. For examples, there was a study on the exaggerated grain growth by addition of TiO<sub>2</sub><sup>2)</sup>, a report on the mechanical properties of Mn-Zn ferrite doped with ZrO<sub>2</sub>-CaO-Na<sub>2</sub>O<sup>3)</sup>, whose resistivity against chipping was improved.

The influence of Na additive on the microstructure, and also on the magnetic and mechanical properties of Mn-Zn ferrites will be described in this chapter.

## 2. Experimental procedure

A coprecipitated spinel powder with a composition of 54.5 mol% Fe<sub>2</sub>O<sub>3</sub>, 27.1 mol% MnO and 18.4 mol% ZnO was used. It had impurities of 0.001 ~ 0.003 wt% CaO, SiO<sub>2</sub>, and SO<sub>4</sub>. The powder was ball-milled with water.

Then dried powder was granulated with NaOH solution which contained 0.005 to 1.0 wt% Na of the weight of dried powder and was molded into a shape of prism (~ 10 x 25 x 38 mm) by cold isostatic pressing of ~ 200 MPa.

Each molded compact was heated up to the sintering temperature in vacuum about  $1.33 \times 10^{-2}$  to  $1.33 \times 10^{-3}$  Pa ( $10^{-4}$  to  $10^{-5}$  Torr) to remove pores from the bodies and sintered in a controlled  $N_2-O_2$  atmosphere at  $1150^\circ \sim 1250^\circ C$  for 4 hr.

The shrinkage of the molded compacts were measured by a dilatometer from room temperature to  $1250^\circ C$  with the heat-up rate of  $300^\circ C/h$  in  $N_2$  flow of 150 cc/min. To check the phase in the compact during heating up process, the X-ray powder diffraction analysis was carried out to determine the amounts (wt%) of spinel phase in the samples, which were prepared by quenching after 10 min heat treatment at the desired temperature in  $N_2$  atmosphere. The wt% of spinel phase in Mn-Zn ferrites were calculated from the X-ray diffraction peak intensity ratio of  $\alpha-Fe_2O_3(104)/spinel(311)$  peak of 0.001, 0.01, 0.1 and 1.0 wt% Na added ferrites. X-ray analysis was also used to measure the accurate values of lattice parameter of the products. Silicon powder was used as an internal standard in this case.

The densities of the sintered bodies were obtained by the Archimedes' method. The microstructures were observed by a scanning electron microscope (SEM).

After the sintered bodies with the dimension of ~ 8 x 20 x 30 mm were cut into bars of approximately 3 x 3 x 6 mm, four of their surface planes were mirror lapped with SiC and diamond abrasives, under a pressure of 490 Pa ( 5 g/cm<sup>2</sup> ).

The average grain size (Gs) was measured from microphotographs of the lapped and etched surfaces.<sup>4)</sup>

Fracture toughness, K<sub>IC</sub>, was measured using an indentation method similar to that described elsewhere<sup>5)</sup>.

The indentation condition was 2.94 N (300 g) and 10 sec.

K<sub>IC</sub> was calculated from the equation of

$$K_{IC} = 0.203 H_v a^{-1/2} (c/a)^{-3/2} \quad (3-1)$$

where 'c' is crack length, 'a' indentation-impression radius, and 'H<sub>v</sub>' hardness. The modulus of rupture was measured in three-point bend test with a span of 30 mm and a crosshead speed of 0.5 mm/min, using ten ferrite bars approximately 3 x 4 x 40 mm with surface roughness R<sub>max</sub> ≤ 0.5 μm.

The dc resistivity, ρ, at room temperature, was measured by the two contact method, using Indium-Amalgam contact. The B/H curve and permeability of ferrites were measured as the same method described in Chapter II.

### 3. Results

#### 3.1 Sintering process

The effect of Na amount on the shrinkage of the compact bodies is shown in Fig. 1. The shrinkage,  $-\Delta l/l_0 = (l-l_0)/l_0$  [ $l_0$ : initial length of compact body,  $l$ : length at  $T$ ], is plotted against temperature as a parameter of Na concentration.

Figure 2 shows precipitation of  $\alpha$ -Fe<sub>2</sub>O<sub>3</sub> in Mn-Zn ferrite bodies occurs between 500 ° and 1100 °C during heating, but increase of Na addition suppress the precipitation at higher temperatures between 800 ° and 1000 °C.

The lattice parameter of ferrites sintered at 1250 °C with ramping rate of 300 °C/h varies from 8.483 to 8.485 Å with an increase of Na concentration (0.001 ~ 0.1 wt%) and is constant of 8.485 Å for 0.1 ~ 1.0 wt% Na additive.

#### 3.2 Microstructure

Tables 1(a) and (b) show the microstructure of the Mn-Zn ferrites with Na additives which were sintered under various sintering conditions.

In Fig. 3, the SEM photographs of the representative microstructure of Mn-Zn ferrite fabricated under the various condition mentioned in Tables 1-(a) and (b) are shown. The Gs as a function of the amount of Na additive are shown in Fig. 4. These ferrites had a porosity less than 0.01 %.

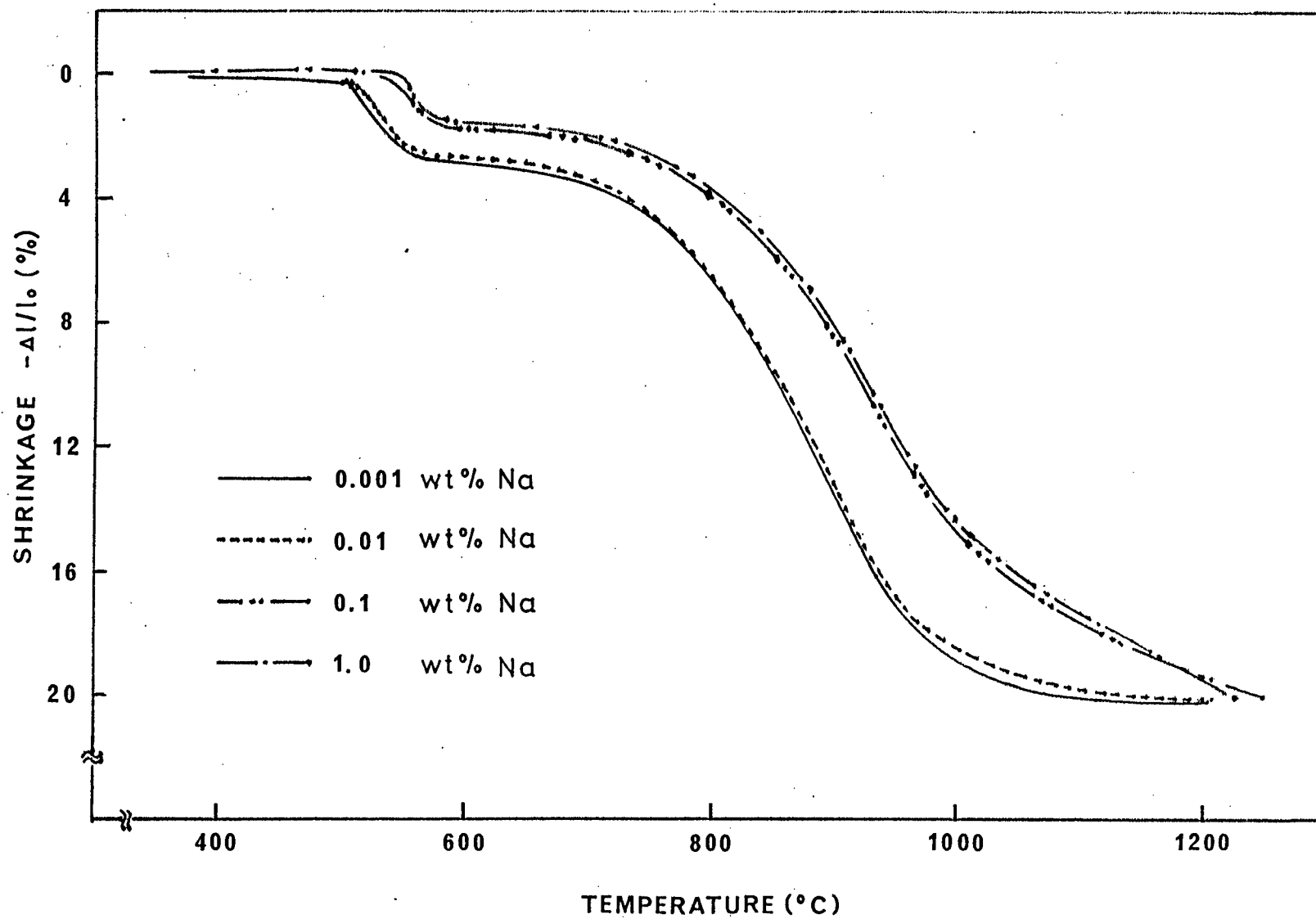


Fig. 1 The shrinkage curves of Na added Mn-Zn ferrite compacts.

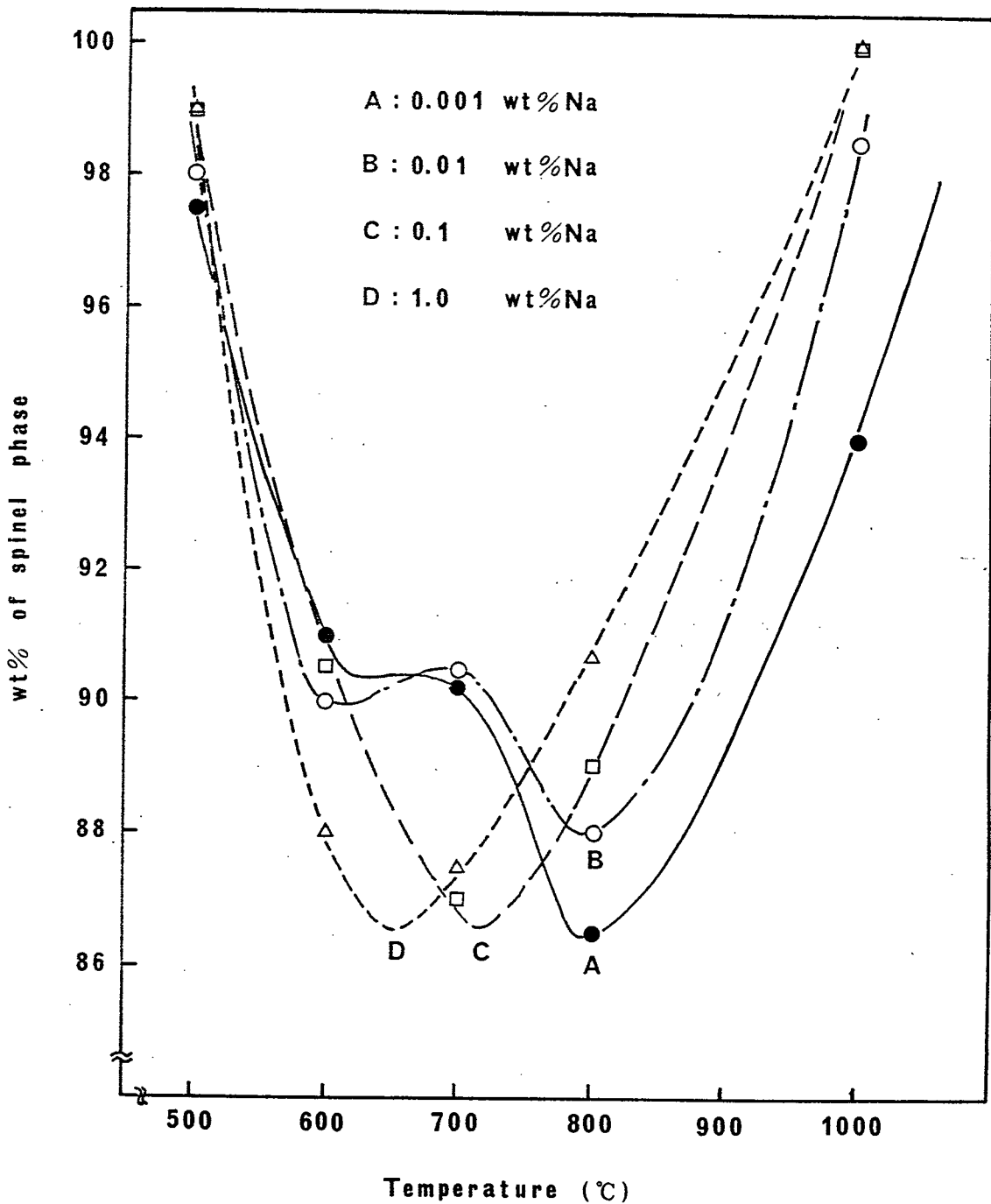
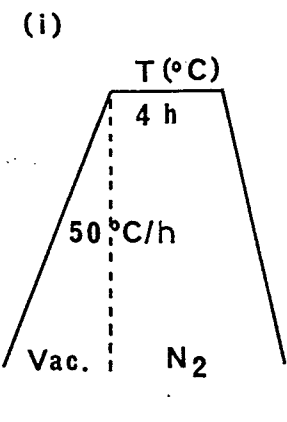


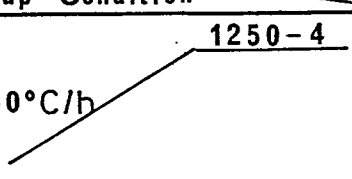
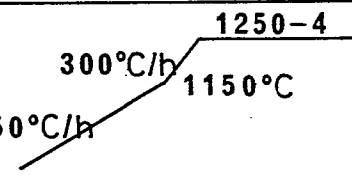
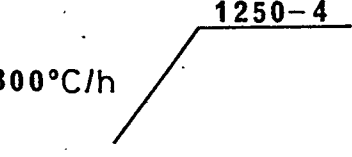
Fig. 2 Amount of spinel phase (wt%) in Mn-Zn ferrites with Na additive (0.001 ~ 1.0 wt%) appeared after the heat treatment at various temperature.



(a)

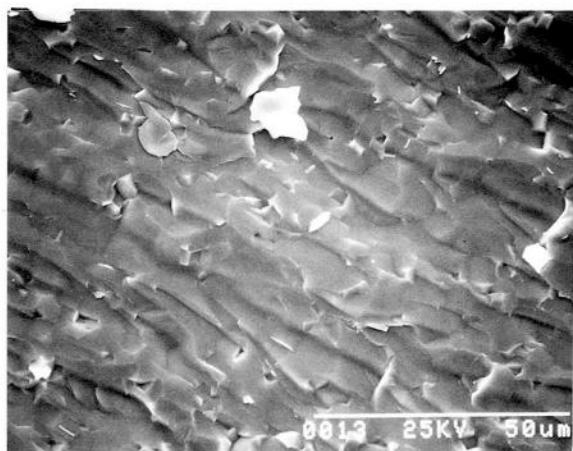
Sintering Condition	Na (wt%)				
	T (°C)	0.001 ~ 0.05	0.05 ~ 0.10	0.10 ~ 1.0	
(i) 	1 2 5 0	Small Grain	Large Grain		
	1 2 2 5		Small Grain	Small Grain	Duplex Structure
	1 2 0 0				
	1 1 5 0	$\alpha$ -Fe <sub>2</sub> O <sub>3</sub> precipitate			
		High Density ◀	▶ Low Density		

(b)

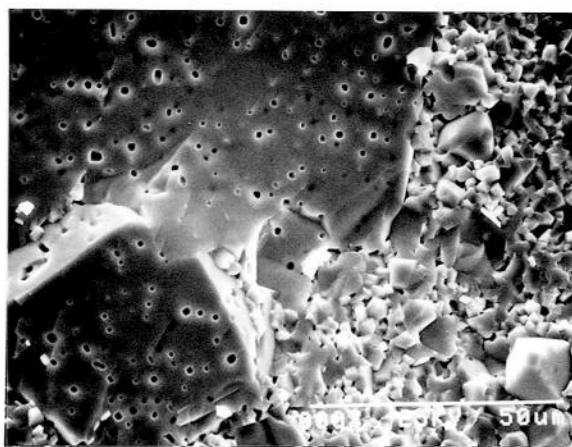
Heat-up Condition	Na (wt%)				
		0.001 ~ 0.05	0.05 ~ 0.10	0.10 ~ 1.0	
(i) 		Small Grain	Large Grain		
(ii) 			Small Grain	Small Grain	Duplex Structure
(iii) 				H. D.	
			L. D.	L. D.	
				L. D.	

H. D.; High Density, L. D.; Low Density

Table 1 The sintering condition vs. the microstructure of Mn-Zn ferrites with Na additives. In Table 1(a), the sintering temperatures are variables. In Table 1(b), the heating rates are variables.



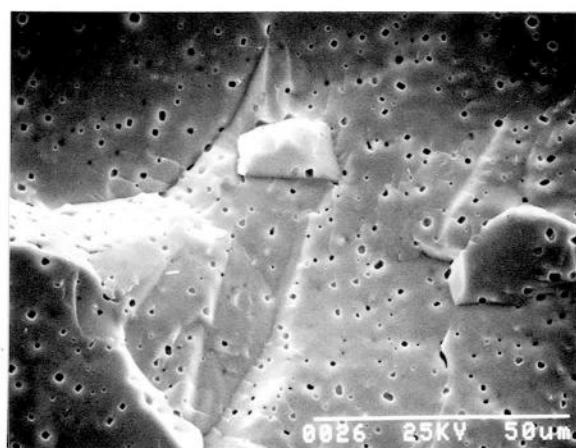
(a)



(b)



(c)



(d)

Fig. 3 The SEM photographs of the representative microstructure of Mn-Zn ferrite fabricated under the various heating rates and sintering temperatures.

(a) 0.05 wt% Na, 300 °C/h-1250 °C-4hr.

(b) 0.1 wt% Na, 50 °C/h-1150 °C, 300 °C/h-1250 °C-4hr.

(c) 0.1 wt% Na, 50 °C/h-1250 °C-4hr.

(d) 1.0 wt% Na, 50 °C/h-1250 °C-4hr.

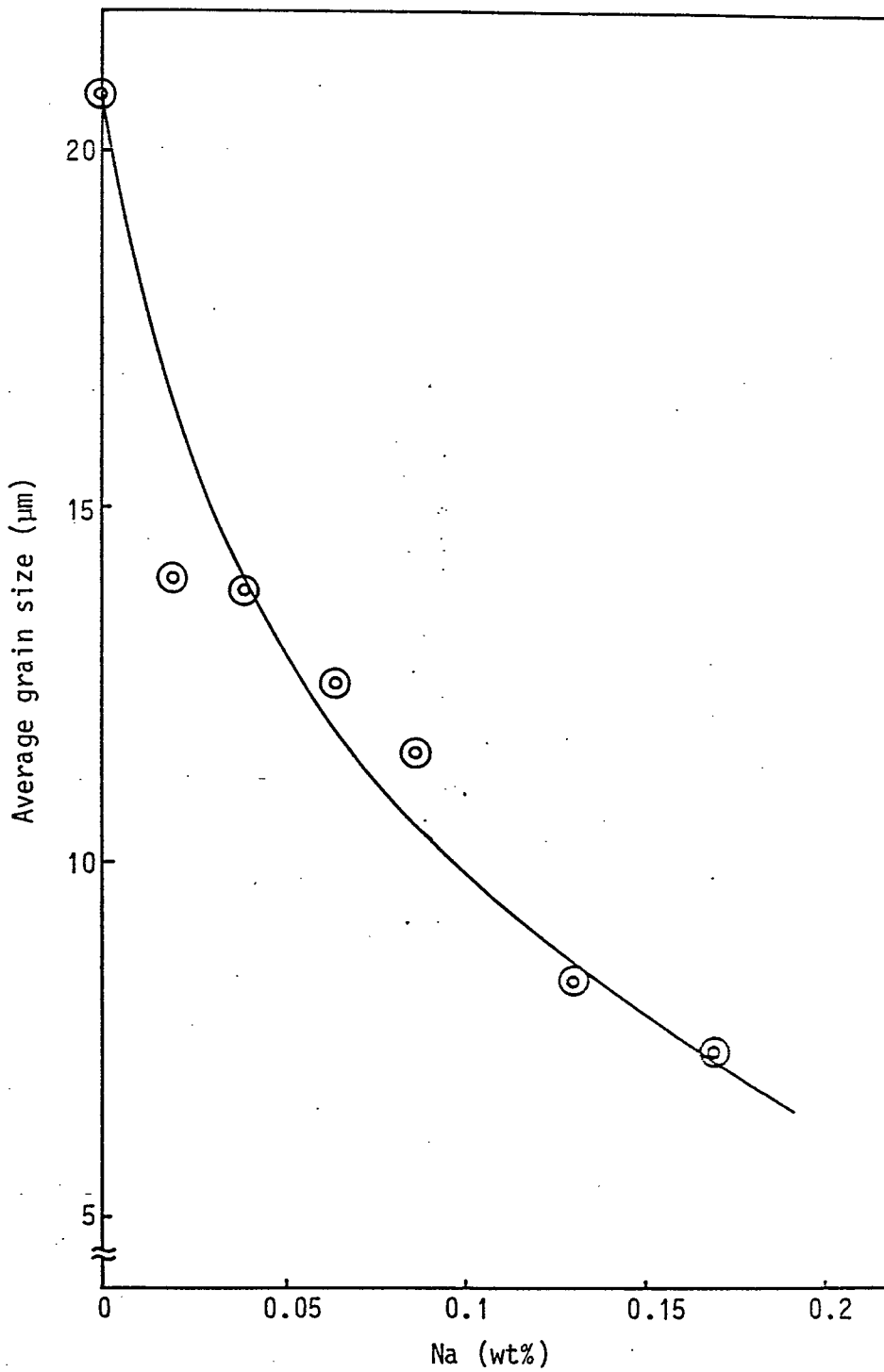


Fig. 4 The grain size of ferrites sintered at 1250 °C with heating rate of 300°C/h and held for 4 hr (300 °C/h-1250°C -4hr) as a function of the amount of Na additive.

### 3.3 Physical properties

The magnetic flux density at an applied field of 796 (A/m) (10 Oe),  $B_{10}$  (T), the coercive force,  $H_c$  (A/m), the permeability at a frequency of 1 kHz,  $\mu$  1kHz, and the disaccommodation of permeability, D.A.(%) vs. the concentration of Na of ferrites produced by the process of 300°C/h-1250°C-4h are plotted in Fig. 5. The changes of dc electric resistivity,  $\rho$ , with Na additives is also shown in Fig. 5.

The mechanical properties such as three-point bending strength,  $\sigma$ , hardness Hv, toughness  $K_{Ic}$ , and Gs of 0.001 wt% and 0.05 wt% Na are listed in Table 2.

### 4. Discussion

Firstly, the effect of Na addition on the microstructure development of the Mn-Zn ferrites are described. During sintering, Na ions reduce the shrinkage rate and suppress the grain growth at temperatures below about 1200°C, as seen in Fig. 1 and Table 1(a). Above 1200°C, however, the shrinkages of Na rich samples (0.1 ~ 1.0 wt% Na) reach the same amount as that of Na less added (0.001 ~ 0.01 wt% Na) samples as illustrated in Fig. 1. These phenomenon can be understood when liquid phase sintering occurs in Na rich ( $\geq$  0.10 wt%) samples above the eutectic point.  $\text{NaFeO}_2$  -  $(\text{Mn}_{0.5}\text{Zn}_{0.5})\text{Fe}_2\text{O}_4$  system is reported to have the eutectic point at 1180°C<sup>6)</sup>.

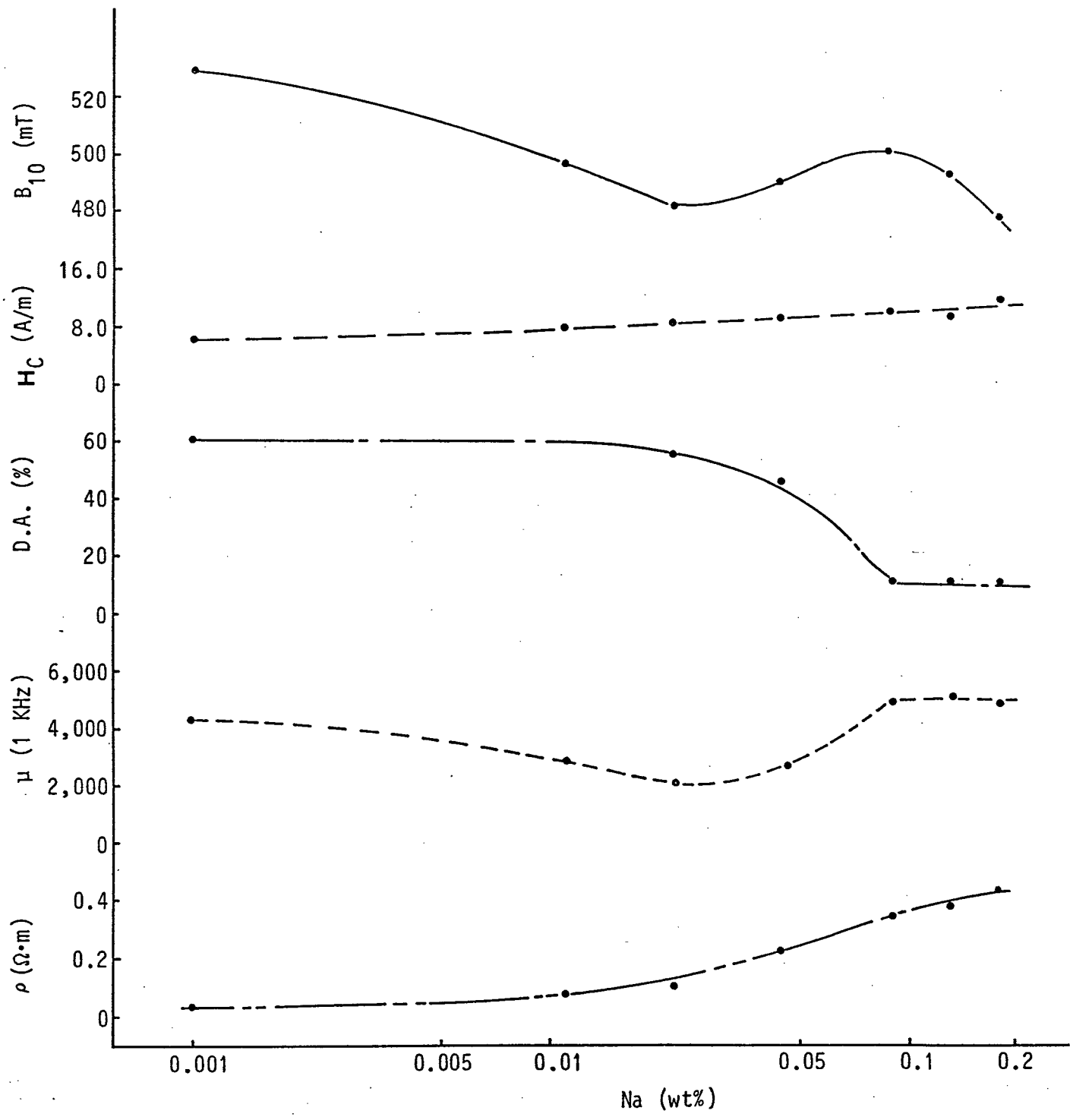


Fig. 5 The magnetic and electric properties of Mn-Zn ferrites with Na additives: magnetic flux density  $B_{10}$ , coercive force  $H_c$ , disaccommodation D.A., permeability  $\mu$  (at 1 kHz), and electric resistivity  $\rho$  are plotted by Na concentration.

additives properties (unit)	0.001 wt% Na	0.05 wt% Na
$\sigma$ (MPa)	168	175
Hv (GPa)	6.40	6.39
K <sub>1c</sub> (MN/m <sup>3/2</sup> )	1.2	1.2 ~ 1.3
G <sub>s</sub> ( $\mu$ m)	20.8	13.8

Table 2 The mechanical properties of Mn-Zn ferrites with 0.001 and 0.05 wt% Na additives fabricated under the heating rate 300 °C/h and sintering temperature 1250 °C for 4 hr.

The result of Table 1(a) also shows that the microstructure of Na added ferrites changes at a critical temperature of about 1200°C and the addition of Na more than about 0.10 wt% induces abnormal grain growth above 1200°C.

Table 1(b) and Fig. 3 show that the microstructures of 0.05 to 1.0 wt% Na added ferrites sintered at 1250°C also depend on the heating rate. When the rate is faster, the grain sizes are reduced and the sintered bodies become denser. The diminution of the average grain size seen in Fig. 4, can be explained by the results mentioned above. The rapid diminution of  $\alpha\text{-Fe}_2\text{O}_3$  in the Na doped ferrites at temperatures between 800° and 1000°C shown in Fig. 2 corresponds to the results of Table 1(a).

The comparison of mechanical properties of 0.01 wt% and 0.05 wt% Na doped ferrite can be explained as follows. A diminution of grain size with addition of Na made little change in both flexure strength and  $K_{IC}$ . On the one hand, hardness  $H_v$  slightly decreases. The variation of the magnetic and electric properties of Na doped samples shows that the effects of Na additives can be divided into three regions in accordance with Na concentration.

The effects caused by Na addition are summarized as follows.

#### 4.1 Products with 0.001 ~ 0.05 wt% Na

It is reported by Kobayashi et al<sup>6)</sup> that 0.05 ~ 0.1 wt% Na dissolves into Mn-Zn ferrite single crystal.

As the amount of Na additive in this region is under the limit of solubility, Na dissolves into the spinel lattice and the lattice parameter 'a' of the ferrites sintered at 1250°C increase with an increase of the Na concentration.

$B_{10}$ , D.A., and  $\mu$  decrease in this range. The permeability has grain size dependency and the permeability becomes lower for smaller grain size. The grain size continuously decrease from 0.001 to about 0.1 wt% Na range and therefore, the decrease of  $\mu$  in this range is probably dependent on the decrease of the grain size.

#### 4.2 Products with 0.05 ~ 0.1 wt% Na

The value of  $B_{10}$  increases in this region to nearly the same as that of value for undoped ferrite. The value of  $\mu$  1kHz increases in the same manner. But, D.A. decreases continuously. At the concentration range higher than 0.05 wt% Na, sintering with liquid phase partially occurs at above the eutectic point.

During sintering, when a heating rate is fast (300°C/h), the grain growth is inhibited because of "impurity drag" effect by addition of Na. The sintered bodies with 0.05 ~ 0.10 wt% Na prepared at 300 °C/h and 1200° ~ 1250 °C, has a high density, more than 99.9 % of the theoretical density with small grain matrix.

On the other hand, when a ramping rate is small (50°C/h), there is enough time for mass transport to result in an enhancement of grain growth.



Therefore, these samples has a relatively low density, 98 ~ 99 % of the theoretical density. They consist of large grains with included pores.

#### 4.3 Products with 0.1 ~ 1.0 wt% Na

As the solubility of Na to the spinel lattice is estimated to be 0.05 ~ 0.1 wt% from the change of the lattice parameter, an addition of 0.1 ~ 1.0 wt% Na is higher than its solubility. At sintering temperature above about 1200 °C, a "micro" liquid phase sintering occurs and it makes both the shrinkage increased and the grain growth enhanced.

The microstructure of 1.0 wt% Na doped ferrite fired at 1250 °C with slow heating rate, consists of exaggerated grains with many pores inside. In this Na rich region, it is thought that Na exists at grain boundaries in the ferrites.

#### 5. Conclusion

The effects of Na addition in the range of 0.001 to 1.0 wt% to Mn-Zn ferrites were investigated. The reduction of both the shrinkage and the precipitation of  $\alpha\text{-Fe}_2\text{O}_3$  by Na addition during sintering were observed.

The microstructure development depended on both the concentration of Na and the sintering condition such as the rate of heating and the firing temperature.

The concentration of Na having an effect on the microstructure were divided into three regions; (I) 0.001 ~ 0.05 wt% Na, (II) 0.05 ~ 0.1 wt% Na, (III) 0.1 ~ 1.0 wt% Na. The fine grain ferrites with high density were sintered in region (I), and large or exaggerated grain with low density in region (III). The microstructure of ferrites was controlled by the heating rate in region (II).

## 6. References

1. T. Akashi, NEC Res. Dev. (Japan) 8, 89 ~ 106 (1966).
2. M. F. Yan and D. W. Johnson, Jr., J. Am. Ceram. Soc., 61, 342 ~ 49 (1978).
3. K. Hirota, Y. Fujimoto, K. Watanabe, and M. Sugimura, Advances in Ceramics edit. F. F. Y. Wang, State Univ. of New York, New York, 15, 385 ~ 92 (1985).
4. D. W. Johnson, Jr., E. M. Vogel, and B. B. Ghate, Proc. Int. Conf. Ferrites 3 edit. H. Watanabe, S. Iida and M. Sugimoto, Center for Academic Publications, Japan, 285 ~ 91 (1980).
5. K. Niihara, R. Morena, and D. P. H. Hasselman, J. Mater. Sci. Lett., 1, 13 ~ 16 (1982)
6. T. Kobayashi and K. Takagi, J. Cryst. Growth, 62, 189 ~ 97 (1983).

Chapter IV. Improvements of mechanical and magnetic properties by adding triple components of Na-Zr-Ca

Abstract

Some effects of additives to Mn-Zn ferrites were studied to improve mechanical and magnetic properties. The grain size decreased when either  $\text{Na}_2\text{CO}_3$  or  $\text{CaCO}_3$  was added. The permeability increased with double additions of  $\text{Na}_2\text{CO}_3$  and  $\text{CaCO}_3$ .  $K_{fc}$  increased with the additions of either  $\text{Na}_2\text{CO}_3$  or the double components of  $\text{CaCO}_3$  and  $\text{ZrO}_2$ .  $\text{ZrO}_2$ -added specimens showed a transgranular fracture surface and long durability against chipping. The Mn-Zn ferrite with high  $B_{10} = 0.58$  T (at 10 Oe [796 A/m]) and  $\mu = 700$  (at 10 MHz) was obtained by triple additions of  $\text{Na}_2\text{CO}_3$ - $\text{CaCO}_3$ - $\text{ZrO}_2$ . It had a small grain size (10  $\mu\text{m}$ ) and showed high resistance against chipping.

## 1. Introduction

High saturation magnetization and high permeability at high frequency are demanded for high magnetic recording density, high reliability, and mass-memory capacity. In addition, fine grain and high toughness are needed for polycrystalline ferrites, because the magnetic head requires a narrow magnetic gap length and a small track width.<sup>1)</sup>

To meet these requests, precise machining is undertaken.<sup>2)</sup> This kind of processing often generates some undesirable defects in the material such as grain pullout or chipping which causes the decrease of production yield and shortening of life time.

A number of results have been reported on the improvement of the magnetic properties of Mn-Zn ferrites,<sup>3)</sup> whereas less discussions have been published on the above-mentioned mechanical properties.

This chapter will describe the effect of additives on the mechanical strength and toughness, and also on the durability against chipping.

## 2. Experimental procedure

Coprecipitated spinel powder with a composition of 55-56  $\text{Fe}_2\text{O}_3$ , 35-37  $\text{MnO}$ , 7-10  $\text{ZnO}$  (mol%) was used. It had impurities of 0.0025  $\text{CaO}$ , 0.0022  $\text{SiO}_2$ , 0.001  $\text{Na}$ , and 0.002  $\text{SO}_4$  (wt%). The fabrication was a traditional ceramic production method.

After a calcination at 600° to 800°C in N<sub>2</sub> atmosphere for 1 to 2 hr, each additive of 0.025 to 0.4 wt% ZrO<sub>2</sub>, CaCO<sub>3</sub>, Na<sub>2</sub>CO<sub>3</sub>, In<sub>2</sub>O<sub>3</sub>, Al<sub>2</sub>O<sub>3</sub> and Sb<sub>2</sub>O<sub>3</sub> and also combined additives of Na<sub>2</sub>CO<sub>3</sub>-CaCO<sub>3</sub> and Na<sub>2</sub>CO<sub>3</sub>-CaCO<sub>3</sub>-ZrO<sub>2</sub> were added to the calcined powders, and the mixed powders were wet ball-milled. The ZrO<sub>2</sub> powder used in these experiments had average particle size of 1.2 μm (diameter) and the monoclinic structure. Dried powder was granulated and molded. The obtained compacts were hot-pressed at 1250° to 1300°C for 2 hr at 29.4 MPa in a controlled N<sub>2</sub>-O<sub>2</sub> atmosphere.

The average grain size (Gs) and the porosity of sintered bodies were measured in the same method described in Chapter III. The occurrences of grain pullout and chipping were observed using a microscope and a scanning electron microscope (SEM). A secondary ion mass spectrometry (SIMS) was used to analyse the segregation or precipitation of Na, Ca, and Zr.

Fracture toughness K<sub>1c</sub> and the modulus of rupture were measured in the same method described in Chapter III.

The dc resistivity, ρ, at room temperature, B/H curves, and permeability, μ were also measured as the same way mentioned in Chapter III.

### 3. Results and discussion

The effects of additive amounts on the Gs are shown in Fig. 1.

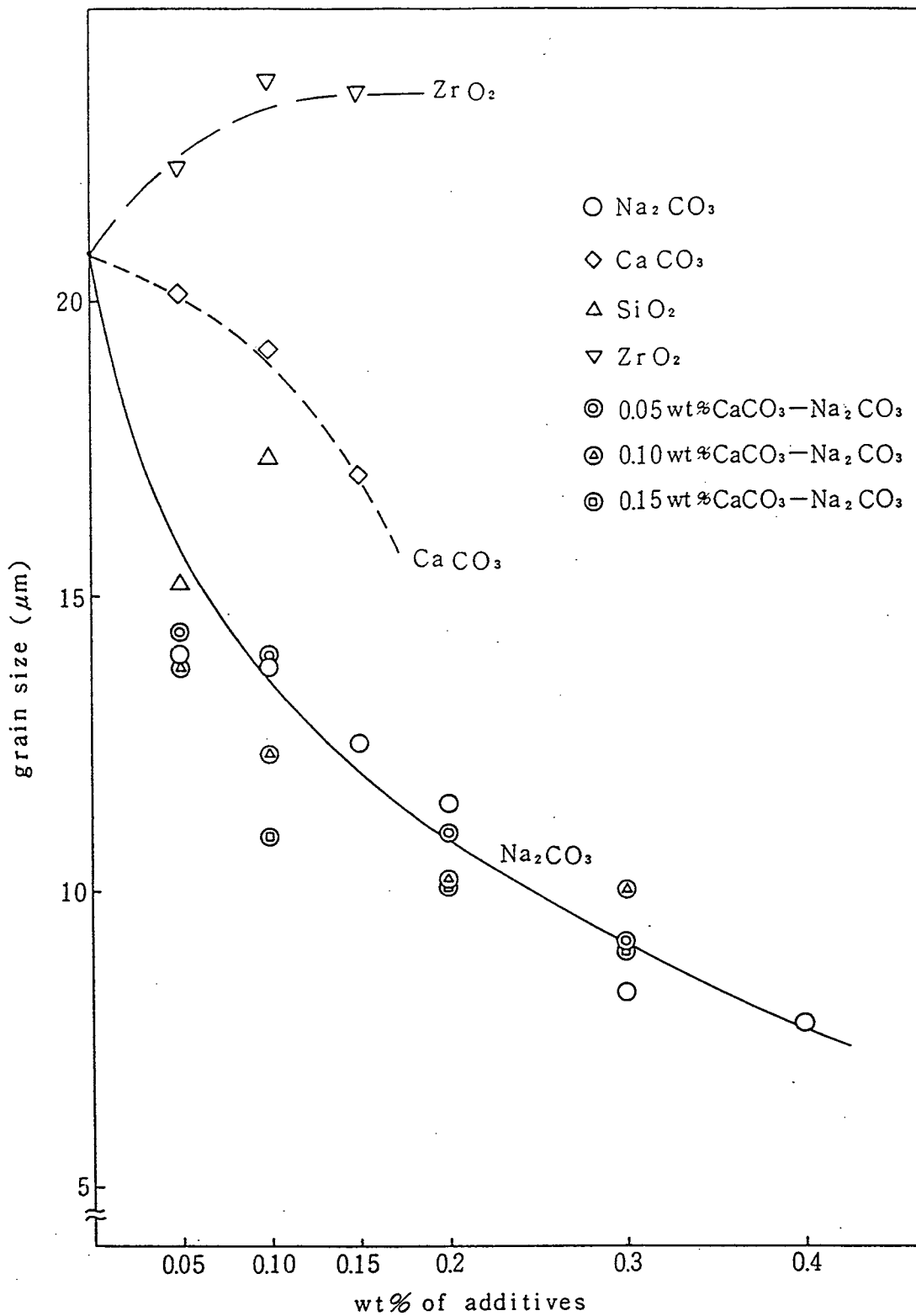


Fig. 1 Variation of grain size with additives.

The Gs for both the  $\text{Na}_2\text{CO}_3$  and  $\text{CaCO}_3$  additions decrease as the amounts of additives increase. The Gs of 0.4 wt%  $\text{Na}_2\text{CO}_3$ -doped Mn-Zn ferrite body is 7.5  $\mu\text{m}$  and that of the sintered body without additives is 22  $\mu\text{m}$ . The combined additives  $\text{Na}_2\text{CO}_3$ - $\text{CaCO}_3$  also decrease Gs.

Another effect of additives on the sintering is seen in the breakdown of the sintered bodies. For example, the additions of 0.05 wt%  $\text{SiO}_2$  and 0.1 wt%  $\text{ZrO}_2$  generate large cracks which make the sintered bodies almost broken down to pieces. No crack is observed in the products in case both  $\text{ZrO}_2$  and  $\text{CaCO}_3$  are added, even when more than 0.1 wt%  $\text{ZrO}_2$  are used.

Additives such as  $\text{CaCO}_3$  and  $\text{Na}_2\text{CO}_3$  increase the modulus of rupture with the increasing amounts. The moduli of rupture of Mn-Zn ferrite without additives and with 0.1 wt% additives of  $\text{Na}_2\text{CO}_3$ ,  $\text{CaCO}_3$ , and  $\text{ZrO}_2$  are shown in Table 1. Those of  $\text{In}_2\text{O}_3$ ,  $\text{Al}_2\text{O}_3$ ,  $\text{Sb}_2\text{O}_3$ ,  $\text{SiO}_2$  are shown in Table 1 as the references. K<sub>ic</sub> of these ferrite samples are also shown in Table 1. Their porosities were less than 0.01 %. Vickers hardness, Hv, also varied with additives as shown in Table 1.

The  $\text{Na}_2\text{CO}_3$  doped Mn-Zn ferrite show nearly the same K<sub>ic</sub> as that of without additives, but a slight decrease in Hv. The effects of  $\text{CaCO}_3$  addition on the diminution of grain size and increase of K<sub>ic</sub>, are reported<sup>2)</sup>. It is expected that  $\text{ZrO}_2$  addition to an Mn-Zn ferrite results in the increase of K<sub>ic</sub>, as are seen in the cases of the systems  $\text{Al}_2\text{O}_3$ - $\text{ZrO}_2$  and in  $\text{ZrO}_2$  added ZnO.

	no additive	Na <sub>2</sub> CO <sub>3</sub>	CaCO <sub>3</sub>	ZrO <sub>2</sub>	In <sub>2</sub> O <sub>3</sub>	Al <sub>2</sub> O <sub>3</sub>	Sb <sub>2</sub> O <sub>3</sub>	SiO <sub>2</sub>
modulus of rupture (MPa)	168	175	171	169	146	160	163	170
K <sub>IC</sub> (MN/m <sup>3/2</sup> )	1.201	1.228	1.305	1.400				
Hv (GPa)	6.40	6.39	6.44	6.50				

Table 1 Modulus of rupture, fracture toughness K<sub>IC</sub>, and Vickers hardness Hv of Mn-Zn ferrites without additive and with 0.1 wt% additives.



This trend is illustrated in Fig. 2, where  $K_{Ic}$  increases in the range from 0 to 0.2 wt% and reaches a constant value over 0.2 wt% of  $ZrO_2$  as is observed in  $ZrO_2$  added ZnO.

Generally, ceramics are durable to compressional stress but weak to tensional stress. The tensional stress is applied to the lower side (the supporting-edge side) of the sample on a three-point bend test.

Both transgranular and grain-boundary fractures were observed at the tension-stressed side of the sample without additive and also  $Na_2CO_3$  added, whereas 0.1 wt%  $CaCO_3$  added sample showed only a grain-boundary fractures at any surface as reported before. This is attributed by CaO segregates at the grain boundaries which mechanically weakens the ferrite, as confirmed by SIMS analysis in Fig. 3. A transgranular fracture was observed at every rupture surface in the sintered body with 0.05 wt%  $ZrO_2$ . The sintered bodies with combined additives of (wt%) 0.1  $Na_2CO_3$ -0.1  $CaCO_3$ -0.1  $ZrO_2$  also showed transgranular fracture surfaces.

The generation of chipping is due to either "grain pullout", which occurs at the grain boundaries, or the breakdown of the grains themselves. Many chippings are observed on the edge of the sintered bodies without additives and with  $Na_2CO_3$  and  $CaCO_3$  additives, as illustrated in Fig. 4(a). A chipped surface therefore consists of a grain-boundary fracture surface. The percentage of chipping generation against the number of all grains on the corner, which is precisely machined, is estimated to be 3 to 7 % of grains in the conventional Mn-Zn ferrite with Gs of 14  $\mu m$ .

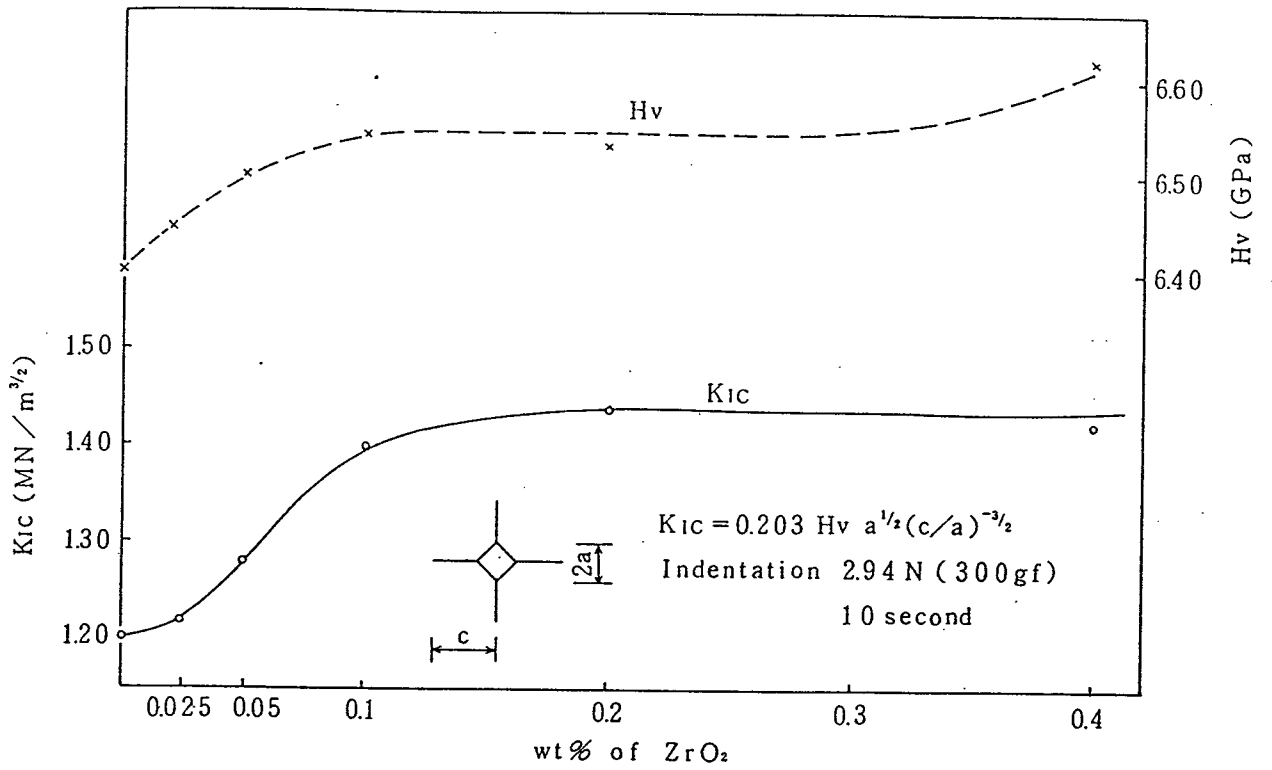


Fig. 2 Fracture toughness,  $K_{1c}$  and Vickers hardness,  $H_v$  of the  $ZrO_2$  added Mn-Zn ferrite polycrystal.

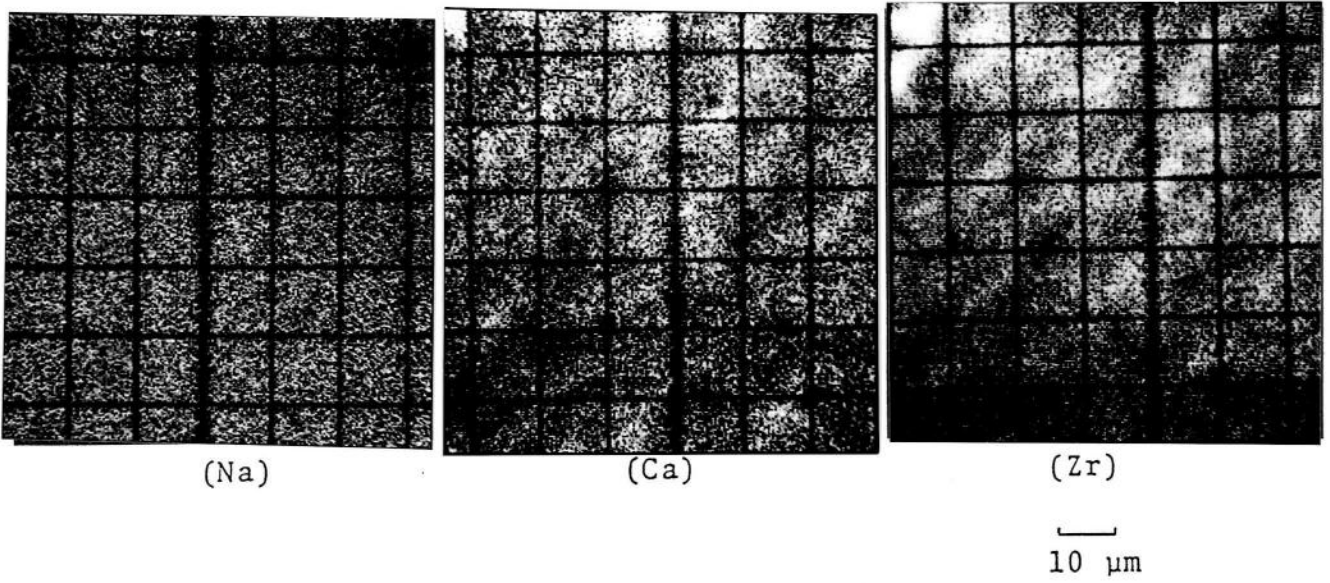
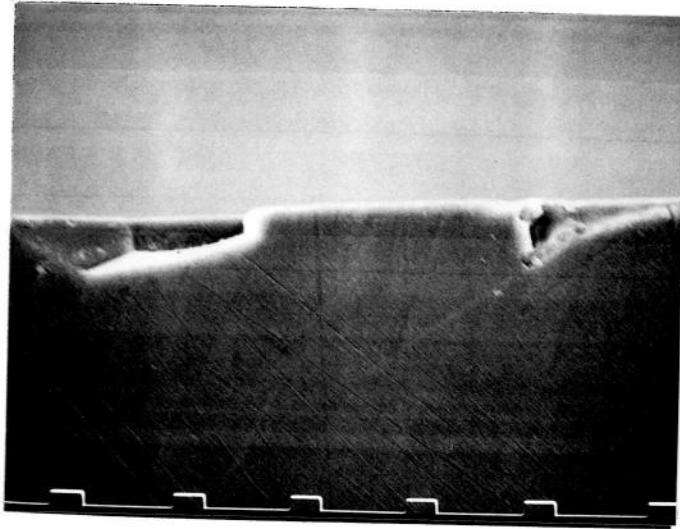
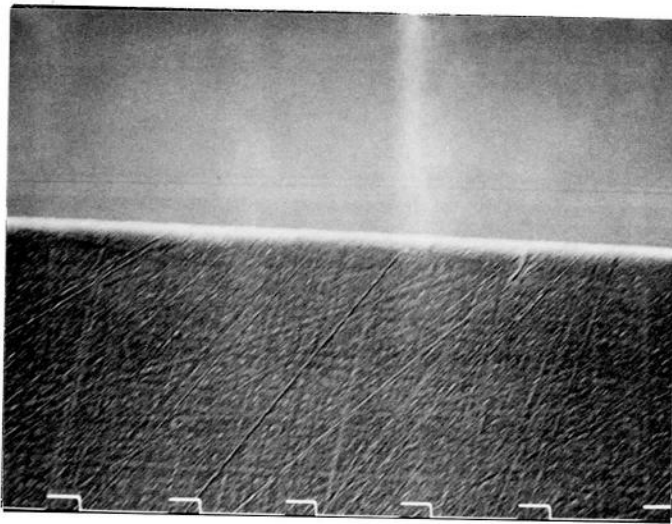


Fig. 3 Photographs of SIMS analysis, which show the distribution of Na, Ca and Zr. The Ca and Zr segregate at the grain boundaries of Mn-Zn ferrites, but Na distributes uniformly.



(a)



(b)

10  $\mu\text{m}$

Fig. 4 Photographs of mirror-lapped edges observed with an SEM show (a) chipping of  $\text{CaCO}_3$  added ferrite and (b) sample mechanically improved by addition of  $\text{ZrO}_2$ .

As shown in the SIMS photographs of Fig.3,  $\text{Na}_2\text{CO}_3$  dissolved mainly into the spinel lattice, and had an effect on the reduction of Gs of the sintered bodies, but had little effect on the microstructural enhancement of fracture toughness.

The  $\text{CaCO}_3$  added Mn-Zn ferrite also had no advantage in durability against chipping, but  $\text{ZrO}_2$  doped ferrite showed high durability and its chipping-generation percentage decreased below 0.7 % per grain. This increased durability suggests that  $\text{ZrO}_2$ , which segregates at the grain boundaries, as shown in Fig. 3, induces compressional stress inside the grains through the grain boundaries, and therefore, the grain boundaries are reinforced by compressional stress. The CaO added Mn-Zn ferrites were also toughened by the addition of  $\text{ZrO}_2$ . For example, the sintered bodies with combined additives  $\text{CaCO}_3\text{-ZrO}_2$  and  $\text{Na}_2\text{CO}_3\text{-CaCO}_3\text{-ZrO}_2$  changed their fracture mechanism from a intergranular fracture to a transgranular fracture by addition of  $\text{ZrO}_2$  and showed high durability to chipping, as shown in Fig. 4(b).

The dc resistivities,  $\rho$ , of the sintered ferrites, as a function of additive content, were measured. Addition of  $\text{Na}_2\text{CO}_3$  increased  $\rho$  compared with that without additives by the factor of 7 to 8. Additional additives, other than  $\text{CaCO}_3$ , had little effect on  $\rho$ , but  $\text{CaCO}_3$  increased it remarkably as shown in Fig. 5.

The frequency dependences of  $\mu$  for samples with and without additives are shown in Fig. 6.

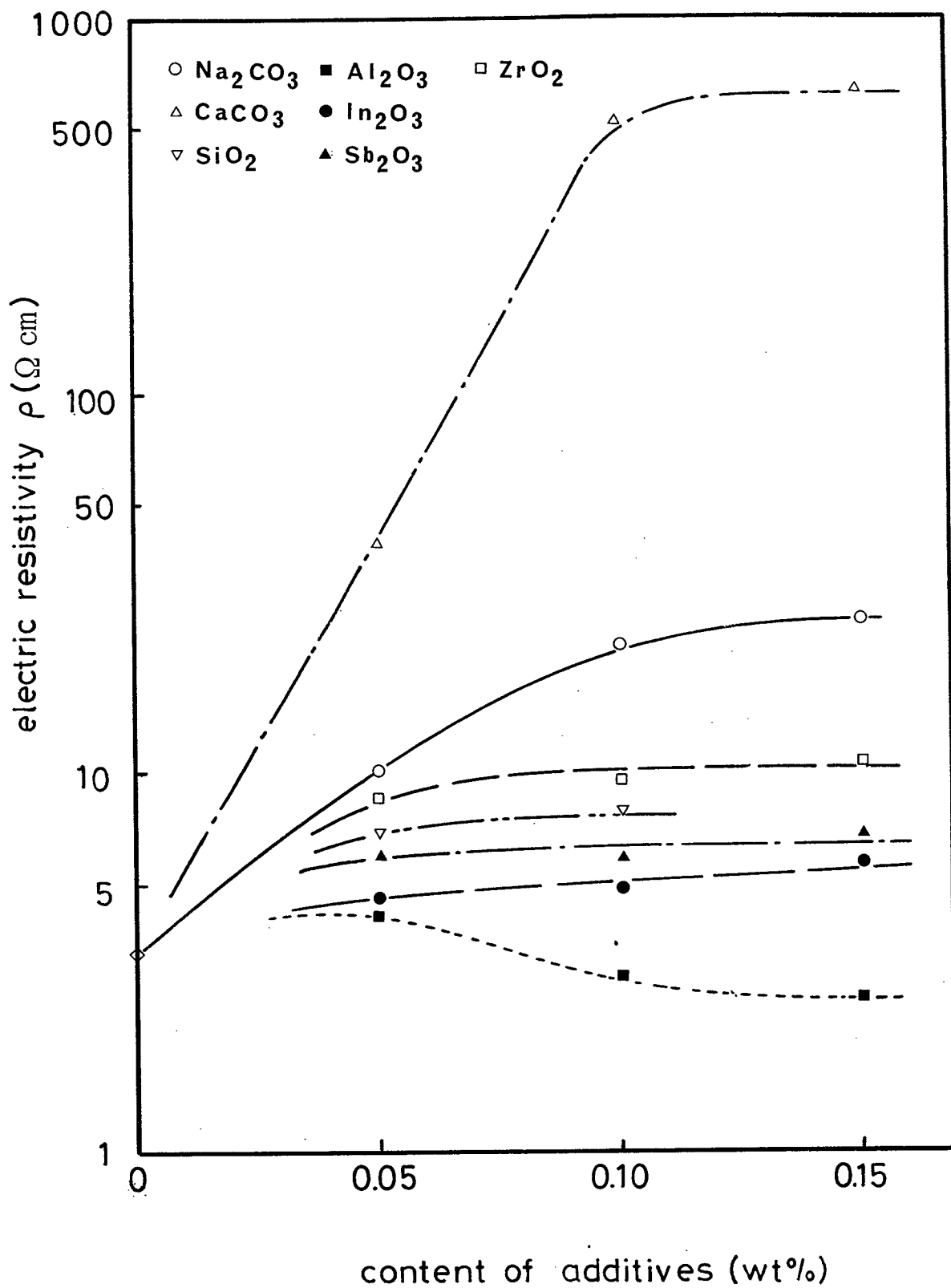


Fig. 5 Effect of additives on the electric resistivity  $\rho$ .

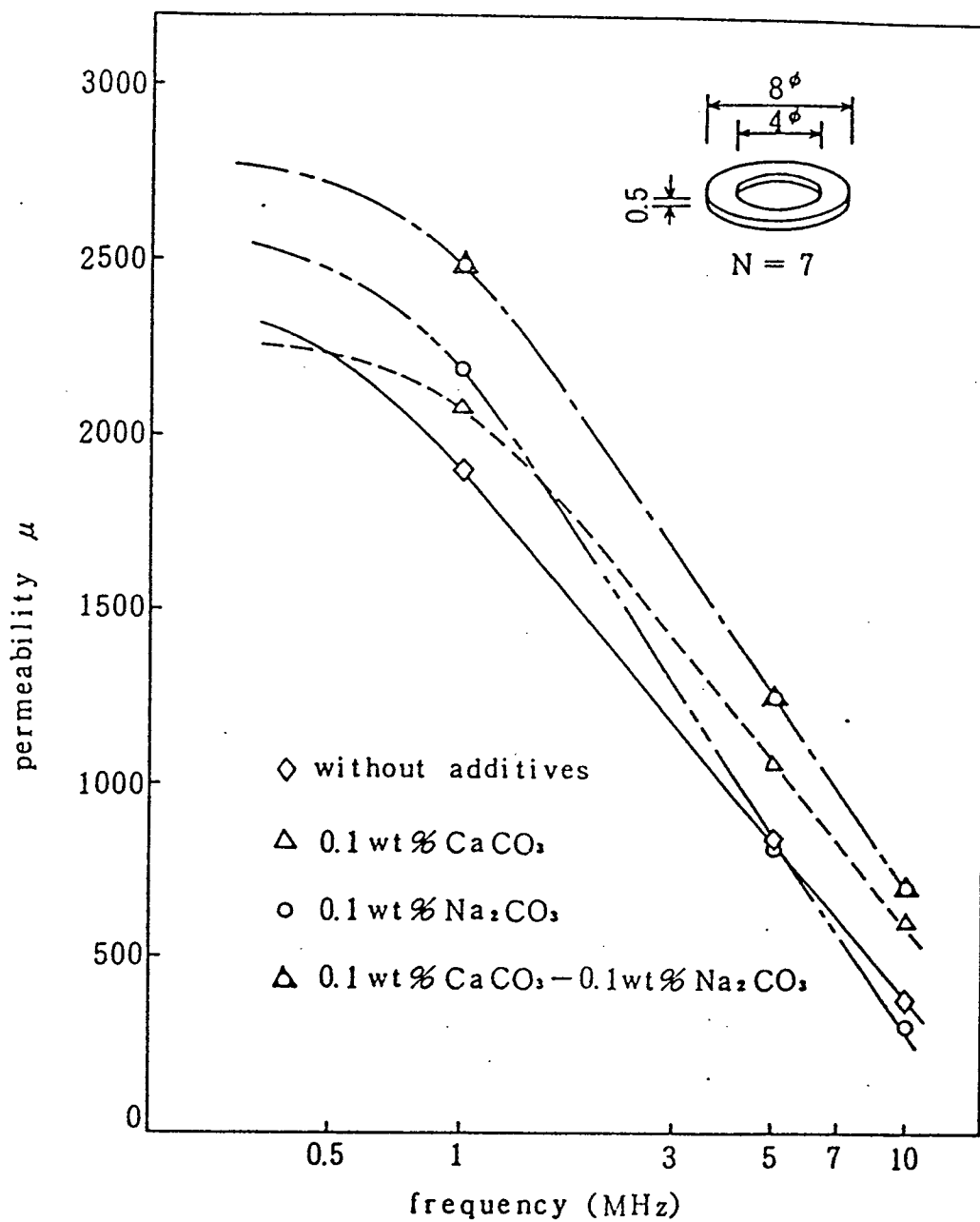


Fig. 6 Frequency dependence of initial permeability of Mn-Zn ferrites with additives.

The  $\mu$ , at high frequency, of  $\text{Na}_2\text{CO}_3$ - $\text{CaCO}_3$  added ferrite was higher than those of respective case of one component,  $\text{CaCO}_3$  or  $\text{Na}_2\text{CO}_3$  added ferrite, and also without additives.

This improvement of  $\mu$  was achieved by widening the grain-boundary area, which had a high electrical resistivity due to the decrease of the grain size.

Variations in the magnetic flux density at 796 A/m (=10 Oe)  $B_{10}$  with the amounts of additives are shown in Fig. 7. The  $B_{10}$  of a polycrystal is decided mainly by the composition, provided that it is sintered in high density under optimum conditions. As most additives are inclined to decrease  $B_{10}$ , it is important to select the correct types and amounts of additives.

The coercive force,  $H_c$ , varied in the range from 7.96 to 23.9 A/m (0.1 to 0.3 Oe) by 0.1 wt% addition of  $\text{Na}_2\text{CO}_3$ ,  $\text{Al}_2\text{O}_3$ ,  $\text{CaCO}_3$ ,  $\text{In}_2\text{O}_3$ ,  $\text{SiO}_2$  and  $\text{ZrO}_2$  additives.

From the results, it is said that the best sample strong against chipping is obtained by the triple addition of  $\text{Na}_2\text{CO}_3$ - $\text{CaCO}_3$ - $\text{ZrO}_2$  in the range from 0.02 to 0.1 wt%.

The properties of Mn-Zn ferrites with improved mechanical strength by the triple addition mentioned above are summarized in Table 2.

#### 4. Conclusion

The effects of the addition of  $\text{Na}_2\text{CO}_3$ ,  $\text{CaCO}_3$ , and  $\text{ZrO}_2$  on the properties of densely sintered Mn-Zn ferrite were surveyed. Other additives were also examined as a reference.



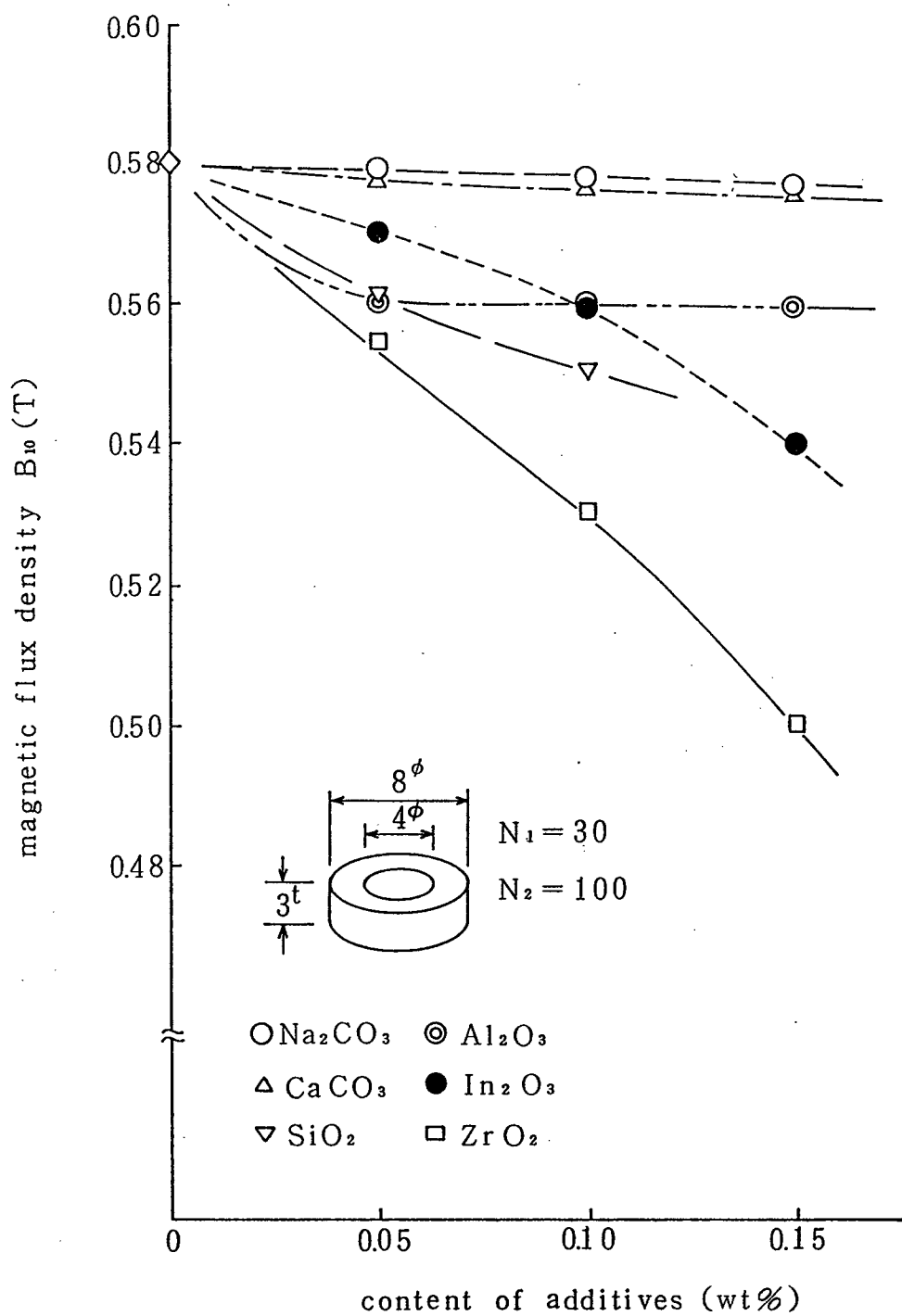


Fig. 7 Magnetic flux density vs. content of additives.

Magnetic-flux density	$B_{10}$ (T)	0.58
Residual-flux density	$B_r$ (T)	0.20
	1 kHz	2800
	1 MHz	2500
Permeability, $\mu$	5	1200
	7	840
	10	700
Curie temperature	$T_c$ ( $^{\circ}\text{C}$ )	240
Electric resistivity	$\rho$ ( $\Omega \cdot \text{m}$ )	>0.1
Vickers hardness	$H_v$ (GPa)	6.42
Thermal expansion coefficient	$\alpha$	$130 \times 10^{-7}$
Grain size	Gs ( $\mu\text{m}$ )	10
Porosity	(%)	0.01
Probability of chipping (%) per grain		<0.7

Table 2 Properties of Mn-Zn ferrite with high  $B_{10}$ ,  $\mu$  and durability to chipping.

The results showed that (a) addition of  $\text{Na}_2\text{CO}_3$  reduced grain size; (b) fracture mechanism of the sintered ferrites was affected by the additives. The addition of  $\text{ZrO}_2$  was useful to suppress the grain boundary fracture; (c)  $K_{IC}$  increased by the addition of  $\text{Na}_2\text{CO}_3$ ,  $\text{CaCO}_3$ , or  $\text{ZrO}_2$ , in sequence; (d) the chipped fracture sample consisted of the grain boundary fracture surface; (e) durability against chipping was improved by the addition of  $\text{ZrO}_2$ ; and (f) the Mn-Zn ferrite with high  $B_{10}$  (0.58 T) and high  $\mu$  (700 at 10MHz) was obtained by a triple addition of  $\text{Na}_2\text{CO}_3$ - $\text{CaCO}_3$ - $\text{ZrO}_2$  and it could have a Gs of 10  $\mu\text{m}$  and showed high durability against chipping.

## 5. References

1. E. Hirota, K. Hirota, and K. Kugimiya, Proc. Int. Conf. Ferrites 3, edit. H. Watanabe, S. Iida and M. Sugimoto. Center for Academic Publications, Japan, 667 ~ 74 (1980).
2. D. W. Johnson, Jr., E. M. Vogel and B. B. Ghate, *ibid.* 285 ~ 91.
3. T. Akashi, NEC Res. Dev. (Japan), 8, 89 ~ 106 (1969).
4. A. G. Evans and E. A. Charles, J. Am. Ceram. Soc., 59, 371 (1976).
5. K. Niihara, R. Morena, and D. P. H. Hasselman, J. Mater. Sci. Lett., 1, 13 ~ 16 (1982).
6. N. Clausen, J. Steeb, and R. F. Pabst, Am. Ceram. Soc. Bull., 56, 559-62 (1977).
7. H. Ruf and A. G. Evans, J. Am. Ceram. Soc., 66, 328-32 (1983).

## Chapter V. Grain growth of Mn-Zn ferrite with additives and its application to the solid state single crystal growth

### Abstract

Grain growth of Mn-Zn ferrite with additives and application of result to the solid state growth of single crystal were studied. Among growth-enhancing additives, the effects of Na and B on the microstructure of Mn-Zn ferrites were investigated. By adhering a seed single crystal plate on the Na doped or the B doped ferrite with ethylsilicate adhesive solution, the polycrystals were converted into a single crystal under the suitable heat treatment conditions, and the mechanism of this conversion was investigated.

The electric and magnetic properties of the crystals at high frequencies was nearly the same as those of the crystal grown by the Bridgman method.

## 1. Introduction.

One of the effects of additives on the microstructure of ceramics is an enhancement of the grain growth during sintering or annealing. This kind of enhancement, which is sometimes called abnormal, exaggerated, discontinuous grain growth, or the secondary recrystallization, is not desirable when the fabrications of densely sintered bodies are attempted. If rapid grain growth occurs, many pores remain in the product and results in spoiling the functional properties such as the magnetic properties and the mechanical strength.

For example, if the soft magnetic Mn-Zn ferrites have the microstructure composed of both the fine and the coarse grains, they have low permeability and high coercive force. These properties are undesirable for soft magnetic materials.

There are many reports about the exaggerated grain growth of Mn-Zn ferrites<sup>1)</sup> and barium titanates<sup>2)-4)</sup>. The abnormal grain growth in barium titanates is due to the existence of liquid phase during sintering, but its origin in Mn-Zn ferrite is not clearly explained so far.

The abnormal grain growth is accelerated in the following cases: a) existence of impurities such as  $\text{SiO}_2$ <sup>5)</sup>, b) unhomogeneous distribution of particle size of the starting powders,<sup>6)7)</sup> c) locally generated pressure worked on the compact during the molding process, d) existence of excess  $\text{Fe}_2\text{O}_3$ , e) fractuation of chemical composition due to insufficient mixing or reaction among the starting

materials, f) existence of liquid phase reaction during sintering,<sup>8)</sup> g) temperature gradient inside the body during sintering.

It has been reported, however, that single crystals such as  $\text{CuFe}_2\text{O}_4$ <sup>9)</sup>,  $\text{Al}_2\text{O}_3$ <sup>10)</sup> were grown by using the process of abnormal grain growth started from polycrystals. Matsuzawa and Kozuka reported that a Mn-Zn single ferrite was produced by a solid state reaction in which an abnormal grain growth was used.<sup>11)</sup>

This chapter will describe the effect of additives on the abnormal grain growth and its application to the single crystal growth of Mn-Zn ferrites.

## 2. Experimental Procedure.

### i) Preparation of polycrystals.

Starting material was coprecipitated spinel powder with a composition (mol%) 53-54  $\text{Fe}_2\text{O}_3$ , 29-30  $\text{MnO}$ , 16-18  $\text{ZnO}$ . This kind of powder was useful to avoid both fluctuation of the chemical composition and unhomogeneity of the particle size distribution. It had impurities of (wt%) 0.0025  $\text{CaO}$ , 0.0022  $\text{SiO}_2$ , 0.001  $\text{Na}$ , and 0.002  $\text{SO}_4$ , the average particle size being 0.15 ~ 0.20  $\mu\text{m}$ .

The starting powder was gently ball-milled with a care not to destroy the particle size distribution. Two kinds of powders were prepared; one without additives and the other with 0.05 wt%  $\text{Na}$ . These powders were dried afterwards.

Dried powders were granulated and molded by using a cold isostatic press with molding pressure 196 MPa to obtain the uniformly densified compact.

The molded compacts were sintered at 1250°C for 6 hr in a controlled N<sub>2</sub>-O<sub>2</sub> atmosphere.

The sintered bodies were cut into pieces rectangular bar of approximately 3 mm x 3 mm x 12 mm in size, with one surface lapped to a mirror surface with SiC and diamond abrasives.

Then, preliminary experiment was undertaken to survey an effect of metal additives on the grain growth enhancements. Twenty-one kinds of acid solutions, each of which contained one of the following ions, K, Mg, Ca, Sr, Ba, Y, La, Ti, Zr, V, Nb, Cr, Co, Cu, B, Al, Si, Sn, Sb, Bi, Te and whose concentration was 5 mol/l were prepared. They were spread on the mirror surfaces of two kinds of ferrite polycrystalline samples prepared before. And then, they were annealed at 1320° to 1340°C for 2 hr in N<sub>2</sub> atmosphere.

The results disclosed that B, Nb, Si, V, Bi, Sn had the noticeable effect on grain growth enhancement.

Again, six kinds of ferrite polycrystals, each of those was added with one of six additive (B, Si, Nb, Bi, V, Sn), were prepared in the same process as described before. Then, these six kinds of polycrystals and one with Na additive, were examined in the following experiment. Na ion is also the grain growth enhancing additive mentioned in Chapter III.

ii) Grain growth.

The sintered polycrystals were annealed at 1250°~ 1420°C for 4 hr in N<sub>2</sub> - O<sub>2</sub> atmosphere to observe the growth of individual grains.

Si contained solution [ethylsilicate Si(C<sub>2</sub>H<sub>5</sub>O)<sub>4</sub> ], which is used as an adhesive solution bonding the polycrystals and a single crystal mentioned afterwards, spread on the mirror surfaces of both B doped ferrite and Na doped one. And then they were annealed at 1250°~ 1420°C for 4 hr in N<sub>2</sub> to observe combination effect of additives and Si on enhancing the grain growth.

iii) Solid state single crystal growth.

A Mn-Zn single crystal grown by Bridgman method was cut into pieces approximately 1 mm x 3 mm x 6 mm, and two of 3 mm x 6 mm surface were lapped to mirror. Each mirror surface was in contact with two kinds of sintered polycrystals (3 mm x 6 mm x 12 mm), which contained 5 ~ 50 ppm B<sub>2</sub>O<sub>3</sub>, and 500 ppm (0.05 wt%) Na, respectively. Metal alkoxide (Si) solution, ethylsilicate, H<sub>2</sub>O and HNO<sub>3</sub> were used as an adhesives.

These "joint samples" were annealed at 1250°~ 1420°C for 4 hr in N<sub>2</sub> - O<sub>2</sub> atmosphere.

iv) Characterization



The shrinkage curves of the molded compacts were measured by a dilatometer in flowing  $N_2$  atmosphere (150 cc/min.) from the room temperature to 1250°C at the heat-up rate of 300°C/h.

The average grain size of each samples after heat treatment was measured from the photographs taken on the joint surface after etching. The porosity was measured by the pores on the mirror surface by a porosimeter.

X-ray diffraction analysis was carried out to determine the crystallographic planes and axis, and SIMS analysis was used to observe the distribution of Si, B and Fe in the samples. Induced coupled plasma analysis (ICP) was used to determine the amount of B remained in the sintered body.

The magnetic properties of the samples were measured as the same way described in Chapter I.

### 3. Results and discussion

#### 3.1) Choice of metal ions for enhancing the grain growth.

Figure 1 shows the grain size of the sintered bodies which contain additives ( $Nb_2O_5$ ,  $SiO_2$ ,  $V_2O_5$ ,  $Bi_2O_3$ ,  $SnO_2$ , Na and B) as a function of the amount of these additives. It has been observed and reported<sup>12)</sup> that grain growth is rapid when a small amount of liquid wets the grain-boundary area. Although a liquid-phase formation alone is not sufficient for an additive to induce exaggerated grain growth in

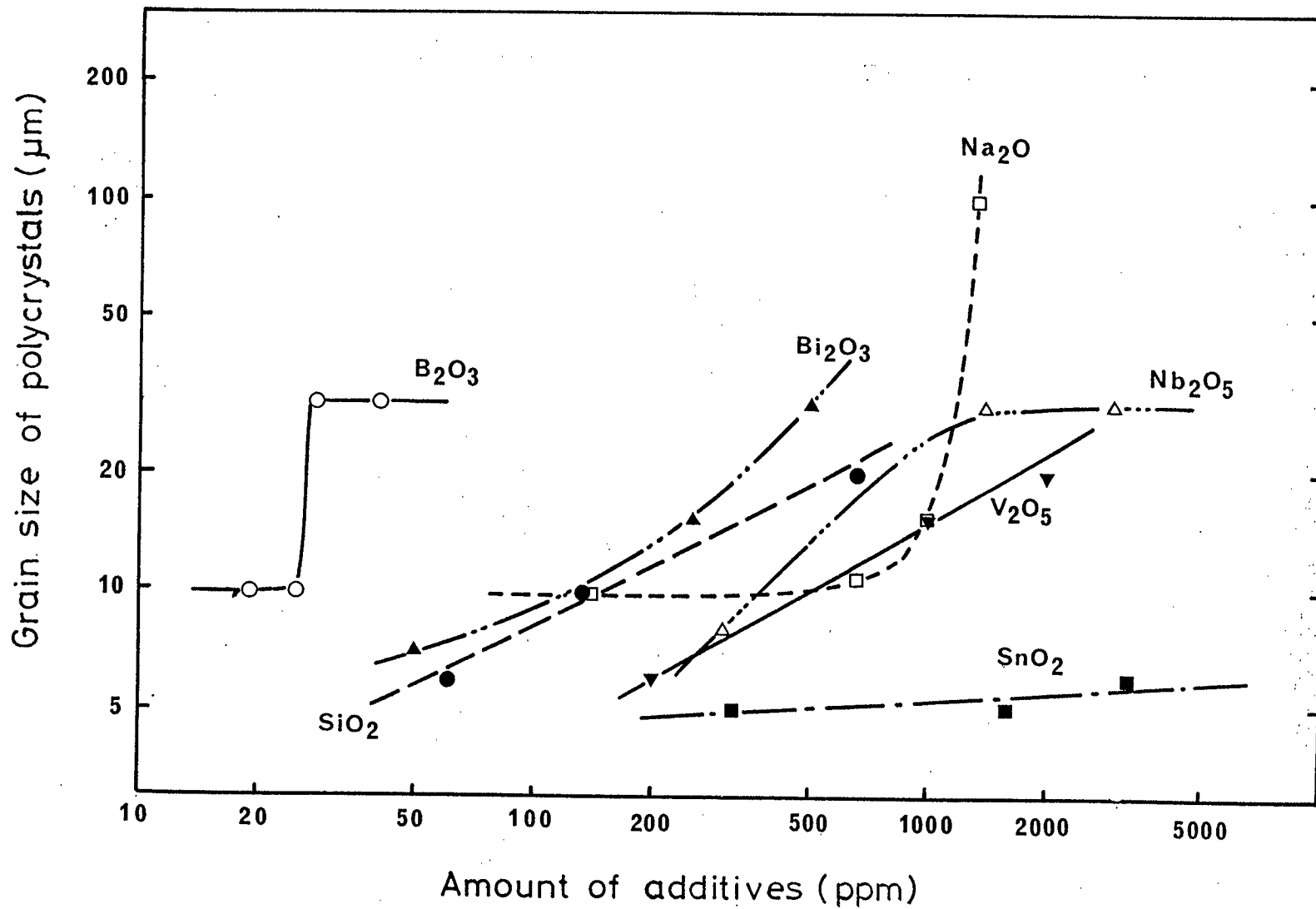


Fig.1 Grain size of Mn-Zn ferrite polycrystals with additives sintered at  $1250^\circ\text{C}$  6 hr in  $\text{N}_2$ - $\text{O}_2$  as a function of amount of additives.

ferrites, it is interesting to observe that many grain-growth-promoting additives either melt or form a low-melting eutectic with the host material at sintering temperatures.

$B_2O_3$  (melting point  $T_m=577^\circ C$ ),  $V_2O_5$  ( $T_m=690^\circ C$ ), and  $Bi_2O_3$  ( $T_m=820^\circ C$ ), melt well below sintering temperature and these molten oxides probably wet the ferrite grain boundaries and promote grain growth.  $SiO_2$  ( $T_m>1700^\circ C$ ) induces exaggerated grain growth in the ferrite and  $SiO_2$  and FeO form a low-melting eutectic at about  $1180^\circ C$  in  $N_2$  atmosphere<sup>13</sup>).

In the case of  $Nb_2O_5$  ( $T_m=520^\circ C$ ), microstructures of ferrite shows planar grain boundaries between the large separate grain and the fine matrix similar to those observed in samples produced by well known liquid-phase-forming dopants such as  $B_2O_3$  or  $V_2O_5$ . The grain morphologies thus suggest that the abnormal and matrix grains are separated by a liquid film and the exaggerated grain growth occurs by dissolution and precipitation in a liquid medium at sintering temperatures, analogous to the phenomenon of Ostwald ripening.

If the amount of a liquid-phase or low-melting eutectic were not enough to wet the ferrite grains, abnormal grain growth were not induced. The preliminary experiment showed that Sn ions induced the grain growth at the surfaces of the Mn-Zn ferrites, but the polycrystals sintered at  $1250^\circ C$  6 hr, which contained  $SnO_2$  ( $T_m=1127^\circ C$ ) as additives, increased the grain size little with the amount of 300 ~ 3000 ppm additives as shown in Fig. 1.

As compared with other additives, the effect of grain-growth-enhancement by  $\text{SnO}_2$  was as small as reported,<sup>1)</sup> the polycrystals with  $\text{SnO}_2$  were not suitable for the following experiments.

As concerns the starting materials for a solid state single crystal growth, there is a limit of additive amount to the polycrystals. Because it uses the abnormal grain growth, which is easy to occur in the fine grain matrix even though adopting the grain-growth-promoting additives, the fine grain is required.

For example, supposing the initial grain size be less than about 30  $\mu\text{m}$ , the limit of the addition of B is less than about 15 ppm and that of Na is less than about 1000 ppm from the result of Fig. 1.

### 3.2) Grain growth of the ferrites after annealing.

The ferrites after annealing had the additives, amounts of which were less than the limit of addition. The results are shown in Fig. 2. The ferrite without additives showed that the grain size remained almost the same on heating up to 1360 °C and the normal grain growth (continuous grain growth) occurred above 1360 °C, but the ferrites with additives such as B,  $\text{SiO}_2$ , Na and  $\text{V}_2\text{O}_5$  showed the abnormal grain growth (discontinuous grain growth) after the annealing higher than 1280 °C. No further experiment using  $\text{Nb}_2\text{O}_5$ ,  $\text{V}_2\text{O}_5$  and  $\text{SiO}_2$  was undertaken, since the effect of enhancing the grain growth was not noticeable compared to the cases of B and Na.

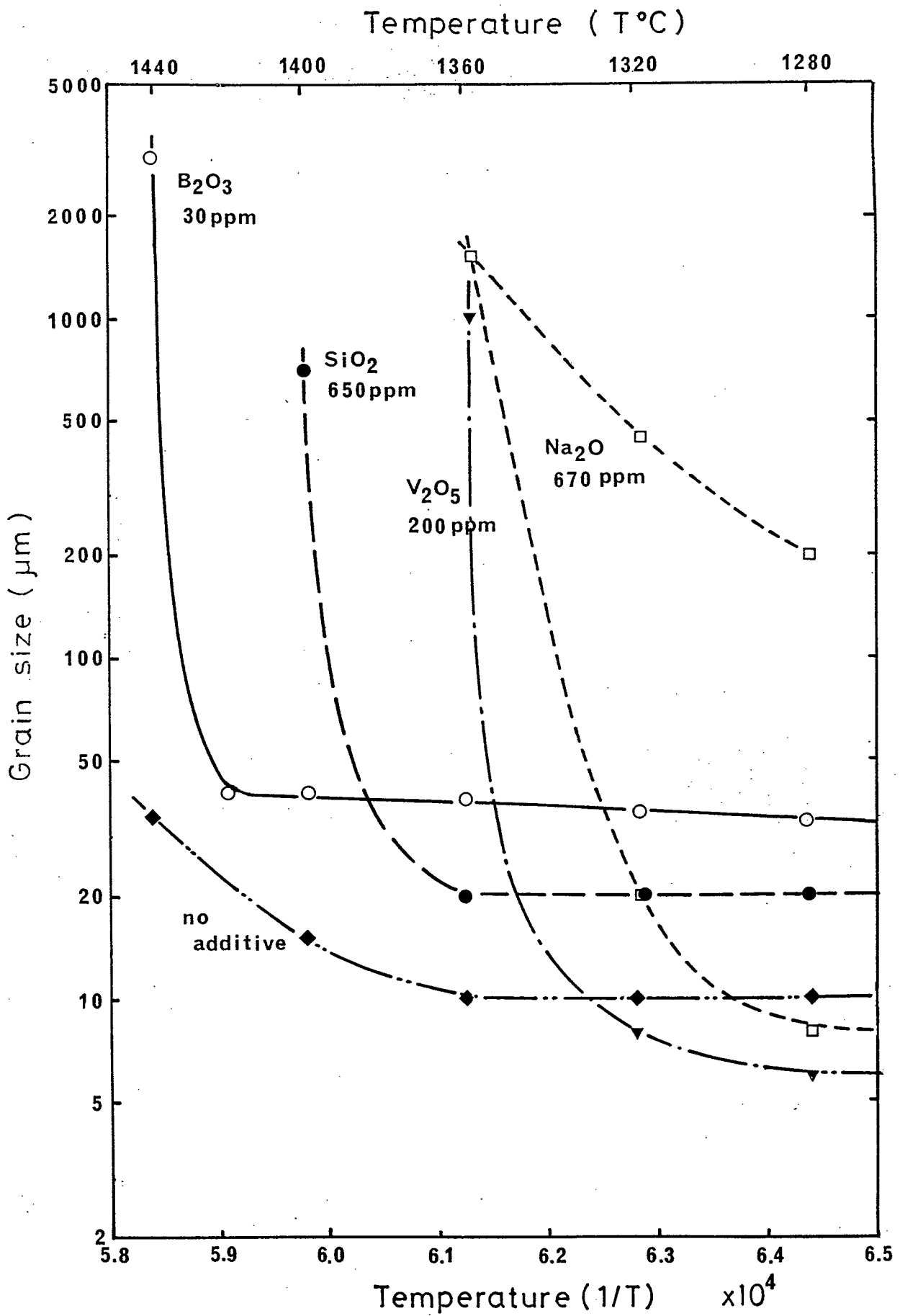


Fig.2 Grain growth of Mn-Zn ferrite polycrystals without and with additives annealed at each temperature for 4 hr in  $\text{N}_2$ .

The Na doped ferrite exhibited the discontinuous grain growth at temperature higher than 1280 °C. This is relatively low compared to the case of other additives. The giant grains were observed near the surface of sintered bodies in Na doped ferrite, implying that the grain growth was strongly related to the atmosphere at the time of heat treatment. On the other hands, the giant grains grew up inside the polycrystals in other additives.

The size of finally obtained grain was 3000 ~ 5000  $\mu\text{m}$  in B doped ferrite and about 1500  $\mu\text{m}$  for other additives. The difference in the final grain size depends on both the kind and the amount of additives.

The onset temperature of the discontinuous grain growth induced by B is higher than that of other additives, and the concentration of nucleus which is the origin of seed crystal can be low because of the small amount of the additive. Accordingly the final grain size is the largest among the additives of this study.

The addition of B induces the largest final grain size, but it is difficult to fabricate sintered body of high density. The addition of Na induces the densely sintered bodies, as described in Chapter III.

The former is important to fabricate the large single crystal in a short heat treatment time and the latter is important when it is used as the material for the magnetic head.

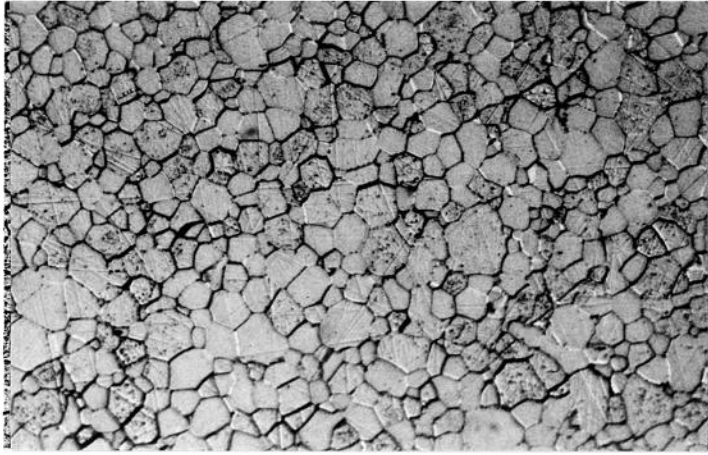
3.3) Preparation of  $\text{B}_2\text{O}_3$  doped Mn-Zn ferrites with high density.

The shrinkage curves during the sintering were measured about the compacts with 0, 25, 45 ppm  $B_2O_3$  dopants. There was little difference among these three curves except the initial shrinkage of the 45 ppm  $B_2O_3$  doped compact between 500 ° and 700°C. But the microstructures of 25 or 45 ppm  $B_2O_3$  doped bodies depend on the sintering condition especially on the heat-up conditions as shown in Na doped ferrites in Chapter III. As the melting point of  $B_2O_3$  is about 580°C, B doped compact is necessary to be heated up with a  $B_2O_3$  liquid at temperatures higher than 580°C.

Generally  $B_2O_3$  is a flux for many oxide ceramics,<sup>14)</sup> and liquid phase helps good process of sintering excluding the case of B doped ferrite.

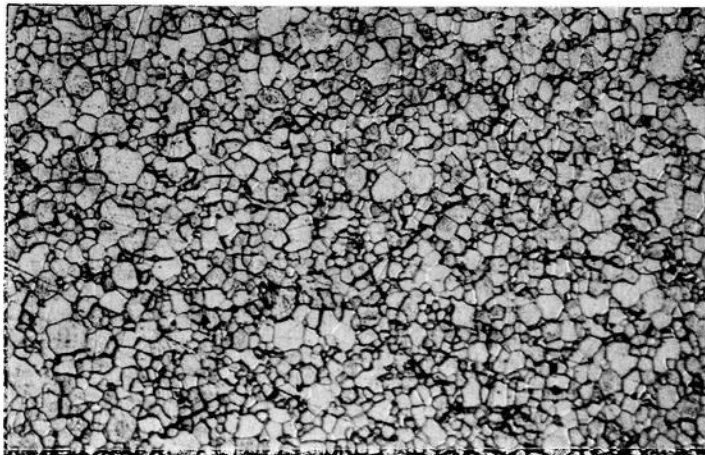
The B doped ferrite sintered at the conventional sintering condition, or the constant heat-up rate of 300°C/h to 1250°C for 6 hr, consists of duplex structures. On the other hand, the ferrites sintered by the controlled rate<sup>15)</sup> (300°C/h; 25° ~ 450°C, 150°C/h; 450° ~ 550°C, 100°C/h; 550° ~ 600°C, 220°C/h; 600° ~ 750°C, 40°C/h; 750° ~ 950°C, 150°C/h; 950° ~ 1050°C, 300°C/h; 1050° ~ 1250°C) consists of small grains. The representative microstructure of the  $B_2O_3$  doped ferrites are shown in Fig. 3; (a) is one prepared under conventional sintering condition, (b) is by the rate controlled sintering.

3.4) Adhesion of a single crystal plate on the polycrystals.



(a)

100  $\mu$ m



(b)

Fig.3 The microstructure of 25 ppm  $B_2O_3$  doped Mn-Zn ferrites. (a) sintered at conventional sintering condition; constant heat-up rate of 300  $^{\circ}C/h$  to 1250  $^{\circ}C$  for 6 hr, (b) sintered by the rate controlled sintering to 1250  $^{\circ}C$  for 6 hr.



To fabricate a single crystal ferrite by a solid state reaction, it is necessary to adhere a single seed crystal to the polycrystal which exhibits abnormal grain growth. The single seed crystal, plays a role of nucleus and an origin of abnormal grain growth, and also controls the crystal growth direction.

The flatness and roughness of the adhesive mirror surfaces of both the single crystal and polycrystal, should be less than  $1 \mu\text{m}/6 \text{ mm}$  and  $0.5 \mu\text{m}$ , respectively. Three kinds of adhesive solutions, ethylsilicate,  $\text{H}_2\text{O}$  and  $\text{HNO}_3$  were tested in comparison.

The joint samples were annealed at  $1100^\circ \sim 1300^\circ\text{C}$  and after that the samples were cut and observed by using a microscope.

The joint samples adhered with an ethylsilicate were tightly connected in solid state on heating at  $1200^\circ\text{C}$  for 1 hr, but other samples adhered with  $\text{H}_2\text{O}$  or  $\text{HNO}_3$  needed treatment at temperature higher than  $1250^\circ\text{C}$  to obtain similar result to ethylsilicate.

Si atoms in ethylsilicate react with Fe in ferrite and forms a Fe-silicate such as fayalite,  $\text{Fe}_2\text{SiO}_4$ . As the melting point of this kind of compounds are around  $1200^\circ\text{C}$ , liquid phase is probably produced at the interface between poly and single crystals and this made the connection tight. No evidence of production of liquid,  $\text{Fe}_2\text{SiO}_4$ , however, was microscopically observed at the interface of poly-single crystals, but the joint sample composed of single-single crystals showed the existence of  $\text{SiO}_2$  layer between them.

These phenomena are explained by the difference of diffusibility of Si to the ferrite single crystal and polycrystal; low volume diffusion in the single crystal and rapid grain boundary diffusion in the polycrystal.<sup>17)</sup>

Since it has been known that Si has an enhancing effect of grain growth, preferred orientations of growth were investigated.

Figure 4 shows the X-ray diffraction intensities of (hkl) planes in the polycrystalline ferrite with 500 ppm Na.

This sample was prepared under the condition; an ethylsilicate solutions was spread on its mirror surface about 1000 ~ 2000 Å thick layer calculated as SiO<sub>2</sub> compound, and then it was annealed at 1320°C-2 hr and 1340°C-2 hr in N<sub>2</sub>.

Since the grain size of annealed samples were as large as about 1000 ~ 1500 μm, X-ray analysis was done by rotating the samples with rotating speed about 300 rpm to measure the X-ray diffraction from the grains of wide area. The depth profile of X-ray diffraction intensities was measured by lapping the surfaces of the samples. In Fig. 4, the horizontal axis shows the depth from the surface of the polycrystal where ethylsilicate solution had been spread.

The X-ray diffraction intensities of (hkl) planes of a "conventional" Mn-Zn ferrite polycrystal are shown in the vertical axis in Fig. 4 as normalized by the intensity of (311) planes [maximum intensity], to compare with the ethylsilicate spread sample. From Fig. 4, it is seen that the intensity ratio of the surface is nearly the same as that of a "conventional" ferrite.

Standard polycrystal

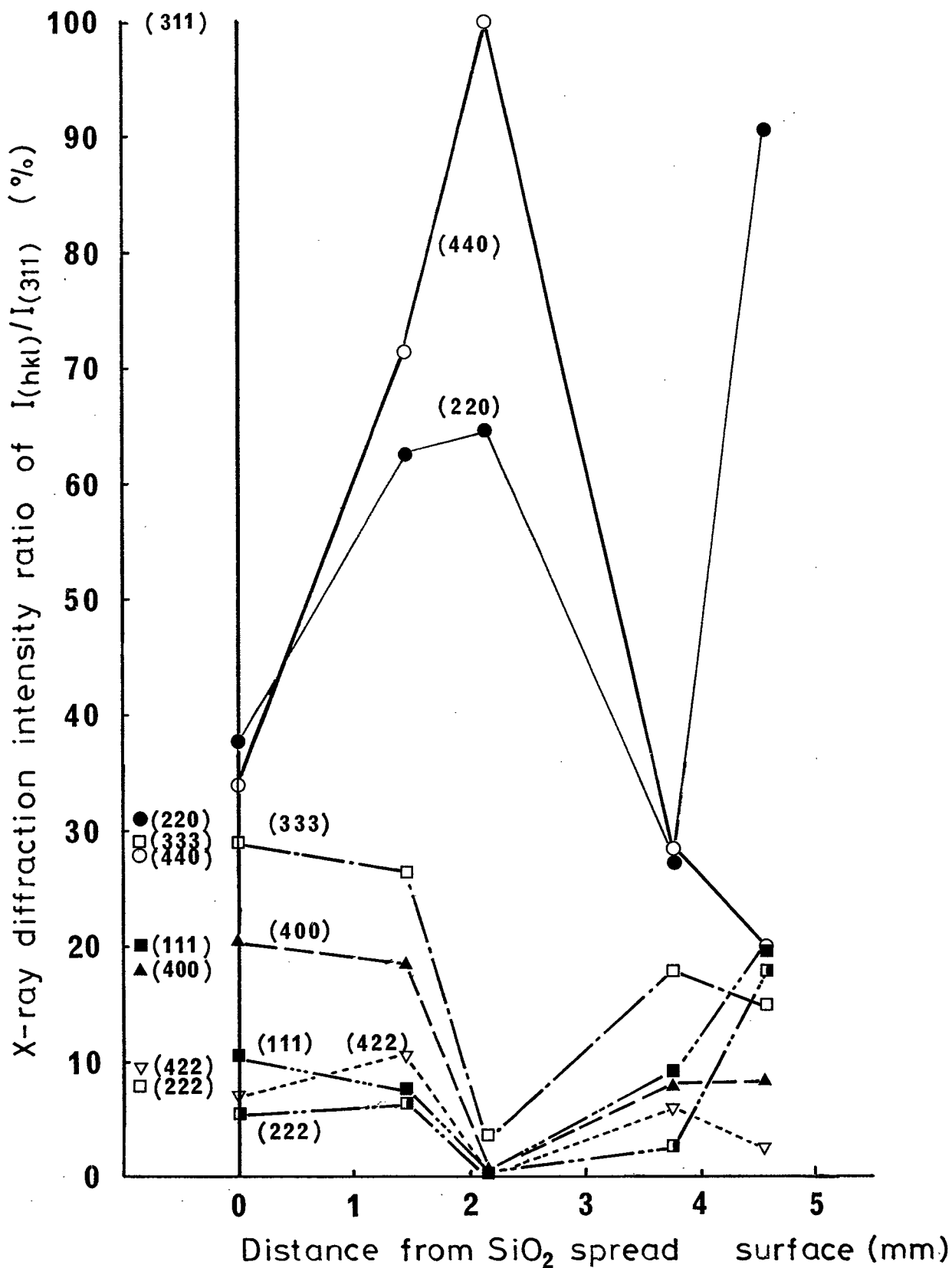


Fig.4 The relation between X-ray diffraction intensity ratios of  $I(hkl)/I(311)$  and the sampling position inside from the ethylsilicate ( $\text{SiO}_2$ ) spread surface. The intensity ratios of standard polycrystal are also shown.

But about 2 mm inside the polycrystal, the diffraction intensities of (220) and (440) planes are strong and predominant compared to other planes, indicating that  $\langle 110 \rangle$  axis is the preferential direction of grain growth. On the contrary, the hard  $\langle 111 \rangle$  and  $\langle 211 \rangle$  axes, which are perpendicular to  $\langle 110 \rangle$ , are difficult direction for grain growth.

### 3.5) Solid state growth of single crystal

The relationship between the heat treatment condition and the length of grown crystal were studied, using the joint samples composed of the single crystal and 5 ~ 50 ppm  $B_2O_3$  doped Mn-Zn ferrite and 500 ppm Na doped Mn-Zn ferrite. Ethylsilicate solution was used as an adhesives, because other samples adhered with  $H_2O$  or  $HNO_3$  did not show the single crystal growth except for the abnormal grain growth of the individual grains in polycrystal.

The relation between the length of the single crystal growth from 500 ppm Na doped polycrystal,  $L_s$  (mm) and reciprocal of the heat treatment temperature,  $1/T$  (1/K) are shown as a parameter of (hkl) planes of a single crystals in Fig. 5. From Fig.5, it is understood that  $\ln(L_s)$  vs.  $1/T$  shows the linear relations and satisfies the following equation;<sup>18)</sup>

$$L_s = \text{const.} \cdot t^{1/n} \exp(-\Delta E/RT) \quad (1)$$

where  $t$  is the annealing time,  $\Delta E$  an activation energy,  $R$  gas constant.

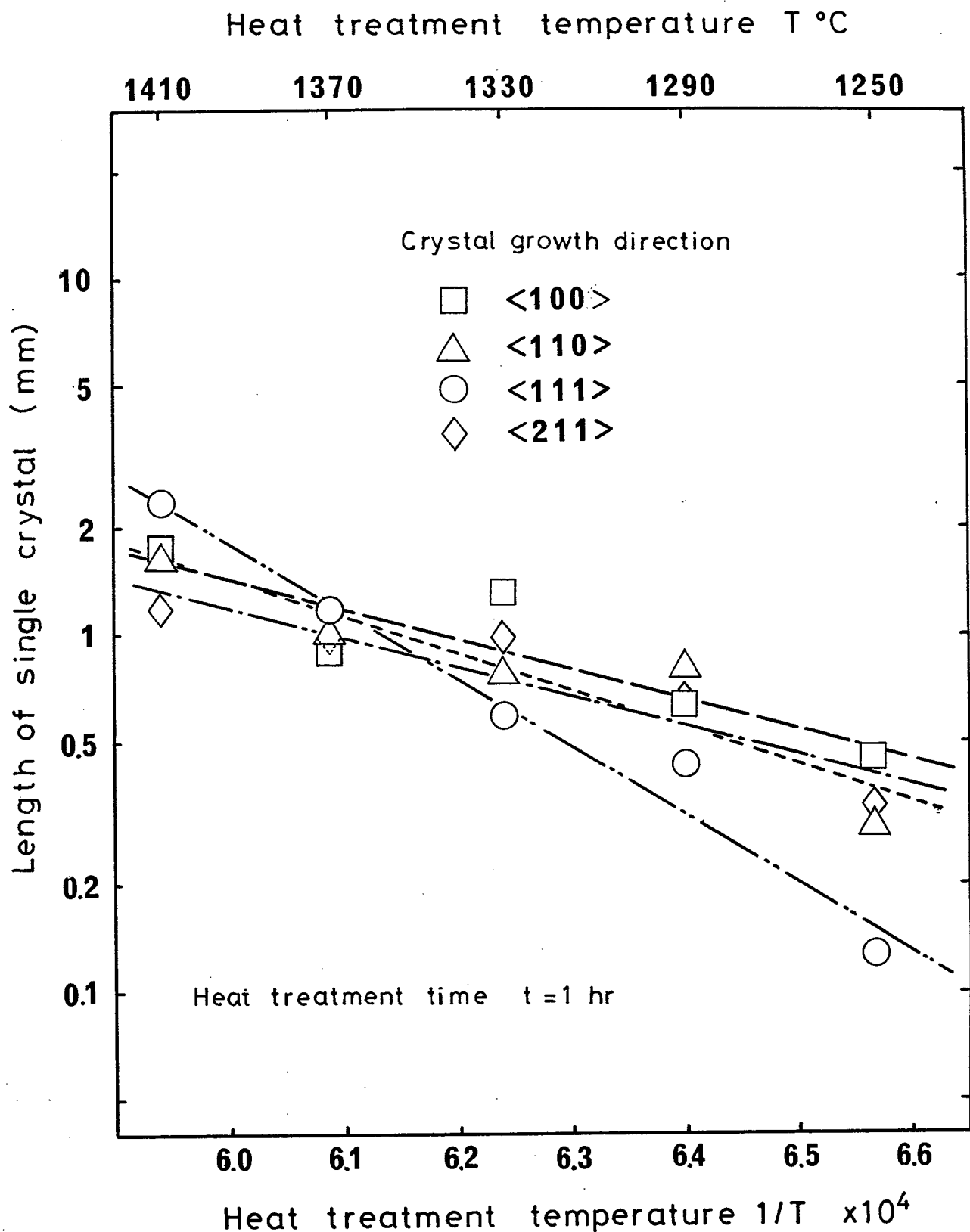


Fig.5 The relation between length of single crystal grown from Na 500 ppm doped Mn-Zn ferrite polycrystal and heat treatment temperature. Heat treatment time was 1 hr and crystal growth direction was varied.

From equation(1), following equation is directly obtained.

$$\ln(L_s) = \text{const.} + 1/n \ln(t) - \Delta E/R \cdot 1/T \quad (2)$$

The least-squares fit gives an activation energy  $\Delta E$  for abnormal grain growth;  $\Delta E$  is  $\sim 67.5$  kcal/mol for  $\langle 111 \rangle$  direction, and  $\sim 42.1$  kcal/mol for other directions. There is good agreement between these values and an activation energy ( $\sim 62.5$  kcal/mol) which was reported on the abnormal grain growth induced by  $\text{TiO}_2$  doping to Mn-Zn ferrite.<sup>1)</sup> From Fig.5,  $L_s$  of each  $\langle hkl \rangle$  direction are,  $L_s[100]$ ,  $L_s[110]$ ,  $L_s[211] > L_s[111]$ , under the temperature of about  $1370^\circ\text{C}$ .

In Fig. 6,  $L_s$  used with 500 ppm Na doped Mn-Zn ferrite are plotted against the annealing time, 't' (hr) under the constant temperature of  $1330^\circ\text{C}$ . From Fig. 6, it is confirmed that  $\ln(L_s)$  vs  $\ln(t)$  also satisfies Eq.(2) and 'n' varies between 1.30 (for  $\langle 111 \rangle$  direction) and 1.98 (for other directions). This  $n=1.98$  value is nearly the same as  $n=2$  which was reported on  $\text{TiO}_2$  doped ferrite.<sup>1)</sup>

In the same way, the joint sample composed of the single crystal and 18 ~ 42 ppm  $\text{B}_2\text{O}_3$  doped Mn-Zn polycrystalline ferrite was heat treated at the temperature between  $1380^\circ$  and  $1420^\circ\text{C}$  for 4 and 12 hr in  $\text{N}_2$  atmosphere.

As is seen in the comparison of final grain sizes between B doped and Na doped ferrites, the single crystal growth length,  $L_s$ , of B doped ferrite is larger than that of Na doped ferrite. The relations between the length of grown crystal,  $L_s$ , and the reciprocal of treated temperature,  $1/T$ , satisfy the Eqs. (1) and (2).

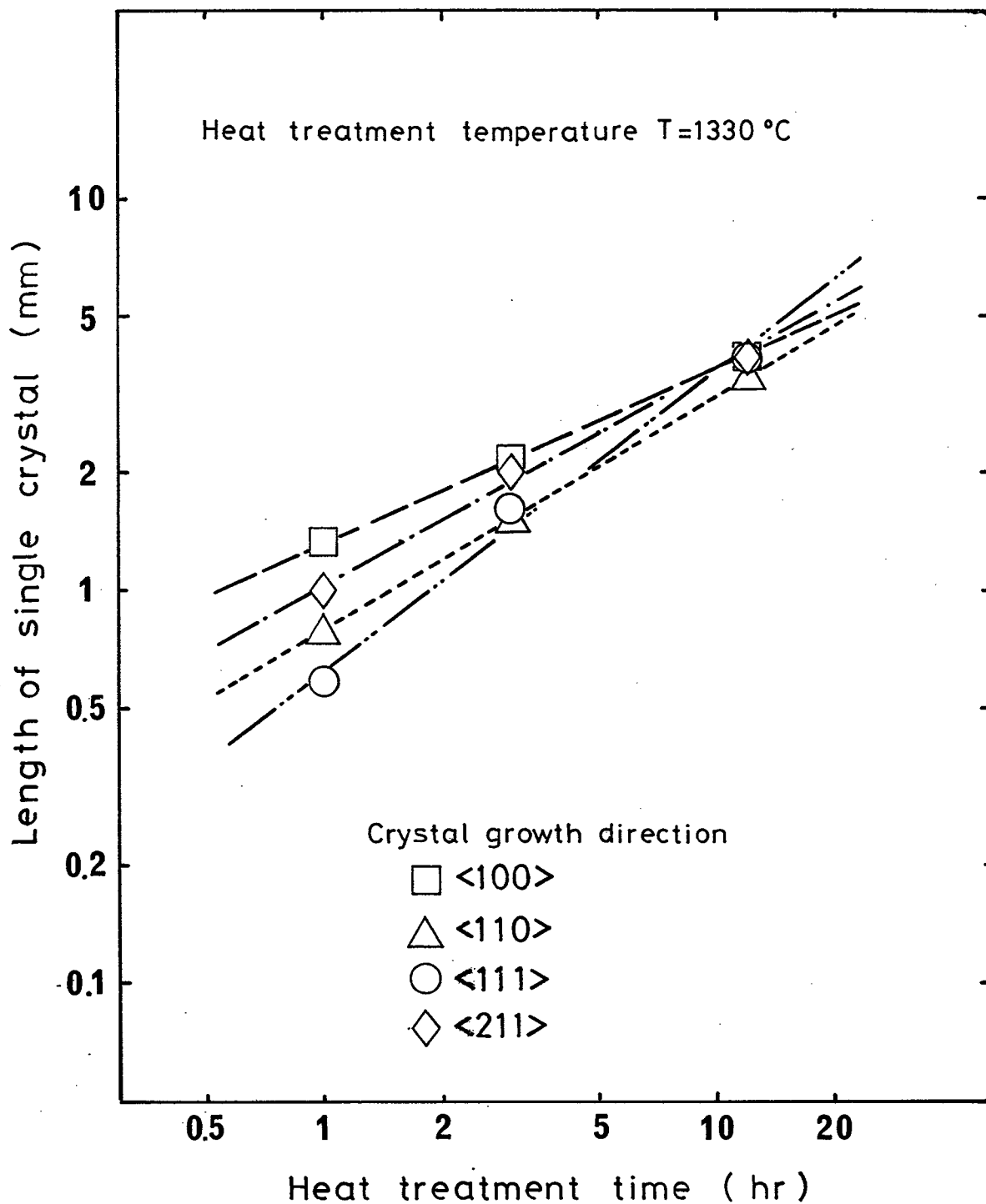


Fig.6 The relation between length of single crystal grown from Na 500 ppm doped Mn-Zn ferrite polycrystal and heat treatment time. Heat treatment temperature was  $1330\text{ }^{\circ}\text{C}$  and the crystal growth direction was varied.

They are shown in Figs. 7 and 8, together with the concentration dependency of Ls.

In Fig. 7, Ls are plotted in two cases of 1400°C-4 hr and 1400°C-12 hr. The blacked out marks mean that the large grains coexist with the grown single crystal in the joint samples. The Ls is proportional to the amount of  $B_2O_3$  in the range between 18 and 30 ppm, and subsequently Ls decreases with the increase of  $B_2O_3$  additive because the existence of the large grains, suppress the single crystal growth.

### 3.6) Mechanism of single crystal growth.

In this study, B and Na addition were used to induce the exaggerated grain growth of the polycrystals and Si, which was contained in an adhesive solution, also takes an important role to promote the single crystal growth.

Figures 9 (a), (b) show Si, B and Fe ions distribution at the cross section of the assembly of crystal, the grown single crystal and the polycrystal of the joint sample after heat treatment. The sample was polished by  $Al_2O_3$  powder abrasives instead of the SiC powder ones because the distribution of Si ion was measured about the polished surface.

The concentrations of Si and B in both the polycrystal and interfaces between the seed single crystal and the grown single crystal are higher than that of the grown single crystal, and inversely the concentration of B of the seed crystal is the lowest among them. On the other hand, the distribution of Fe ion is constant.



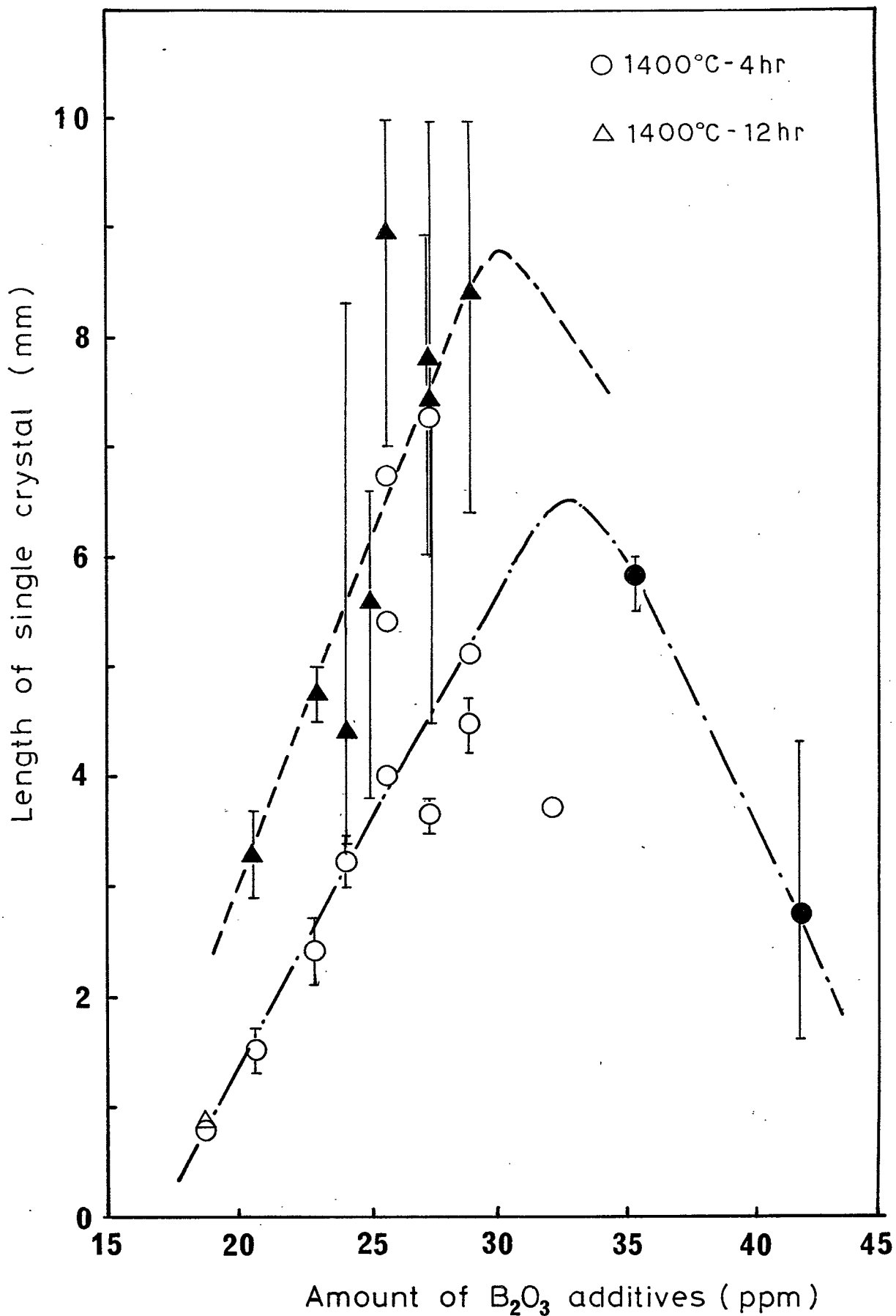


Fig.7 The relation between length of single crystal grown from B<sub>2</sub>O<sub>3</sub> doped ferrite polycrystals and the amount of B<sub>2</sub>O<sub>3</sub> additive. Heat treatment condition were 1400 °C-4 hr and 1400°C-12 hr in N<sub>2</sub>.

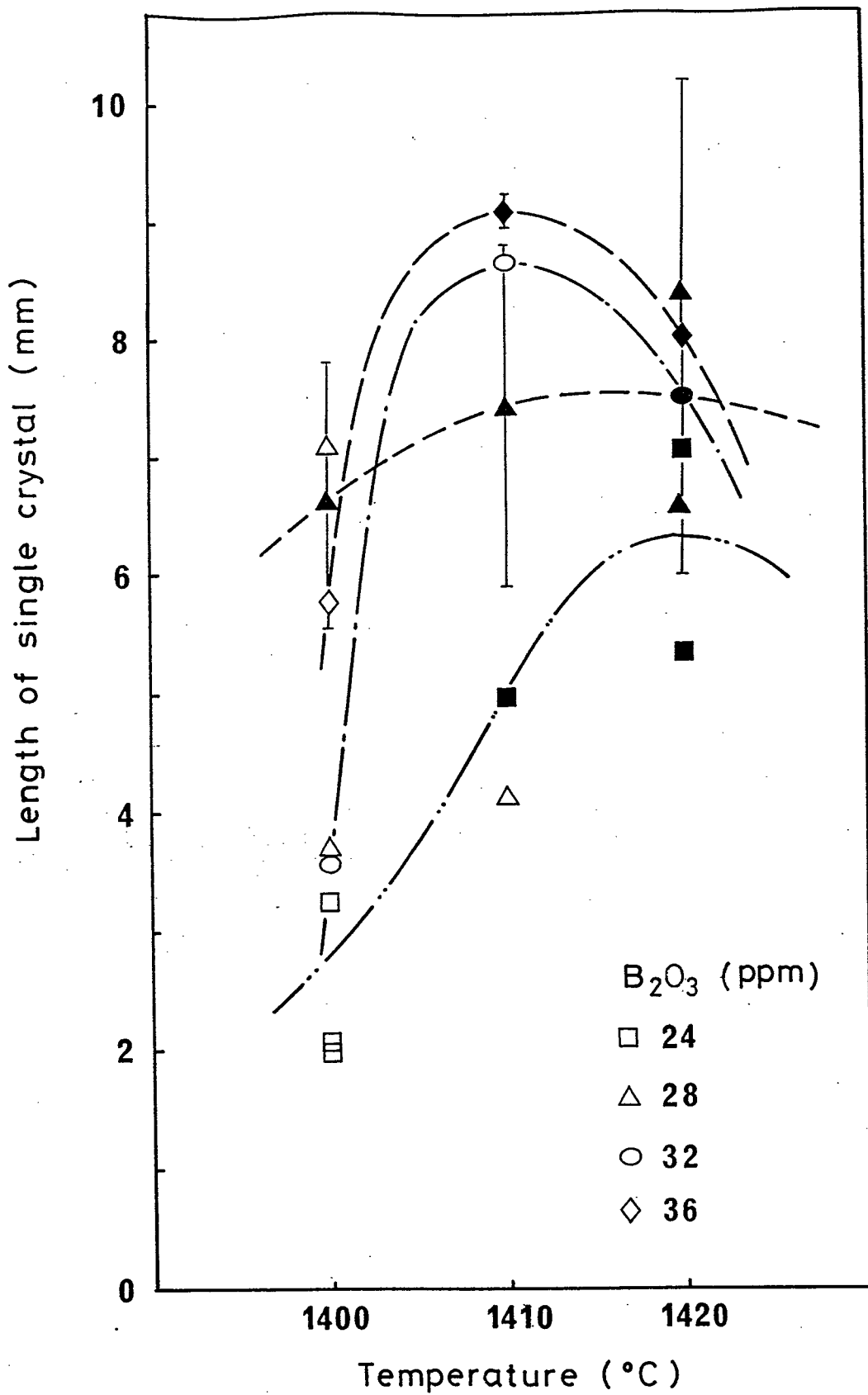


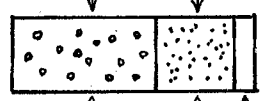
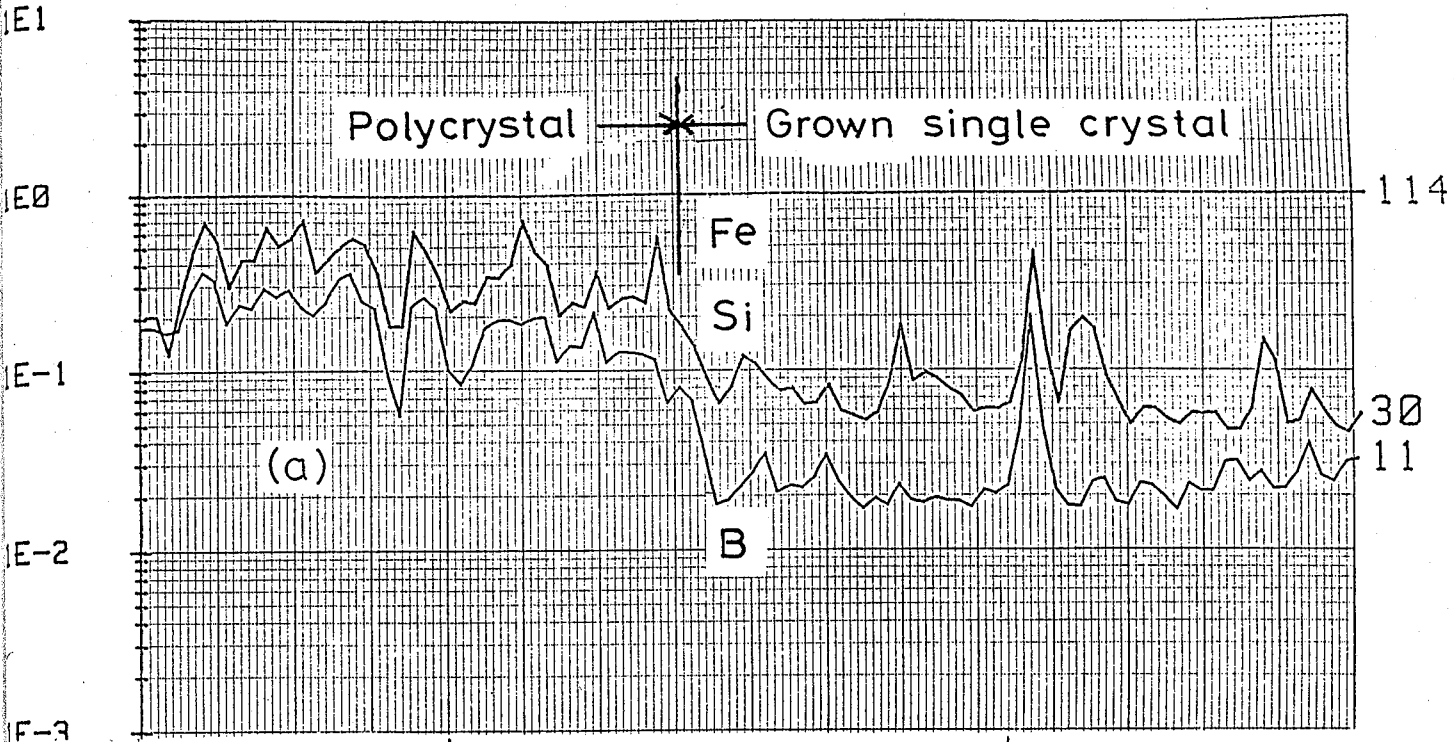
Fig.8 The relation between length of single crystal and heat treatment temperatures as a parameter of amount of B<sub>2</sub>O<sub>3</sub> addition.

Therefore, Si and B is considered to be swept from the grown single crystal to the polycrystal portions.

The distribution intensities of Si and B are nearly the same in both the polycrystals and the grown single crystal as shown in Fig. 9 (a), (b). It is said that Si and B ions are segregated at the grain boundaries of polycrystal.<sup>19)-21)</sup>

A model of growth mechanism of single crystal is illustrated in Fig. 10. Figure 10 (a) shows the joint sample composed of a seed single crystal, adhesive layer and the polycrystal which has the tendency to abnormal grain growth by the additives. Figure 10 (b) illustrates the distribution of the additives involved in the joint sample. The abscissa and ordinate represent the distance from the contact surface of the seed crystal and the concentration of the additives respectively, where  $C_1$  is the initial concentration in the polycrystal,  $C_x$  is the level at which the abnormal grain growth is generated at the given temperature of  $T=T_1$ , and  $C_0$  is the initial concentration of the additive.

Figure 10 (c) illustrates the relation between the grain size of the polycrystal and the heat treatment temperature, where temperature  $T=T_x$  denotes the onset temperature of the abnormal grain growth under the condition of the additive concentration level  $C=C_1$ . If the additive concentration changes from  $C_1$  to  $C_x$ , the onset temperature shifts towards lower temperature  $T_1$ .



0.5 mm

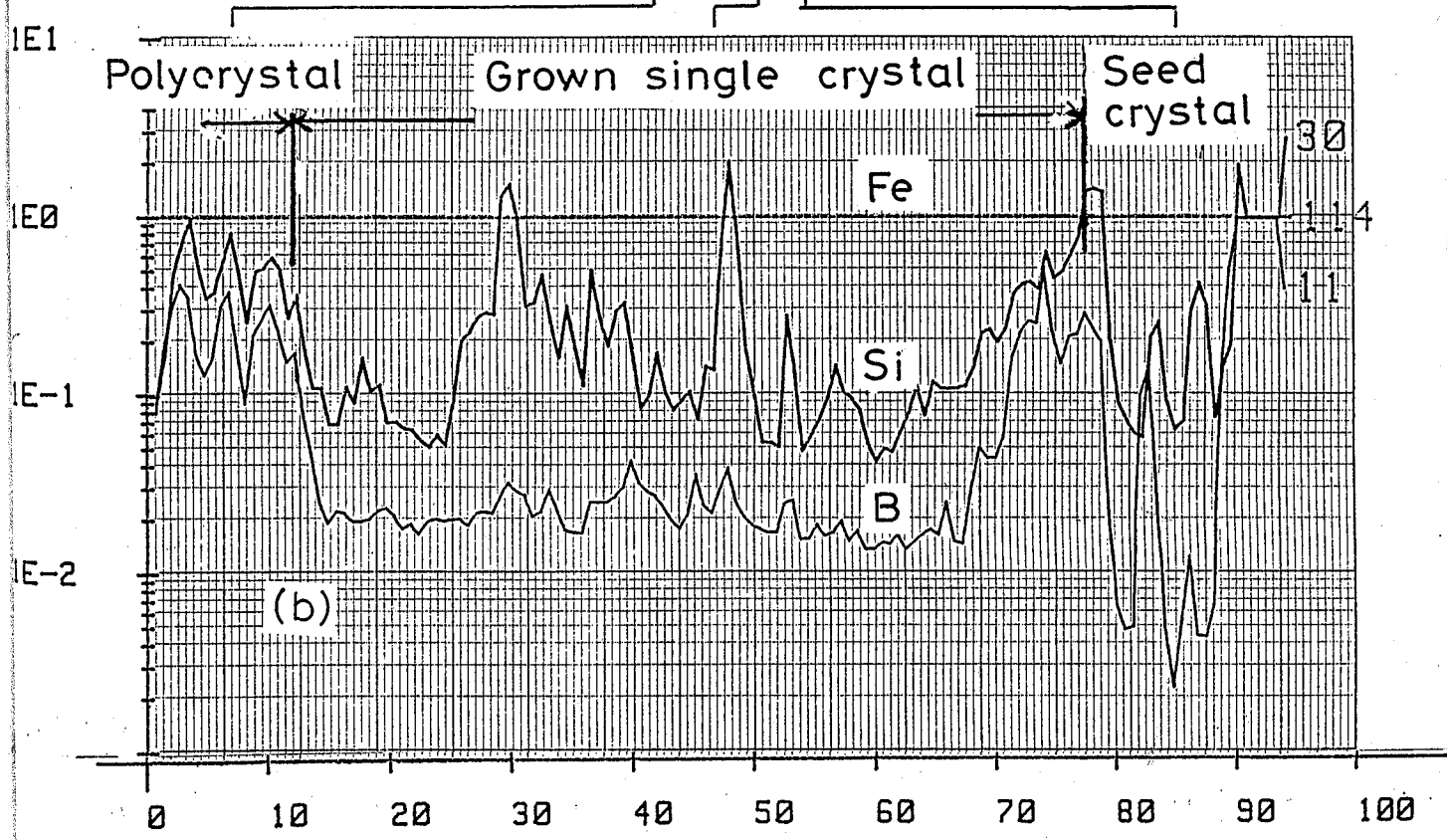


Fig.9 The distribution of B, Si and Fe in the joint sample composed of seed single crystal,  $B_2O_3$  doped Mn-Zn ferrite polycrystal, and grown single crystal. Analyses were undertaken by SIMS; (a) shows the portion of polycrystal and grown single crystal, (b) shows polycrystal, grown single crystal and seed single crystal.

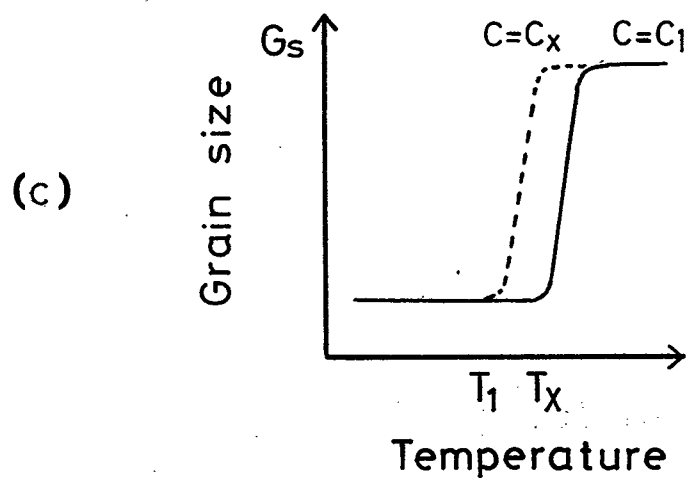
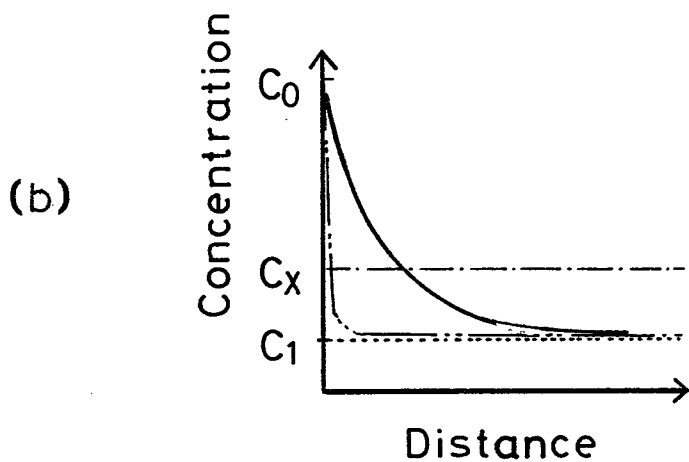
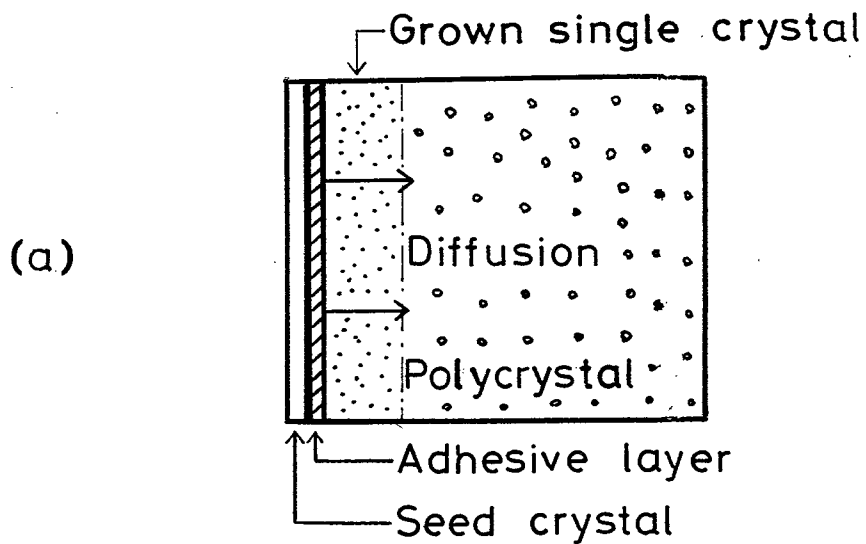


Fig.10 (a) Schematic figure of the joint sample. (b) illustrates the relation between the concentration of additive and the distance from the interface or the adhesive layer. (c) illustrates the relation between grain size and temperatures as a parameter of the additive concentration.

When the joint sample is held at temperature  $T_1$ , and heat treatment time reaches  $t_1$ , the distribution curve of the additive ion changes by diffusion and the concentration level in the polycrystal reaches  $C_x$ , where the abnormal grain growth begins and the single crystal grows.

Once the single crystal grows, the additives B and Si are swept out from the grown single crystal to the front boundary of the grown single crystals. This model can be correlated to the result of Fig. 9.

### 3.7) Magnetic properties of grown single crystal

The magnetic properties of Mn-Zn ferrite polycrystal and single crystal are listed in Table 1.

The polycrystal without additives was prepared by a sintering condition of 1250°C for 6 hr in 1 vol%  $O_2$ - 99 vol%  $N_2$  gas.

In the case of measuring the magnetic properties by using a toroid of single crystal, a vertical axis of the toroid was parallel to  $\langle 111 \rangle$  axis of the single crystal.

The polycrystal ferrite has relatively large coercive force and high disaccommodation, compared with the single crystal ferrites, because the former is due to existence of the grain boundaries and impurity segregation or precipitation in the sintered body, the latter is due to the oxidative sintering atmosphere, respectively.

Among single crystals, SX-Na-1 has high coercive force and low permeability and after annealing of 2 vol%  $O_2$  atmosphere, coercive force and permeability were improved (SX-Na-2).

Samples Properties	Poly.	SX-Na-1	SX-Na-2	SX-B	SX-1
Magnetic flux density $B_{10}$ (T) in field of 795.8 (A/m)	0.47	0.47	0.47	0.47	0.47
Remnant magnetization $B_r$ (T)	0.25	0.12	0.12	0.12	0.16
Coercive force $H_c$ (A/m)	19.1	7.9	5.6	2.4	1.35
Disaccommodation D.A. (%)	8	0	0	1.5	1.0
Permeability $\mu$ at 0.1 MHz	2400	1700	2500	3500	8000
0.5	2400	1600	2000	2400	3700
1.0	2500	1350	1600	1800	2500
5	1200	650	780	900	900
10	700	450	450	600	600

Table 1. The magnetic properties of Mn-Zn ferrites of poly and single crystal with the same composition. Poly.: a polycrystal used as the starting material, SX-Na-1: a grown single crystal started from Na 500 ppm doped ferrite, SX-Na-2: an annealed SX-Na-1 at 1300 °C in 2 vol% O<sub>2</sub>, SX-B: a grown single crystal started from B<sub>2</sub>O<sub>3</sub> 25 ppm doped ferrite, SX-1: a single crystal produced by Bridgman method.

SX-B shows the best magnetic properties among the single crystals. This is probably due to both the kind of additive and the amount of additive. Since Na is univalent and the amount of additive is much, vacant sites for metal ion or a lot of  $\text{Fe}^{3+}$  are produced in the lattice, while B is trivalent and its amount is very little, therefore there is little influence of additive on the lattice. This explains that Na doped single crystal is improved by annealing because of re-adjustment of the ratio of  $(\text{Fe}^{2+}/\text{Fe}^{3+})$  and that B doped one does not change the magnetic properties after annealing.

There is a little difference in magnetic properties between solid state single crystal (SX-B) and Bridgman single crystal (SX-1); SX-1 has higher permeability at low frequencies than that of SX-B. This is attributed to the difference in the fabrication process. This probably results in the dislocation density in the product and SX-1 has better quality as far as the lattice perfection is concerned. These dislocations have some influence on the permeability at low frequencies and coercive force.

The magnetic head requires high permeability at high frequencies and this kind of defect hardly affect the practical use of the solid state single crystal as VTR head.

#### 4. Conclusion.



Grain growth of Mn-Zn ferrites with additives was examined and its application to the crystal growth was attempted. Among grain growth enhancing additives, the effect of Na and B on the microstructure were investigated in detail.

Conversion of polycrystal to a single crystal was tried using an assemblage of polycrystals adhered to seed single crystal and the mechanism of formation of single crystal was discussed.

The magnetic properties of these single crystals were measured and compared with both the starting polycrystal and a single crystal prepared by the Bridgman method.

The solid state single crystal made from B doped ferrite showed to possess nearly the same permeability at high frequencies as the Bridgman single crystal.

## 5. References

1. M. F. Yan and D. W. Johnson, Jr., J. Am. Ceram. Soc., 61, 342 ~ 349 (1978).
2. D. F. K. Hennings, R. Janssen and P. J. Reynen, *ibid.*, 70, 23 ~ 27 (1986).
3. H. Schmelz, Sci. Ceram. 12, 341 ~ 347 (1984).
4. Y. Matsuo and H. Sasaki, J. Am. Ceram. Soc., 54, 471 (1972).
5. Y. Bando, J. Jpn. Soc. of Powder Metallurgy, 15, 414 ~ 419 (1969).
6. G. R. Chol, J. Am. Ceram. Soc., 54, 34 ~ 39 (1971).
7. N. Yoneda and I. Katoh, *ibid.*, 61, 465 (1978).
8. G. Petzow and W. A. Kaysser, Sci. Ceram., 10, 269 ~ 278 (1980).
9. H. Tamura and T. Yoshida, J. Ceram. Soc. Jpn, 83, 28 ~ 33 (1975).
10. M. Kinoshita, *ibid.*, 82, 295 ~ 296 (1974).
11. S. Matsuzawa and Y. Kozuka, Advances in Ceramics edit. F. F. Y. Wang, State Univ. of New York, New York, 15, 527 ~ 532 (1985).
12. M. F. Yan, R. M. Cannon and H. K. Bowen, Ceramic Microstructures '76, edit. R. M. Fulrath and J. A. Pask, Westview Press, Boulder, Colo., 276 ~ 307 (1977).
13. W. C. Allen and R. B. Snow, J. Am. Ceram. Soc., 38, 264 ~ 280 (1955).
14. D. Elwell, A. W. Moriss and B. W. Neate, J. Cryst. Growth 16, 67 ~ 70 (1972).

15. M. L. Huckabee and Hayne Palmour III, Am. Ceram. Soc. Bull., 51, 574 ~ 576 (1972).
16. C. Scott and V. B. Tran, *ibid.*, 64, 1129 ~ 1131 (1985).
17. S. Ogawa, J. Phys. Soc. Jpn., 23, 179 ~ 184 (1967).
18. G. C. Jain and B. K. Das and N. C. Goel, Indian J. Pure Appl. Phys., 14, 87 ~ 92 (1976).
19. T. Akashi, NEC Res. Dev., 8, 89 ~ 106 (1966); 19, 66 ~ 82 (1970).
20. P. E. C. Franken and W. T. Stacy, J. Am. Ceram. Soc., 63, 315 ~ 319 (1980).
21. A. Nakata, H. Chihara and A. Sasaki, J. Appl. Phys. 57, 4177 ~ 4179 (1985).

## Chapter VI. Summaries

Syntheses of Mn-Zn ferrites were studied to improve their magnetic properties and mechanical properties. These ferrite materials were used for the magnetic recording heads such as video tape recorder (VTR) or computer disk memory.

This paper consists of three contents;

1. A new attempt was done to fabricate a Mn-Zn ferrite polycrystal with a cube-texture in order to make use of both the mechanical anisotropy of single crystals and the productivity of polycrystals. This Mn-Zn ferrite was fabricated by adopting thin strip  $\alpha$ -FeOOH and  $\gamma$ -MnOOH as starting powders, those had shape anisotropy. Since  $\alpha$ -FeOOH was main component powder because of  $\text{Fe}_2\text{O}_3$  rich composition ( $\text{Fe}_2\text{O}_3$ : 50 - 55 mol%), large  $\alpha$ -FeOOH powder was newly developed. These hydroxides, fine ZnO powder and binder system were mixed and extruded into the green sheets. By both extrusion and rolling the sheets, the powder oriented compacts were prepared. Topotactic reaction and the grain growth during hot pressing made the Mn-Zn ferrite with grain oriented structure. Developed Mn-Zn ferrite had high orientation of  $Q(110) \geq 95\%$  and  $Q(111) \geq 90\%$  at the same time due to the large  $\alpha$ -FeOOH and new process. This ferrite showed nearly the same wear resistance as the single crystal and intermediate magnetic properties between that of a polycrystal and a single crystal.

2. To control the microstructure of Mn-Zn polycrystal ferrites, the effect of additives such as  $\text{Na}_2\text{O}$ , and  $\text{Na}_2\text{O}-\text{CaO}-\text{ZrO}_2$  were studied.

2-1) At first, the effect of Na dopant in the range of 0.001 ~ 1.0 wt% was investigated. The microstructure depended on both the concentration of Na and the sintering condition such as the rate of heating ( $50^\circ\sim 300^\circ\text{C/h}$ ) and the firing temperature ( $1150^\circ\sim 1250^\circ\text{C}$ ).

The amount of Na having an effect on the microstructure was divided into three regions; (I) 0.001 ~ 0.05 wt% Na, (II) 0.05 ~ 0.1 wt% Na, (III) 0.1 ~ 1.0 wt% Na. The fine grain ferrites with high density were sintered in region (I), and large or exaggerated grain with low density in region (III). The microstructure of ferrites was controlled by the heating rate in region (II). The effect of Na additive on the microstructure in relation to the sintering condition was cleared for the first time.

2-2) Then, to increase the mechanical strength, especially to improve the resistance to chipping during the magnetic head (computer disk memory head) fabrication process, a triple addition of  $\text{Na}_2\text{O}-\text{CaO}-\text{ZrO}_2$  was examined. It was cleared from the present study that  $\text{ZrO}_2$  increased toughness of the polycrystals, with contribution of the fine grain matrix which was induced by small amount of  $\text{Na}_2\text{O}$ . By  $\text{ZrO}_2$  addition, the microstructure showed the intragranular fracture, even though CaO were added to the polycrystal.

The ferrite with CaO, or Na<sub>2</sub>O-CaO showed the grain boundary fracture, where CaO was added in order to get high permeability at high frequencies. It was also cleared that the polycrystal which showed the grain boundary fracture was low resistance to chipping, and on the other hand one with intragranular fracture had high resistance to chipping. Mechanically improved Mn-Zn ferrites by a triple addition were suitable for the material of the hard disk magnetic recording heads.

3. In relation to the results of Na doped Mn-Zn ferrites, the abnormal grain growth was investigated. Among many kinds of additives, effects of B<sub>2</sub>O<sub>3</sub> and Na<sub>2</sub>O on the grain growth were studied.

And the solid state single crystal growth was attempted by using a joint sample which composed of a polycrystal and a seed single crystal. By fine control of the amount of B<sub>2</sub>O<sub>3</sub> in the polycrystal, and adopting ethylsilicate solution as an adhesive for the joint sample, the polycrystal was converted into the single crystal with the crystal growth length of ~ 8 mm under the condition of 1400°C for 12 hr.

Mechanism of single crystal growth was proposed and the properties of grown single crystal was evaluated.

A grown single crystal showed nearly the same properties as that of the Bridgman single crystals, which is suitable for the material of VTR head.

## ACKNOWLEDGMENT

The author wishes to express his thanks to Dr. T. Nitta, Chief of Central Research Laboratory of Matsushita Electric Ind. Co., Ltd, Dr. E. Hirota, Managing Director of Matsushita Technology Institute, Mr. Y. Ise, Group Manager of Central Research Laboratory of Matsushita Electric Ind. Co.,Ltd, for their help and supervisions, and to Dr. K. Kugimiya, Central Research Laboratory of Matsushita Electric Ind. Co.,Ltd, for his help and discussion in this work, and to Messrs. M. Satomi, Central Research Laboratory of Matsushita Electric Ind. Co.,Ltd, M. Sugimura, K. Watanabe, Y. Ito, and K. Matsuyama, Miyazaki Matsushita Electric Co.,Ltd, for the preparation of test specimens and measurement of their magnetic properties and mechanical properties and their kind suggestion and discussions in this work.

The author wishes to express his thanks to Professor S. Kume, Osaka University, for his critical reading of the manuscript and helpful discussions.